NASA Contractor Report 185120

On Finite Element Implementation and Computational Techniques for Constitutive Modeling of High Temperature Composites

A.F. Saleeb, T.Y.P. Chang,
T. Wilt, and I. Iskovitz

University of Akron
Akron, Ohio

July 1989

Prepared for
Lewis Research Center
Under Grant NAG3-901

National Aeronautics and
Space Administration

TABLE OF CONTENTS

TABLE OF CONTENTS (Continued)

TABLE OF CONTENTS (Continued)

TABLE OF CONTENTS (Continued)

PART I: AN OVERVIEW

1. Introduction

At present, metal matrix composites are the primary materials for use in the propulsion systems of space vehicles due to the light weight/high performance requirements. During its service life, the composite will experience, to a large extent, severe thermal and mechanical loading cycles under high temperature environments. As a result, such composite components undergo considerable inelastic deformations, leading to phenomena like ratcheting, and eventually to their fatigue failure. Obviously, effective utilizations of high temperature composites require proper design technology, including life prediction methodologies, for "typical" composite structural components; such as turbine blades and combustor liners in the form of *composite laminates* with flat (plate-type) or curved (shell-type) geometries.

A valid assessment of the structural integrity, reliability, and life expectancy of these components requires the development of an improved numerical capability for their complete, "global-local" (also called progressive-failure) analysis. This in turn requires consideration of (a) generalized material behavior, and (b) analytical solution procedure. It is noted here that for such a development, a general framework of wide applicability is still lacking. The research work reported here is concerned with several contributions to this end.

The term "generalized material behavior" refers to the multiaxial constitutive equations which describe the basic characteristics, and experimentally-observed phenomena, of the composite material subjected to complex thermo-mechanical load cycles. These are the most fundamental relations required in

any analysis; in fact, their "accuracy" determines the "quality" of the entire numerical results. Ideally, these constitutive models should then provide accurate mathematical representations of the pre-failure, failure, and post-failure (or damaged) materials response modes.

However, in view of the extremely complex nature of the many phenomena exhibited by composite materials at elevated temperatures (e.g., strong initial anisotropy; inelasticity; time- and temperature-dependent effects like creep, relaxation, and recovery mechanisms; failure in the form of fiber breakage or matrix-dominated ductile rupture; constituent matrix-fiber interactions such as debonding and delamination failure, etc.), a concensus favoring a particular approach for developing a "comprehensive" constitutive model for composite deformation-strength behavior is not yet in evidence. Nevertheless, progress is currently being made on several fronts by various groups at NASA Lewis [e.g. 1-9]. Considering the "output" composite constitutive idealizations resulting from this research activity, an immediate and important issue in this connection concerns their use in nonlinear structural analysis.

The term "analytical procedure" used above refers collectively to all mathematical/numerical aspects of calculations needed to obtain a solution. To this end, the finite element method is often utilized as a general framework. The present work is mainly concerned with issues related to accuracy, reliability, and efficiency of algorithmic strategies employed in the (materially/ geometrically) nonlinear finite element solutions for laminated composite plates and shells under static/dynamic loadings.

More detailed discussions are given below on specific areas and problems investigated in the subsequent parts of the report.

2. Composite Constitutive Modeling

Metal matrix composites are typically multi-phase materials, comprised of "stiff" reinforcing fibers, metal matrix (resin), as well as their interphases. The mathematical characterization of their "macroscopic" thermomechanical deformation/strength properties should therefore ideally be based on a consideration of the more basic "microscopic" properties of the individual constituents and their interactions; i.e. in the spirit of the so-called "mesomechanics" approach [6].

In one such micromechanics approach, the overall response of the aggregate composite is "derived" using the rule of mixtures, and often utilizes some simplifying assumptions regarding the fibers' geometry and packing, for a representative volume element of the composite [1,8,9]. For example, this has led to the development of a set of "simplified" nonlinear constitutive relationships by Chamis and his colleagues at NASA Lewis [e.g. 1].

Other more comprehensive developments of micromechanics-based inelastic constitutive models for composites at elevated temperatures are currently underway at NASA Lewis using the method of homogenization. For instance, based on the periodicity of the composite microstructure, a combined experimental/finite element effort is made by Onat and Leckie [7] to formulate constitutive/damage models for the "equivalent" homogenized composite material. In addition, homogenization techniques based on Green functions/Fourier series are employed by Walker [3] in developing viscoplastic models for general periodic/nonperiodic heterogeneous composites, which can also account for surface effects in thin structures.

However, in an alternative approach for composite material modeling, the microscopic effects can be "averaged" at the outset, and the phenomenological (experimentally-observed) aspects of the composite can then be idealized as for an initially-anisotropic continuum. Various classes of such continuum-based constitutive representations have been recently developed at NASA Lewis; i.e., unified viscoplastic models by Robinson and co-workers [e.g. 4, 10].

In view of their generality and ability to account for many important cyclic load/time-dependent phenomena, these multiaxial viscoplastic equations; e.g., as suggested in [4] for transversely-isotropic composites, are presently among the most well-developed and promising models for practical applications. They are therefore used here as a *base-form* for the finite element capability developed. Note that further extensions/refinement of this basic formulation are also currently under investigation; e.g. to include high-temperature damage (creep damage, low- and high-cycle fatigue damage, etc. [7]). We also note that the recent research efforts on homogenization in [3,7] will most likely lead to constitutive macromodels of this same basic structure.

With regard to the above viscoplastic constitutive modeling, a major part of the present work is concerned with the study of various computational/implementation aspects associated with their usage in large-scale finite element analysis [e.g. 5, 11-17]. More specifically, the main objectives here are:

(1) Development of efficient/accurate integration schemes [e.g. 11-14] for the resulting system of *stiff* nonlinear differential equations using explicit/implicit methods with error control;

(2) Design of special procedures for the *structured-coding* organization of the material model implementation into the finite element software NFAP [18], such that it becomes not only transparent but also immediate to constitutive researchers at NASA Lewis for future work.

(3) Development of a "refined" *automatic* local/global time incrementing algorithm [e.g. 15-17] capable of handling general loading; e.g. monotonic or low-rate time varying load histories, as well as transient or high-cycle thermomechanical loadings, etc.

Detailed descriptions of the above items and results of the numerical tests for the schemes developed are given in Part III of this report.

Several other aspects that are not addressed in this report, but will be considered in our future research, are associated with the introduction of the "damage" response [19] in the viscoplastic model. It is now well-known that this presents unique numerical difficulties and calls for a careful investigation of the computational procedure utilized. For example, a typical continuum-damage model is likely to eventually lead to some sort of "strain-softening" [20,21]. This may cause the finite element solution to exhibit pathological behavior in the form of oscillations and strong element-size/mesh sensitivity, unless suitable "localization limiters" are introduced in the numerical model [21]. Also, depending on the particular continuum-damage theory used, the resulting "damaged" material-moduli matrix may become "unsymmetric" [20,22]; i.e., an efficient symmetrization procedure may thus be needed.

Finally, there are cases in which composite structures may fail due to excessive or "moderately-large" viscoplastic deformations (e.g. strains of the order of a few percent, as opposed to the infinitesimal-strain assumption typically used). One crucial question in such cases is how should these "moderate" inelastic strains be treated in the finite element analysis? For example, the inelastic deformations appear as an additive term in the constitutive equations of the unified viscoplastic theory, thus leading to the so-called initial strain approach which is typically employed in finite element analysis. This is equivalent to an explicit or constant-stiffness formulation for "small-strains" viscoplasticity. It is known that the explicit method may present numerical instability or slow convergence problem, especially when the composites experience large strains. In this latter case, a need therefore arises for the development of variable-stiffness or implicit methods [e.g. 23], which has been traditionally used for time- and rate-independent plasticity. This in turn requires careful studies of the possible ways for deriving appropriate material "tangent-stiffness" matrices for viscoplastic models.

3. Laminated Composite Plate/Shell Elements

A very important ingredient in the nonlinear analysis of composite structural components is the use of suitable plate/shell elements representing structural action of thin/moderately-thick/thick laminated composites. It is presently well-established that the most effective approaches for geometric modeling of plates and arbitrary curved shells are: (a) degenerated shear-flexible (middle-surface) elements for thin and relatively-thick situations; and (b) two-surface elements (3-D solids) for the thick regime. Despite

their popularity, displacement-based models of these types are also known to exhibit several difficulties [e.g. 24, 25, 27] in applications to isotropic as well as anisotropic problems (e.g., shear/membrane locking for thin structures, kinematic deformation modes for reduced integration, etc.).

Alternative formulation approaches have therefore been advocated, e.g. using various hybrid/mixed methods. In particular, a class of effective and simple hybrid/mixed plate and shell elements have recently emerged from our previous research work with NASA Lewis [25-30]. More specifically, a large variety of critical test problems, for both linear [25, 27] as well as geometrically-nonlinear [30] situations, have clearly demonstrated the robustness and accuracy of our simple quadrilateral element (HMSH5) for isotropic-elasticity. A major portion of the present work was thus devoted to mixed element-technology development applied to composites, for both static and vibration analyses, as detailed in Part II of the report.

In such a development of mixed composite elements for plates and shells, at least three numerical problems can be anticipated. First, because of their anisotropy there will be strong interactions among various stress and strain components in a composite element, which may induce the so-called locking effect. This needs careful examination. For example, an attempt has been made by Spilker [32] to formulate a locking-free 8-noded hybrid stress element for laminated plates. However, in that approach, independent stress functions were assumed for each individual lamina. This leads to a very large number of independent stress (strain) parameters per element, thus rendering the analysis prohibitively expensive. Instead, we propose to use a fixed set of stress (or strain) functions for a "designated" number of laminae (plies or layers).

This "designated" number has to be determined on the basis of numerical study. In fact, the extreme assumption of utilizing *layer-number-independent* strain interpolation for the laminate element, is utilized here, and was shown to be successful in all the test cases investigated in Part II. This is certainly of great advantage from the standpoint of computational efficiency.

Second, there is a need in using an efficient "through-thickness" integration scheme to obtain the overall constitutive properties of the laminated composite from the corresponding (viscoplastic rate) equations for the individual plies (laminae). The familiar Gauss quadrature rule for isotropic materials is not suitable for laminated composites since it fails to capture the material behavior of each lamina. For numerical expediency, we developed an "interpretive" scheme for thickness integration that is combined with conventional Gauss quadrature for in-plane lamina integration. That is, a few sampling points in the thickness direction are preselected to calculate the material matrices for an equivalent unidirectional material. Then, the corresponding quantities for each lamina are interpolated according to its thickness-location and fiber-orientation. It is believed that this scheme combines the attributes of computational *efficiency* as well as numerical *accuracy*.

Finally, from the viewpoint of general applicability to *arbitrary* curved shells (i.e., nonflat/nonrectangular elements), the need will arise for the appropriate definition of "fiber-orientations" or "material-symmetry" axes for the "equivalent" material at each in-plane (lamina) integration point. To this end, we have implemented a simple "shape-function" interpolation (isoparametric-type) scheme based on their values associated with the nodal points

defining the element geometry; i.e., the so-called nodal fiber or *material triads*. Note that for rectangular-element meshes for flat plates, this can be reduced to simply specifying (as input) the angle of inclination of material-symmetry axes with respect to the global axes of the composite plate.

The various aspects above have been incorporated in the mixed formulation of the composite element HMSH5, and its applications to a number of test cases are described in Part II of the report. Emphasis is placed on demonstrating its response characteristics with regard to: 1) mesh-convergence properties; 2) accuracy of stress and displacement prediction in static analysis; and 3) frequency and mode predictive capability for vibration analysis.

4. Fully-Nonlinear Analysis Capability for Shell Applications

In addition to material nonlinearities, geometric nonlinearities in the form of 1) *large rotations*, and 2) large or *non-infinitesimal strains*, must be also considered in the development of a fully-nonlinear solution procedure of plates and shells [e.g. 30, 31]. For example, item (1) is crucial in studies related to any buckling phenomenon (e.g. creep buckling). Significance of (2) appears in the analysis of failure or damage due to excessive deformations. In these latter cases, moderate strains (on the order of 3-5%) will be typically involved. Based on our previous experience [30], these should be properly accounted for in the iterative solution scheme to improve its convergence properties.

In this final part of the investigation, the general framework of fully-nonlinear curved shells is developed for the mixed elements. Adopting an updated-Lagrangian approach, a consistently-linearized form of the incremental

modified Hellinger/Reissner mixed variational principle is utilized to derive the element nonlinear governing equations. Emphasis is placed on devising effective solution procedures to deal with

(1) element configuration-update in the presence of large rotations in space;

(2) accurate integration of spatial stress and strain fields.

A rather comprehensive account of the various aspects of this development has been recently compiled in a report [30], which was provided to NASA-Lewis earlier this year (1989). Therefore, only a summary of the essential points and results in some validation tests will be included in Part IV of this report.

5. Objectives, First-Year Accomplishments, and Outline

In summary, the overall objectives of the present work are given as follows:

1) To develop robust and effective laminated plate/shell elements based on the mixed method for the analysis for static and vibration problems.
2) To develop efficient implementation and time-stepping/numerical-integration schemes for unified viscoplastic constitutive models for high-temperature composites.
3) To develop a general framework for the fully-nonlinear structural analysis of shells.

Considering the above three items, our first-year accomplishments are summarized as follows:

With regard to item (1), we have completed the formulation and testing of an "extended" hybrid-mixed *composite* element HMSH5 for *static and vibration*

analyses. Emphasis is placed in this development on: i) robustness, ii) computational efficiency, as well as iii) general applicability to arbitrary curved shells, and several noteworthy aspects are included here. With regard to (i) a careful selection is made for the polynomial functions in the assumed strain field, thus leading to stiffness formulation that is kinematically *stable*, *free from locking* for large "thickness" aspect ratios, relatively *insensitive to* geometric distortions, etc. In addition, with a view toward (ii), and in contrast with other previously-developed hybrid composite plate elements, we utilized a *fixed* set of parameters; i.e., a layer-number-independent assumption, for the strain field discretization, together with an *efficient* "through-thickness" integration scheme for the stiffness calculations in terms of the *anisotropic* elastic/viscoplastic properties of the laminated element. A *simplified* mass matrix was also used, thus obviating the need for expensive "dynamic condensation" of its fifth node's degrees-of-freedom. Finally, from the viewpoint of general applicability to *arbitrary* curved shells (i.e., nonflat/nonrectangular elements) in (iii), appropriate definitions of "fiber-orientations" or "material-symmetry" axes for the "equivalent" material at each in-plane (lamina) integration point were made through the implementation of a simple "shape-function" interpolation (isoparametric-type) scheme based on their values associated with the nodal points defining the element geometry; i.e., the so-called nodal fiber or *material triads*.

In connection with research areas in item (2) above, the major contributions of the first-year study consist of: i) four different viscoplastic constitutive models (for isotropic and anisotropic responses), and the associated integration methods, are coded as a separate module in NFAP so that any

future extension or coding modification can be done easily by a user, ii) "reduced" forms of viscoplastic models were made readily available for applications to various structural components represented by a 2/D continuum, or plate/shell elements, iii) further understanding of the numerical schemes employed for practical analysis, and iv) development of a "refined" automatic local time incrementing algorithm capable of handling general time-varying load histories.

Finally, in the first-year investigation associated with item (3), the *general framework* of fully-nonlinear analysis of curved shells has been developed for our mixed finite elements. Adopting an updated-Lagrangian approach, a consistently-linearized form of the incremental modified Hellinger/Reissner mixed variational principle is utilized to derive the element nonlinear governing equations in the form of *tangent* (*variable*) *stiffness* solution. Emphasis is placed on devising *effective* solution procedures to deal with: i) element *configuration-update* in the presence of large rotations in space; and ii) *accurate integration* of spatial stress and strain fields when large non-infinitesimal strains occur. Within this framework, the newly-developed nonlinear element HMSH5 was tested and shown to exhibit *improved* convergence characteristics compared to other available elements.

Following the overview given in this first part, the remainder of the report is conveniently divided into three separate parts, II, III and IV, describing the research work completed in each of the above three areas (1), (2), and (3), respectively. Each part contains a review of pertinent literature, detailed theoretical and algorithmic developments, results of numerical test problems for validation, as well as conclusions summarizing the research items planned for future work.

PART II: MIXED ELEMENTS FOR LAMINATED PLATES AND SHELLS

1. Introduction

In order to analyze and design some of the complex composite structural applications, finite element techniques are now almost invariably used in many, if not all, phases of the design process. In addition to the design phases, recent interest has also begun to focus on the failure and various damage mechanisms associated with composite materials, i.e. matrix cracking, delamination/debonding, ply failure, etc. These types of applications demand accurate stress predictions.

Because of the above mentioned points, considerable interest and effort has focused in developing accurate and efficient composite finite elements. In this connection, we summarize here the results of our recent research activity on the development of an effective quadrilateral plate/shell element, of the hybrid/mixed type, for the static and dynamic analysis of anisotropic elasticity.

2. Background and Literature Review

2.1 Composite Finite Elements

A laminate is typically constructed of a series of plies stacked and bonded together to form the laminate. Each of the individual plies are composed of two distinct constituents, fibers and surrounding matrix material, which possess markedly different properties. In particular, due to the difference in shearing stiffness of the matrix and fibers, high ratios of elastic moduli to shear moduli are developed. Thus, the cross-sectional warping, i.e. shear deformation, of the laminate is dependent on the ply orientations in addition to the plate/shell thickness. Because of this, it is

known that shear deformation has a more pronounced effect in laminated structures than in the case of isotropic structures.

In classical lamination theory (CLT) the usual Love-Kirchoff assumptions of plane sections remaining plane are in effect, thereby neglecting shear deformations totally. Obviously, this type of theory is of no value except in very thin plate or shell applications. A theory used in thick plates is that attributed to Reissner-Mindlin type of assumptions. In this case, a constant shear angle through-the-thickness of the plate is assumed and has been referred to as the constant shear angle theory (CST). Typically, some form of shear correction factor, κ, is chosen to account for the through-the-thickness shear deformation. These types of Reissner-Mindlin elements are those typically used for composite analysis.

It has been suggested that while this type of assumption is satisfactory for isotropic plates, it may not be sufficient for laminated plates and shells because of the varying shear moduli through-the-thickness of the laminate. Thus, a layerwise constant shear angle theory (LCST) has been used in which, as the name implies, a constant shear deformation angle is used for *each* ply.

Using the terminology of Bert [33], the majority of composite finite elements can be categorized into two distinct groups, namely, (1) a "smeared laminate model" (SLM), and (2) a "discrete layer model" (DLM). In the SLM elements, the laminate is not considered as a series of individual layers but a heterogeneous, anisotropic medium. In terms of shear deformation, the constant shear angle theory (CST) type of elements are in effect smeared models since they do not distinguish the shear strain angles on an individual layer basis. In the DLM elements, each layer retains its own identity and in some cases is treated as a "sub-element" of the total element. In terms of shear

deformation, the layerwise constant shear angle theory, (LCST) are discrete models since each layer is permitted to have its own shear angle.

In addition, the above classifications may be further subdivided into groups which utilize lower-order and higher-order approaches. The criteria for distinguishing between a lower-order versus a higher-order approach depends on the order of thickness-coordinate (z) terms included in the expansion of various displacement components. That is, expansions including only up to linear terms in z are described as lower-order approaches, whereas, those including higher-than-linear powers of z are collectively referred to as higher-order approaches. It should be noted that application of either approach can be made on the *entire laminate*, as in the SLM elements, or to *individual layers*, as in the DLM element.

At this point, it may be useful to briefly discuss the higher-order theories in general. There have been numerous higher order theories developed, Reddy [34], Lo [35] and Murakami [36], to account for shear deformation. In these approaches, higher-order expressions containing quadratic and cubic terms are used for the displacement or stress field equations. By using such expressions, accurate predictions of in-plane displacements, shear strain and stress distributions through-the-thickness are obtained. The goal and motivation for using these higher-order theories is to be able to obtain an accurate prediction of the laminate behavior while still using a 2-dimensional approach, as compared to 3-dimensional or elasticity approaches. Thus, the higher-order theories attempt to strike a balance between complexity and accuracy.

In the above, two approaches have been used to develop the higher-order theories, namely, a displacement-field assumption or a stress-field assump-

tion. The most commonly used is the displacement-field assumption, where in this case, the new laminate theory is based upon a kinematically admissible displacement field.

The main thrust of the "higher-order theory" models is to primarily deal with the complex cross-sectional warping of the laminate. All of the literature reviewed, i.e. Reddy. Lo, Murakami, emphasizes how well their particular approach can predict the "zig-zag" shape of the in-plane displacement distributions. In reality, the crucial test appears to be how well the theory predicts the through-the-thickness distribution of shear stresses. In fact, accurate methods to predict such transverse shear stress variations is currently one of the very active research areas in composite modeling; see additional related discussions in Sec. 4.2.

For example, Reddy [34] gives results showing through-the-thickness shear stress distributions obtained directly from constitutive equations and equilibrium equations. The distributions obtained from the constitutive equations are quite poor with stress discontinuities occurring at the layer interfaces. The only improvement over the lower-order theory, i.e. CLT, is the parabolic shear stress distribution within each layer and the ability to satisfy the stress free conditions at the top and bottom surfaces of the laminate. On the other hand, if ply equilibrium equations are used to calculate the shear stresses, more accurate and correct shear stress distributions are obtained. As will be shown later in Sec. 4, the present element can also obtain such a prediction through the use of a modified shear strain distribution method, which is simpler than using higher-order theory. In the results of Murakami [36], the shear stresses are obtained from equilibrium equations, and as ex-

pected show good agreement with the exact solution, while Lo [35] makes no mention of the shear stress distribution results, only flexural stresses.

2.1.1 Discrete Layer Model (DLM) Elements

A group of 8-node isoparametric hybrid-stress elements for thin to thick laminated plates have been developed by Spilker [37,38,39]. Together with a higher-order approach the hybrid-stress formulation is utilized. The latter is claimed to be preferred since it is easier to satisfy interlayer stress continuity and laminate surface conditions exactly. The main feature of this element is that displacements and non-normal cross-section rotations are independent from layer to layer [37]. Thus, each layer possesses its own degrees of freedom (d.o.f.) and remains a discrete layer. In addition, individual stress expressions are written for each layer. Stress continuity through-the-thickness is then established by relating certain terms of the adjacent i^{th} and $i+1^{th}$ layers. Also, certain displacements of the adjacent layers are related to establish displacement continuity through-the-thickness. The DLM approach is used in order to account for the severe cross-sectional warping on the laminate. This point is emphasized by the fact that *within each layer*, a higher-order displacement assumption is used. Specifically, the in-plane displacement, v, is on the order of z^3 and the transverse displacement, w, is of z^2 order, where z is the thickness coordinate. This is in contrast to the usual applications of the higher-order theory, which is usually applied on the laminate level.

Because each layer is considered to be discrete, forming the element stiffness becomes an involved process. Basically, an assembly process is

required to form the element, or laminate, stiffness from the individual layer stiffnesses. Reference [38] likens the process to the conventional element "assembly" operations in finite element codes. That is, stress parameter "pointers" and nodal displacement "pointers" are required to add individual layer stiffness contributions to the overall element stiffness. Thus, the element requires a large amount of computation just to form the element stiffness. As a matter of fact, Spilker does point out that the number of d.o.f. and laminate stress parameters grow rapidly as the number of layers increase, and computer core storage may limit the number of layers allowed [37].

In reference [38], in an attempt to eliminate some of the layer dependency of the element, "kinematic constraints" are introduced. These constraints are such that a number of the individual layer displacements are related to a laminate set of d.o.f. located at the mid-plane of the laminate. The element d.o.f. are only those associated with the mid-plane reference surface making the element's d.o.f. layer independent. Thus, the element now has a total of 40 d.o.f. independent of the number of layers. Also, the higher-order displacement assumptions of [37] are simplified to again decrease the complexity of the element. Thus, in effect, the detailed in-plane displacement response is neglected, yet the element still retains the higher-order stress expressions. By using such a compromise, the element still gives accurate transverse displacement as compared to CLT and good through-the-thickness stress distributions as compared to elasticity.

Finally, in reference [39] Spilker introduces an element which is totally layer independent. For moderately thick laminates, $0.01 < h/L < 0.1$, shear deformation affects structural behavior but the individual layer warping ef-

fects are not significant. Thus, individual layer non-normal cross-section rotations and individual stress parameters may not be necessary. In this element, the total number of d.o.f. and stress parameters are independent of the number of layers. First, the nodal d.o.f. are related to the in-plane and transverse displacements at the mid-plane reference surface of the laminate, and to the non-normal cross-section rotations of the laminate. Second, the stress fields in each layer are expressed in terms of laminate stress parameters. All the through-the-thickness integrations can therefore be isolated and they are then analytically evaluated. Specifically, this refers to the calculation of the laminate material properties, i.e. axial, bending, and coupling stiffnesses. In effect, laminate theory is used to calculate these quantities, thus effectively eliminating any numerical integration through-the-thickness. Since these are the only layer dependent quantities for the element, the computation time will increase slowly as the number of layers increase.

The element predicts transverse displacements quite well, as compared to exact solutions, for laminate thickness ratios of $0.01 < h/L < 0.25$, where h is the total thickness of the laminated plate, and L is a characteristic "spanwise" length. The stress distributions show good agreement with exact solutions for thickness ratios of $0.01 < h/L < 0.10$, i.e. up to moderately thick laminates. The stress distributions for thick laminates, $h/l=0.25$, are not in good agreement. This is attributed to some of the above mentioned simplifications introduced into this element to improve its efficiency. Details of improved CPU times can be found in [39], and in general this element proves to be more efficient than the previous elements.

Thus, the trend is to move away from the true discrete layer model, which is inefficient from a computational standpoint, to a semi-discrete layer model. While the DLM elements give very detailed displacement and stress information, one needs to question whether or not such detail is necessary. Spilker states that such detail may only be required for special cases such as non-linear post-first-ply failure, laminate strength measurements, etc. [37]. But for typical structural applications such detail is not necessary.

Chaudhuri and Seide [40] present a triangular 6-node displacement based element. It is somewhat similar to Spilker's original element [37], in that the total d.o.f. of the element is layer dependent. The total laminate element consists of N "layer elements" for a N-layer laminate. Each layer element is triangular in shape and consists of 6-nodes with 5 d.o.f. per node. This element is different from Seide's previous work in that the element can assume a general triangular shape. The reason given for choosing a triangular over a quadrilateral shape is that it allows easier modeling of holes and cut-outs.

In terms of the d.o.f., each "layer element" has two independent in-plane displacements and two independent rotations. Because each layer has independent rotations, i.e. shear angles, Seide uses the term layerwise constant shear angle, LCST, to describe this type of element. The remaining d.o.f., transverse displacement, is not independent from layer to layer. That is, each element shares the same transverse displacement with the adjacent nodes that have the same in-plane coordinates through-the-thickness. This satisfies the assumed condition of transverse inextensibility, i.e. laminate thickness does not change, and interlayer continuity.

However, Seide's element differs from that of Spilker's layer-dependent element in one important aspect. That is, because of its underlying displacement-based formulation, the former element must satisfy the displacement continuity requirement, thus allowing the typical numerical integration scheme to be used through-the-thickness to form the element stiffness from the individual layer stiffnesses. In contrast, since Spilker used assumed-stress fields, which are not continuous through-the-thickness, the complex "pointer" method was required. Seide uses Heaviside functions to write a continuous function through-the-thickness of the laminate for the in-plane displacements, with the resulting expressions being similar to those used in the higher-order theory approaches. The expression for transverse displacement is constant, as discussed.

The results produced by this element shows good agreement with the elasticity solutions. In particular, the transverse displacement predictions for a thick laminate, i.e. L/h = 4, the CLT error is around -78% while the LCST and CST give -3% and -5.2%, respectively. Thus, for thick laminates, Seide believes that LCST is required for acceptable results. But it should be noted that for moderately thick laminates, L/h = 10 to 20, both the error between the LCST and CST theories becomes almost negligible. Thus, since CST theory gives adequate results for thin to moderately thick laminates, is LCST necessary?

2.1.2 Smeared Laminate Model (SLM) Elements

Another classification of composite finite elements are what may be termed as smeared laminate model (SML) elements. Most of the original compos-

ite element developments fall under this particular category. The elements of Panda and Natarajan [41], Chang and Sawamiphakdi [42], Reddy [43], Rogers and Knight [44], and Haas and Lee [45], reviewed in this paper, use a "smeared" laminate in the sense that the element does not retain the discrete ply structure, as do the DLM elements discussed previously. Instead, by either numerical integration through-the-thickness or the application of laminate theory an equivalent laminate or element stiffness is formed. In most cases, the use of this smearing technique is sufficient for predicting the global structural response.

The elements of Panda [41] and Chang [42], can be considered as representative examples of early composite finite elements based upon a "degenerated" solid shell theory. In particular, the element of Panda is a simplification of an element originally developed by Mawemya and Davies [46]. This original element considered independent rotations for each layer, thus the total degrees of freedom of the element was dependent on the number of layers. Panda states that the use of independent layer rotations does not necessarily give improved results, but does increase the size of the problem considerably [41]. Thus, the element of Panda uses a constant normal rotation through-the-thickness of the laminate. Also, details are provided on the method of integrating through-the-thickness using a "thickness concept" to effectively account for the different layer material properties. This change of variable scheme is common to most elements which integrate through-the-thickness to form the element stiffness. The results provided by Panda show good agreement with elasticity solutions. For $L/h > 20$ errors in deflections and stress are on the order of -7% and for $L/h > 10$, the deflections are within -15% and

stresses are within -10%. Panda shows that this particular method of integrating through-the-thickness provides good accuracy for thin plates and reasonable accuracy for thick plates [41].

A limitation of the previous displacement based "degenerated" elements is in dealing with the problem of locking. That is, most shell elements have a tendency to overpredict the element stiffness as the thickness becomes small, which leads to locking. In reference [45], Haas and Lee present a nine-node assumed strain degenerate solid shell element, which was chosen because it has been shown that the problem of locking is eliminated. This is achieved by segregating the energy expression into components of in-plane, bending, and transverse shear strain energy terms. Also, coupling strain energy terms are included since coupling effects are present in non-symmetric composite laminates (for symmetric laminates or isotropic materials, this term will vanish). By segregating the in-plane and transverse shear strain terms, the source of locking is eliminated. The strain polynomial assumptions were chosen to produce a stable element with no spurious kinematic modes [45]. An important point is that these strain polynomials are used to describe the behavior of the *entire* laminate through-the-thickness, unlike the stress polynomials of Spilker [37]. Because of this, the element degree's of freedom are not layer dependent.

Results are presented for symmetric laminated plates subjected to a sinusoidal load. For square laminated plates with length-to-thickness ratios of $10 < L/h < 400$, the element shows good agreement with elasticity and thick plate theory [45]. One interesting point is that no mention is made of any shear correction factors for shear deformation, yet reasonable results are obtained.

Recall that previously the higher-order theory was shown as applied on an individual basis, in particular, the DLM elements of Spilker. On the other hand, Reddy [43] uses the higher-order approach on a laminate or element level. The element, as described in reference [43], is classified as a SLM element where the higher-order displacement fields are used to describe the entire laminate through-the-thickness. Specifically, Reddy's element is based upon the previously discussed theory set forth in reference [34]. Again, as most proponents of the higher-order theory emphasize, the classical plate theory based upon the Kirchhoff-Love assumption is not adequate to describe the behavior of moderately thick laminates. By using a higher-order theory, the parabolic distribution of the transverse shear stresses is accounted for and thereby eliminates the need for the shear correction factors, [43].

Results are presented covering deflections, stresses, buckling loads, and vibration frequencies. If attention is focused primarily on deflection and stress results, the higher-order element does show excellent agreement with exact elasticity solutions for the cases presented here. Reddy again emphasizes the discrepancy between the CLT and HSDT, with the difference becoming more significant as the ratio of longitudinal to transverse moduli increases.

But as is common with the higher-order approach, Reddy does point out the associated drawbacks. First, higher-order stress and moment resultants arise from the formulation which are difficult to understand physically. This same problem is evident in the elements of Spilker. And secondly, the theory contains derivatives of the transverse deflections. Thus, the element requires functions with C^1 continuity [43].

In reference [47], Lakshminarayana and Murthy present a shear flexible finite element which is based upon a generalized theory of Yang, Norris, and Stavsky, YNS. It is "shear flexible" in the sense that shear deformation is accounted for. Using this theory, the coupled bending and stretching response of the laminated plate is expressed in terms of five unknowns. That is, three displacements; u,v,w, and two rotations; θ_x,θ_y, of the normal [47]. The element itself is triangular in form and has three nodes located at the vertices. Complete cubic polynomials are used to approximate the displacements and rotations within the element and were chosen because the authors believe that higher-order elements have advantages over lower-order elements when dealing with laminated composite plates and shells [47]. There are 15 degrees-of-freedom per node; three displacements, two rotations, and their derivatives. The authors believe that by using the derivatives of displacements and rotations at the nodes is an advantage because it allows evaluation of the stresses directly at the nodes instead of at Gauss points which is common in most other elements. But this also makes the element very computationally expensive since for three nodes with 15 degrees-of-freedom per node gives a total of 45 degrees-of-freedom for the element. Thus, one must question whether the luxury of having the stresses directly at the nodes is really advantageous. Again, as with previous SML elements, the element stiffness is partially based upon laminate theory to reduce the multi-layer composite into a smeared single layer plate.

Lakshminarayana and Murthy present a large number of cases with a variety of geometry, loading, support conditions, and plate thicknesses to access the performance of the element and the importance of shear deformation effects. In each case, the performance is measured by comparing to either analytical or

other finite element solutions obtained from a reference by Noor and Mathers. The element appears to agree very well with the other solutions, both finite element and exact, in all cases presented. Because of the large amount of detailed results and the varied cases, this reference will serve well as a source of benchmark problems for the present composite finite element development.

Rogers and Knight [44] present a higher-order element with a specific application to filament-wound composite pressure vessels. It is pointed out in the paper, that the main motivation for the development of the element is to provide an efficient and simple means of modeling the complex composite structure found in the pressure vessels. Also, because of the low shear stiffness of the material, significant shear effects between the layers develop, thus requiring a higher-order displacement field. The proposed element is similar to the higher-order elements previously discussed, but a distinguishing feature presented is that the order of the through-the-thickness polynomial is user selectable. The element subroutine internally generates the appropriate shape functions using Lagrange interpolation polynomials. This is unlike most elements in which the shape functions are permanently coded into the element subroutines. This eliminates the need to manually derive the shape functions and their derivatives. Whether or not this feature is really an advantage is not clear. By using such a higher-order element, the typical multi-layer composite can now be effectively modeled using one element through-the-thickness. As proof of the need of a higher-order element, data is presented which shows the amount of computation time saved by using one higher-order element through-the-thickness, as compared to the use of individual elements for each ply.

The element stiffness is generated by performing numerical integration through-the-thickness on a layer-by-layer basis. Unlike most composite elements reviewed that use this technique, this element uses a zeroth-order rule (rectangular integration rule) with the weighting factors being proportional to the layer thickness in which the integration point resides. This allows the effects of each individual layer's material properties to be effectively modeled. The authors do point out though, that no relationship exists between the polynomial order, n, and the number of integration points required to integrate the polynomial exactly using this zeroth-order integration (unlike standard Gauss quadrature). This creates a variable in the accuracy of the finite element solution which can be only eliminated by experience with this particular element [44].

All of the papers reviewed thus far, have been limited to linear problems with regard to deflections, vibrations, and buckling loads. One of the obvious reasons for such limited work in nonlinear composite analysis is the added complexity of the problem. Indeed, considering composite literature in general, closed-form or "exact" solutions that do exist are further limited to a very narrow class of problems; i.e., for the most part, to symmetrically layered cross-ply and angle-ply laminates. This is due to the presence of coupling terms, which are peculiar to composite materials, that often make any analytical solution for unsymmetric laminates intractable. This accounts for the repeated use of the 0/90 class and other symmetric laminates, which do not contain these coupling terms, as reference solutions in most finite element literature; e.g. Pagano [48] and Whitney [49].

A comprehensive review of research on both linear and nonlinear analysis of composites was given in [50]. In addition, a penalty-type formulation to overcome shear locking for thin plates together with the composite theory by Yang, Norris, and Stavsky (YNS), and various classical first-approximation shell theories were utilized in [50] to develop a displacement-based element for nonlinear analysis. Similar applications of these types of elements can also be found in [52,53].

3. Present Element Formulation

The element to be presented here is the extension of earlier work by Saleeb et.al. [27] to the modeling of multi-layered composite materials. It is the objective of this investigation to see how well the element will perform with the minimum amount of modifications to its basic formulation. If the element yields satisfactory results, as such, a good foundation will have been established in which to build upon for future work. It is also desirable to keep the element as "simple" as possible thereby minimizing the computational expense, i.e. an element which has the total d.o.f. independent of the number of layers.

This element may be classed as a hybrid/mixed or assumed-strain shell element. That is, in the underlying variational principle, both the displacement and strain fields are approximated independently. Since the ultimate goal of the research is the application of the elements for high-temperature metal-matrix composite structural analysis, i.e. non-linear material analysis, it appears that utilizing a strain assumption, as opposed to a stress assumption, is most desirable. That is, in the case of material non-linearity it is

still entirely valid to assume a linear variation of bending strains through-the-thickness of the "thin" laminate, while such an assumption for associated stresses is certainly not valid. Also, choosing a strain field *a priori* is much easier to justify than it would be for a particular stress field assumption.

What is different in the present approach from some of the previously mentioned elements is that the assumed strain field used represents the *entire* laminate. Thus this element can be classified as a smeared laminate model, SML, type, utilizing a first-order or constant shear angle (CST) theory. Its general formulation is derived from a "modified" form of the Hellinger-Reissner variational principle, as described in the sequel.

3.1 Mixed Variational Principal

The "modified" Hellinger-Reissner principle, including the kinetic energy term for the dynamics problem, is expressed as

$$\pi_R = \int_\tau \Big[\int_V \Big[-\frac{1}{2}\,\underset{\sim}{\epsilon}^T \underset{\sim}{\underset{\sim}{D}}\,\underset{\sim}{\epsilon} + \underset{\sim}{\epsilon}^T \underset{\sim}{\underset{\sim}{D}}\,\underset{\sim}{\hat{\epsilon}} + \frac{1}{2}\,\rho\,\dot{\underset{\sim}{u}}^T \dot{\underset{\sim}{u}} - \underset{\sim}{f}^T \underset{\sim}{u} \Big] dV - \int_{S_\sigma} \underset{\sim}{\bar{T}}^T \underset{\sim}{u}\, dS_\sigma$$

$$- \int_{S_u} T^T (u - \bar{u})\, dS_u \Big] d\tau \qquad (1)$$

where

$\underset{\sim}{\epsilon}$ = independently assumed strains

$\hat{\epsilon} = \underset{\sim}{B}^{\ell} \underset{\sim}{q}$ = strains derived from assumed displacements

$\underset{\sim}{D}$ = material stiffness matrix

ρ = material density

$\underset{\sim}{u}$ = assumed element displacements

$\dot{\underline{u}}$ = element velocities

$\underline{T}$ = boundary tractions

$\underline{f}$ = boundary force

V = volume

τ = time

All quantities with an overbar, $(\bar{})$, are prescribed quantities, and S_δ and S_u are portions of the element boundary over which tractions and displacements are prescribed. By taking the first variation of the functional with respect to the strains $\underline{\epsilon}$, and displacements $\underline{u}$, and invoking the stationarity conditions $\delta\pi_R = 0$,

$$\delta\pi_R = \int_\tau \left[\int_V \left[-\underline{\underline{D}}\,\underline{\epsilon}\,\delta\underline{\epsilon}^T + \underline{\underline{D}}\,\hat{\underline{\epsilon}}\,\delta\underline{\epsilon}^T + \rho\ddot{\underline{u}}^T\delta\underline{u} - \underline{f}^T\delta\underline{u} \right] dV - \int_{S_\sigma} \bar{\underline{T}}^T\delta\underline{u}\, dS_\sigma \right] d\tau \qquad (2)$$

the equilibrium equations, strain-displacement relations, i.e.,

$$\underline{\epsilon} = \hat{\underline{\epsilon}} = \underline{\underline{B}}\,\underline{u} \quad \text{in } V$$

$$\underline{\underline{B}}^T\underline{\sigma} + \underline{f} = \rho\ddot{\underline{u}} \quad \text{in } V$$

together with the associated surface-tractions and displacement boundary conditions on S_σ and S_u, respectively, are recovered. In the above, $\underline{\underline{B}}$ is a differential strain-displacement operator, and $\underline{\underline{B}}^T$ is the associated "matrix-divergence" operator.

3.2 Element Stiffness and Mass Matrices

The derivation of the stiffness and mass matrices will be obtained from the previously described functional π_R, now referring to *lamina-coordinate* systems. Justification for choosing such a reference frame is given in detail

in our previous work [27]. Thus, the functional can be expressed as,

$$\pi_R = \int_t \left[\int_V \left[-\frac{1}{2} \underline{\epsilon}^T \underline{\underline{D}} \underline{\epsilon} + \underline{\epsilon}^T \underline{\underline{D}} \underline{\hat{\epsilon}} + \frac{1}{2} \rho \underline{\dot{u}}^T \underline{\dot{u}} \right] dV - \int_{S_\sigma} \underline{\bar{T}}^T \underline{u} dS_\sigma \right] dt \qquad (3)$$

where $dV = dxdydz = |\underline{J}|drdsdt$, in which r,s,t are the natural (isoparametric) coordinates and $\underline{J}$ is the Jacobian-of-coordinate-transform matrix. For the finite element discretization, the displacements, u, are interpolated from the nodal degrees-of-freedom,

$$\underline{u} = \sum_{k=1}^{5} N_k \underline{u}_k + \frac{t}{2} \sum_{k=1}^{5} h_k N_k \left[-\theta_1^{(k)} \underline{e}_2^{f(g)} + \theta_2^{(k)} \underline{e}_1^{f(k)} \right] \qquad (4)$$

where the N_k are the two-dimensional shape functions in terms of local (isoparametric) coordinates, r and s, for node k. For simplicity in terms of the derivations, the above equation can be written symbolically as,

$$\underline{u} = \underline{\underline{N}} \underline{q} \qquad (5)$$

where $\underline{\underline{N}}$ are "modified" shape functions obtained by combining terms in Eq. (4). In the above, $\underline{e}_i^{f(g)}$, with i = 1,2,3, are the components of the fiber triad associated with node (k), which are defined as in [27].

The independently-assumed strains, $\underline{\epsilon}$, are approximated in terms of the strain parameters, $\underline{\beta}$, as follows

$$\underline{\epsilon} = \underline{\underline{P}} \underline{\beta} \qquad (6)$$

where $\underline{\underline{P}}$ is the strain interpolation matrix. Again for brevity, we refer to

[27] for details of the form for the interpolation matrix $\underline{P}$. The strains, $\hat{\underline{\epsilon}}$, derived from the assumed displacements are expressed as

$$\hat{\underline{\epsilon}} = \underline{B}^{\ell}\underline{q} \tag{7}$$

where B^{ℓ} is now a *local* strain-displacement matrix.

Now, substituting Eqs. (5), (6) and (7) into Eq. (3), the functional becomes

$$\pi_R = \int_\tau \Bigg[\int_V \Bigg[-\frac{1}{2}(\underline{P}\underline{\beta})^T \underline{D}(\underline{P}\underline{\beta}) + (\underline{P}\underline{\beta})^T \underline{D}(\underline{B}^{\ell}\underline{q}) + \frac{1}{2}\rho(\underline{\ddot{N}}\underline{\dot{q}})^T(\underline{\ddot{N}}\underline{\dot{q}}) \Bigg] dV$$

$$- \int_{S_\sigma} \bar{T}^T(\underline{\ddot{N}}\underline{q}) dS_\sigma \Bigg] d\tau \tag{8}$$

Equation (8) can be simplified and written as

$$\pi_R = \int_\tau \Bigg[-\frac{1}{2}\underline{\beta}^T \underline{H}\underline{\beta} + \underline{\beta}^T \underline{G}\underline{q} + \frac{1}{2}\dot{\underline{q}}^T \underline{M}\dot{\underline{q}} - \underline{Q}^T\underline{q} \Bigg] d\tau \tag{9}$$

where the matrices $\underline{H}$, $\underline{G}$, $\underline{M}$ and $\underline{Q}$ are defined as,

$$\underline{H} = \int_{-1}^{1}\int_{-1}^{1}\int_{-1}^{1} \underline{P}^T \underline{D}\underline{P} |\underline{J}| dr ds dt \tag{10}$$

$$\underline{G} = \int_{-1}^{1}\int_{-1}^{1}\int_{-1}^{1} \underline{P}^T \underline{D}\underline{B}^{\ell} |\underline{J}| dr ds dt \tag{11}$$

$$\underline{M} = \int_{-1}^{1}\int_{-1}^{1}\int_{-1}^{1} \underline{\ddot{N}}^T \rho \underline{\ddot{N}} |\underline{J}| dr ds dt \tag{12}$$

$$\underline{Q} = \int_{-1}^{1} \int_{-1}^{1} \underline{N}^T \underline{T} |\underline{J}| dr ds dt \tag{13}$$

In order to eliminate the strains on the element level, stationarity is invoked on Eq, (8) in terms of $\underline{\beta}$ variables, thus yielding

$$\underline{\beta} = \underline{H}^{-1} \underline{G} \underline{q} \tag{14}$$

Now, substituting Eq. (14) back into the functional π_R and taking the variation with respect to nodal displacement parameters, we finally get the element stiffness equations as follows,

$$(\underline{G}^T \underline{H}^{-1} \underline{G} \underline{q} + \underline{M} \ddot{\underline{q}} - \underline{Q}) \delta \underline{q}^T = 0$$

or

$$\underline{M} \ddot{\underline{q}} + \underline{K} \underline{q} = \underline{Q} \tag{15}$$

where the stiffness matrix $\underline{K}$ is defined as

$$\underline{K} = \underline{G}^T \underline{H}^{-1} \underline{G} \tag{16}$$

and the mass matrix $\underline{M}$ is defined previously in Eq. (12).

3.3 Through-the-Thickness Integration for Composites

According to Eqs. (10) and (11), the component matrices for the present "smeared" element stiffness (see Eq. 16) are obtained by simply integrating through-the-thickness and taking into account the differences in material

properties of each layer. That is, since the element now represents a multi-layered composite, the material matrix $\underset{\sim}{D}$ is no longer constant through-the-thickness. Thus, individual layer material matrices, $\underset{\sim}{D}_\ell$, must be formed, transformed, and then "combined" during integration to form the smeared laminate stiffness.

Specifically, each layer is assumed to be in a state of *plane stress* ($\sigma_{33}=0$), i.e. the stresses in local *material fiber* or *symmetry-axes* coordinates are ordered as

$$\{\sigma\}_\ell = \{\sigma_{11},\sigma_{22},\tau_{12},\tau_{23},\tau_{13}\}_\ell \tag{17}$$

and the corresponding layer constitutive relation is,

$$\begin{Bmatrix} \sigma_{11} \\ \sigma_{22} \\ \tau_{12} \\ \tau_{23} \\ \tau_{13} \end{Bmatrix}_\ell = \begin{bmatrix} D_{11} & D_{12} & 0 & 0 & 0 \\ D_{21} & D_{22} & 0 & 0 & 0 \\ 0 & 0 & D_{33} & 0 & 0 \\ 0 & 0 & 0 & D_{44} & 0 \\ 0 & 0 & 0 & 0 & D_{55} \end{bmatrix}_\ell \begin{Bmatrix} \epsilon_{11} \\ \epsilon_{22} \\ \gamma_{12} \\ \gamma_{23} \\ \gamma_{13} \end{Bmatrix}_\ell \tag{18a}$$

or symbolically,

$$\{\sigma\}_\ell = [D]_\ell\{\epsilon\}_\ell \tag{18b}$$

in which the $\underset{\sim}{D}_\ell$ matrix elements are defined as,

$$D_{11} = \frac{E_{11}}{1 - \nu_{12}\nu_{21}} \quad ; \quad D_{22} = \frac{E_{22}}{1 - \nu_{12}\nu_{21}}$$

$$D_{12} = D_{21} = \frac{-\nu_{12}E_{22}}{1 - \nu_{12}\nu_{21}} \tag{19}$$

$$D_{33} = G_{12} \qquad D_{44} = \frac{5}{6} G_{23} \qquad D_{55} = \frac{5}{6} G_{31}$$

where E_{11} and E_{22} are the longitudinal and transverse elastic moduli, respectively, the G's are the transverse and in-plane shear moduli and ν's are Poisson's ratios, with all quantities being defined in material fiber coordinates. Now, the layer matrix $\underset{\sim}{D}_\ell$ needs to be transformed from material fiber direction to the direction of the global axes. This is accomplished by using the standard coordinate-transformation relation:

$$[\bar{D}]_\ell = [T]_\ell^T [D]_\ell [T]_\ell$$

where $[\bar{D}]_\ell$ is the transformed layer material matrix and [T] is an appropriate transformation matrix. This latter matrix will generally vary along the lamina surface (i.e., t=0 surface) from one integration point to another (with different r,s-coordinates), depending on the composite's material-fiber layout, in a generally-distorted (non-rectangular) and curved shell element. However, for the special case of flat plate problems with "regular" meshes, as in the numerical simulations reported later in Sec. 4, a simplified <u>unique</u> transformation matrix can be utilized; i.e.,

$$[T]_\ell = \begin{bmatrix} \cos^2\theta & \sin^2\theta & 2\sin\theta\cos\theta & 0 & 0 \\ \sin^2\theta & \cos^2\theta & -2\sin\theta\cos\theta & 0 & 0 \\ -\sin\theta\cos\theta & \sin\theta\cos\theta & \cos^2\theta - \sin^2\theta & 0 & 0 \\ 0 & 0 & 0 & \cos\theta & \sin\theta \\ 0 & 0 & 0 & -\sin\theta & \cos\theta \end{bmatrix} \qquad (20)$$

where the quantity θ is the angle the material fiber makes with respect to the x-axis, as shown in Fig. 2.

Thus, the stress-strain relation in "global" coordinates for layer ℓ is finally written as

$$\begin{Bmatrix} \sigma_x \\ \sigma_y \\ \tau_{xy} \\ \tau_{yz} \\ \tau_{xz} \end{Bmatrix}_\ell = \begin{bmatrix} \bar{D}_{11} & \bar{D}_{12} & \bar{D}_{13} & 0 & 0 \\ \bar{D}_{21} & \bar{D}_{22} & \bar{D}_{23} & 0 & 0 \\ \bar{D}_{31} & \bar{D}_{32} & \bar{D}_{33} & 0 & 0 \\ 0 & 0 & 0 & \bar{D}_{44} & \bar{D}_{45} \\ 0 & 0 & 0 & \bar{D}_{54} & \bar{D}_{55} \end{bmatrix}_\ell \begin{Bmatrix} \epsilon_x \\ \epsilon_y \\ \gamma_{xy} \\ \gamma_{yz} \\ \gamma_{xz} \end{Bmatrix}_\ell \tag{21}$$

Finally, in order to facilitate the integrations indicated in the above $\underset{\sim}{H}$ and $\underset{\sim}{G}$ matrices, we utilize the following simple "change-of-variable" procedure [41]:

$$t = -1 + \frac{1}{h_c}\left[-h_\ell(1-t_\ell) + 2\sum_{j=1}^{\ell} h_j\right] \tag{22}$$

which yields, upon differentiating with respect to t_ℓ,

$$dt = \frac{h_\ell}{h_c}\, dt_\ell \tag{23}$$

(See Fig. 3 for definitions of the various quantities used in the above expressions). Thus, the matrices H and G now have the forms,

$$\underset{\sim}{H} = \sum_{\ell=1}^{n} \int_{-1}^{1}\int_{-1}^{1}\int_{-1}^{1} \underset{\sim}{P}^T \bar{\underset{\sim}{D}}_\ell \underset{\sim}{P} |\underset{\sim}{J}| \frac{h_\ell}{t_c} dt_\ell dr ds \tag{24a}$$

$$\underset{\sim}{G} = \sum_{\ell=1}^{n} \int_{-1}^{1}\int_{-1}^{1}\int_{-1}^{1} \underset{\sim}{P}^T \bar{\underset{\sim}{D}}_\ell \underset{\sim}{B}^L |\underset{\sim}{J}| \frac{h_\ell}{t_c} dt_\ell dr ds \tag{24b}$$

which are evaluated using standard numerical integration; i.e., two Gauss quadrature points per layer, and the indicated summation is over the total number of layers, n.

4. Numerical Studies

In this section, we present a series of numerical simulations for selected problems taken from various literature sources, to demonstrate the capabilities of the element in representing the static and dynamic behaviors of composite laminates. These problems involve varied boundary conditions, aspect ratios, loading conditions and laminate configurations. For several of these problems, comparisons are made with available "exact" analytical solutions as well as other independent finite element solutions. The quantities of interest are predictions of laminate global response, i.e. deflections, and natural frequencies with corresponding vibration modes, and laminate local responses, namely, bending, in-plane, and transverse shear stresses. For transverse shear stresses in particular, a series of alternative methods are investigated in an attempt to "improve" its accuracy.

In the following results, the elements of Lakshminarayana and Murthy will be conveniently referred to as TRIPLT [47] and those of Spilker as MQH3R [39] and V2R [28]. These particular elements are chosen because they appear to provide accurate results for comparison.

4.1 Static Test Problems: Deflections and Stresses

4.1.1 A Cantilever Beam with In-Plane Point Load

The following problem, taken from Lakshminarayana and Murthy [47], is used to access the element's prediction of the in-plane response of a laminated composite beam; i.e., a slender cantilever beam subjected to an in-plane point load of magnitude P = 1.0 lb (Fig. 4). The material used has E_{11} = 30 x 10^6 psi, E_{22} = 0.75 x 10^6 psi, G_{12} = 0.45 x 10^6 psi, ν_{12} = 0.25. A variety of laminate configurations are used, i.e. 1-, 4-, and 8-layer laminates. Such a

variety of multi-layer laminates will provide for a validation test of the new element subroutines for layer-transformation and integration through-the-thickness schemes. The "exact" solution is based upon that of Lekhnitskii, and the TRIPLT element is used for comparison.

As shown in the results summarized in Table 1, the present element compares quite well with the exact solution in all cases analyzed. In addition, although its "overall" accuracy is comparable to that of TRIPLT, the present element's results is evidently superior in the $\theta = 30$ single-layer case.

4.1.2 A Single Layer Clamped Rectangular Plate Under Uniform Pressure

The problem analyzed here is a single layer rectangular plate subjected to a uniformly distributed pressure load of magnitude q_0. This problem was also taken from Lakshminarayana and Murthy, and even though no "exact" solution is available, it is felt that the TRIPLT element has proven to provide accurate results. This problem is a difficult test for the element due to the combination of plate aspect ratio, boundary conditions, and high material anisotropy. The geometry of the plate has an aspect ratio of 2, and has totally clamped boundary conditions, Fig. 5. The material used has the following properties, $E_{11} = 30 \times 10^6$, $E_{22} = 0.75 \times 10^6$, $G_{12} = 0.45 \times 10^6$, $G_{23} = 0.375 \times 10^6$ $\nu_{12} = 0.25$.

Because of the demanding nature of the problem, a mesh convergence study was performed to assess the elements behavior as a function of mesh size. Due to a lack of material symmetry, the entire plate was modeled. The results for the TRIPLT element were obtained using an 8 x 8 mesh. Recall the TRIPLT element uses 3 nodes with 15 d.o.f. (degrees of freedom) per node, thus giving a total of 1215 d.o.f. for the 8 x 8 mesh. The present element's 10 x 10 mesh

contains 605 d.o.f. As shown in the convergence results in Table 2, for most material fiber angles, convergence is attained at the 8 x 8 mesh with the 10 x 10 mesh giving the best results. Thus, the present element is able to model the problem, accurately using less d.o.f.

Table 3 summarizes the above results for normalized center deflections in a 10 x 10 mesh for the present element and an 8 x 8 mesh for the TRIPLT element.

4.1.3 Two-Layer Clamped and Simply Supported Square Plates Under Uniform Pressure

A square, 2-layer plate subjected to a uniformly distributed pressure ρ_0 is considered here. The plate was analyzed using both simply supported and clamped boundary conditions. Note that the simply supported boundary conditions have, in addition to the transverse displacement, the in-plane displacement normal to the plate edge restrained. The clamped boundary conditions have all d.o.f. restrained along the plate edge. The material properties for the problem are; $E_{11} = 40 \times 10^6$ psi, $E_{22} = 1 \times 10^6$ psi, $G_{12} = 0.5 \times 10^6$ psi, $\nu_{12} = 0.25$.

The results are compared to exact solutions as well as other finite element results using the TRIPLT element, and the MQH3T and V2R thin plate elements of Spilker [38,39]. Both of these latter elements contain 8 nodes with 5 d.o.f. per node. A 6 x 6 mesh of MQH3T elements is used for the clamped plate (665 d.o.f.) and a 4 x 4 mesh of V2R elements is used in the simply supported plate (325 d.o.f.). The TRIPLT element utilized a 6 x 6 mesh (735 d.o.f.). The present element used a 10 x 10 mesh for both cases (605 d.o.f.). Again, due to a lack of material symmetry, the entire plate was modeled, and

the results are summarized in Tables 4 and 5. Clearly, the present element agrees well in both cases with the exact solutions.

In addition to displacements, bending moments M_{xx} and M_{yy} were calculated for the simply supported plate, and are given in Tables 6 and 7.

4.1.4 Cylindrical Bending of Symmetric Laminates Under Sinusoidal Pressure

In the present example, the cylindrical bending of a symmetric laminate is considered. The problem is a simply supported plate subjected to a sinusoidal pressure load of maximum intensity q_0. The material properties are; $E_{11} = 25 \times 10^6$ psi, $E_{22} = 1 \times 10^6$ psi, $G_{12} = 0.5 \times 10^6$ psi, $G_{23} = 0.2 \times 10^6$ psi, $\nu_{12} = 0.25$.

Exact solutions for this specific problem have been obtained by Pagano [56,57], providing detailed stress distributions, in addition to deflections. Thus, this example will provide a means of determining the present elements prediction of laminate local behavior; in particular, transverse shear stresses, which will be discussed in the next section in some detail.

Figures 6 and 7 show deflections, $\bar{w}$, as predicted by the present element and compared to the exact solutions, where

$$\bar{w} = \frac{100E_{22}h^3}{q_0 l^4} w$$

Figures 8 and 9 show the predicted through-the-thickness, (T-T-T) distribution for in-plane stress, σ_x, which matches that of Classical Plate Theory (CPT) quite well, as expected.

4.2 Treatment of Transverse Shear Stress

As mentioned previously, one of the desirable features of any composite element is its ability to accurately predict the "detailed" stress distribution within the composite. However, in this regard, one of the obvious limitations of the element presented here is the assumption of constant transverse shear strain through-the-thickness (see Fig. 10 with the same problem as described in Section 4.1.4 being considered here). The resulting transverse shear stress, if directly obtained from the constitutive relations, are discontinuous through-the-thickness, and as Fig. 11 shows, will be grossly in error. Thus, some consistent means needs to be established to allow more accurate transverse shear stress distributions through-the-thickness. Again, it was still desired to avoid any modifications to the element's basic formulation itself. Thus some form of "post-processing" of the transverse shear stresses was attempted while still keeping the "computationally-efficient" global scheme of utilizing constant through-the-thickness and layer-number independent distributions for transverse shear strains. To this end, several approaches are described next.

4.2.1 Approach 1: Modified Shear Stress Distribution

The first approach involves the simple redistribution of the transverse shear strain into a parabolic form through-the-thickness. This type of assumption is believed to be more reasonable in that the conditions of zero shear strain at the top and bottom surfaces are automatically satisfied. The value of the constant shear strain obtained directly from the finite element results γ_{ave}, is redistributed parabolically, i.e.

$$\gamma_{max} = \frac{3}{2}\,\gamma_{ave} \quad ; \quad \gamma(z) = \gamma_{max}\left[1 + 4\left[\frac{z}{h}\right]^2\right] \tag{25}$$

The corresponding transverse shear stress is then computed using "layer" constitutive equations,

$$\{\tau\}_k = [D]_k \{\gamma\}_k \tag{26}$$

where the subscript k corresponds to layer k.

As shown in Fig. 12, using this method does produce more accurate transverse shear stress distributions, yet the stresses remain discontinuous at the layer interfaces. Note, however, that the magnitudes of the shear stress are closer to the exact values. It may also be noted that this type of distribution is similar to that of a higher-order theory presented by Reddy [34].

4.2.2 Approach 2: Equilibrium-Based Method

In the alternative method investigated here, an attempt is made to eliminate the transverse shear stress discontinuities noted previously at the layer interfaces. In particular, the methodology outlined by Chanduri and Seide [58,59] was chosen. In this approach, "layerwise" equilibrium and stress continuity conditions are imposed. One problem arises, however, in choosing the values of average layer shear stress, $\bar{\tau}_k$. Note that the exact methodology as given in [58,59] cannot be applied here to achieve the same good results due to the rather significant differences between the elements utilized. As discussed previously, the element of Seide's, for which this method was developed, is a layer-dependent element of the displacement type, i.e. the total degrees of freedom are layer-dependent quantities. In contrast, the mixed element presented here, has in effect, only one "layer" to model the entire laminate thickness.

Initially, the average shear stress values used were those obtained directly from the finite element analysis (refer to Fig. 11). The transverse shear stress distribution as compared to the exact 3-D solution is shown in Fig. 13. The shear stresses in the middle 90-layer are grossly underestimated and the stresses in the outer two layers (both 0) are overestimated. Obviously, no improvement has been attained. Thus, two additional cases using different values for the average layer shear stress $\bar{\tau}_k$ were investigated. In one case, the average layer transverse shear stresses were calculated by taking the average distribution as predicted by the previous Approach 1; see Fig. 12. Using these values for $\bar{\tau}_k$, produced the distribution shown in Fig. 14, where we note that the shear stress values in the middle layer are still underestimated. In the second case, the value of $\bar{\tau}_k$ was taken to be the value of the average shear stresses at the interface of any two adjacent layers, and the resulting distribution is shown in Fig. 15. The persistent problem of the poor stress prediction in the middle layer remains. But it should be noted that at the layer interfaces the value of the shear stresses match those of the exact solution rather well.

4.2.3 Approach 3: Simplified Strength-of-Materials Concept

Finally, the third approach investigated is based upon a basic strength of materials concept, specifically, the transformation of the various layers to "equivalent" cross sectional areas depending on their elastic moduli. This is a method used frequently in the design of heterogeneous materials (e.g., reinforced concrete). The layer cross-sectional areas are modified by using the following "modular" ratio, n,

$$n = \frac{E_k}{E_o} \tag{27}$$

where E_o is the selected "reference" elastic modulus and E_k is the elastic modulus for layer k. Thus the equivalent cross-sectional area is simply,

$$A_k' = nA_k \tag{28}$$

Once the cross section of the laminate is transformed into an equivalent section, the transverse shear stress distribution is then calculated by the following formula,

$$\tau(z) = \frac{VQ}{It} \tag{29}$$

where V is the total shear force acting on the cross section; Q the statical moment of cross-section about the neutral axis; I the moment of inertia of the transformed cross-section; and t the width of the layer at a point z.

The calculation of the total shear force V, per unit length, is obtained from the transverse shear stress distribution obtained directly from the finite element solution (Fig. 11), i.e.,

$$V = \sum_{k=1}^{n} \tau_k h_k \tag{30}$$

The results of this method are shown in Fig. 16, and clearly illustrate the excellent stress distribution obtained. The quality is far better than

either of Approaches 1 or 2. Of course, the major limitation to this approach is the fact that the expression for transverse shear is based upon a linear distribution of stress, thus linear material behavior is necessary. Since the immediate goal is to extend the current element formulation to non-linear composite material behavior, this type of approach will need to be modified.

4.2.4 Additional Remarks on Alternative Approaches for Transverse Shear Stress Computations

Approaches 1 and 2 above produced rather "mixed" results. Approach 1 is still attractive from the standpoint that the assumptions made for the current linear analysis are still applicable to non-linear analysis. But, as mentioned, the drawback is the stress discontinuities at the layer interfaces. Concerning Approach 2, a point of difficulty is in the determination of the values for $\bar{\tau}_k$. A somewhat "ad hoc" procedure was used and such a methodology is not desirable.

With regards to Approach 3, it is certainly appealing in view of its extreme simplicity. Some initial thoughts have already been given for the extension to non-linear analysis, and it appears that some workable extension is possible. In this, the restrictive condition of linear through-the-thickness distributions of in-plane normal stresses will be replaced by a modified "piecewise-linear" assumption for each layer, and the "local" form of equilibrium conditions are imposed to derive the applicable formula for transverse shear stress distribution. Whether or not this approach will work as well and provide as accurate results in the non-linear regime as it did for the linear case, remains to be seen. Some additional numerical studies in the linear, as

well as the non-linear cases will need to be conducted. And this is a part of our planned future research work.

The difficulties associated with accurate distributions of transverse shear stresses serve to show the inherent limitations of the "smeared" composite element approach. The accurate distributions obtained by other composite elements are at the expense of using rather computationally-expensive formulations. Very detailed distributions are simply not possible using the type of elements as the one presented here. But again, one must question how crucial is it that the element be capable of detailed "local" quantities in addition to accurate "global" quantities, such as displacements, vibration frequencies, etc. It is our view that such detailed "local" responses will always necessitate very refined, and also complicated, formulations that can best be used only for critical parts of the laminated structure determined on the basis of a less-expensive "overall" analysis of the "global" response.

4.3 Test Problems for Dynamic Analysis

As described in [27], a feature of the element presented here is that the element is defined by five nodes, four of which are defined externally and the fifth node being generated internally. The fifth node's degrees-of-freedom are then condensed out of the element stiffness matrix before assembly into the global stiffness matrix. It is this feature which presents some difficulty when dealing with the mass matrix for dynamic analysis. This point can be made more clear by looking at the eigenvalue problem being solved. That is, the associated eigenvalue problem can be expressed as,

$$(\underset{\sim}{K} - \lambda \underset{\sim}{M})\ \{\underset{\sim}{d}\} = 0 \qquad (31)$$

where $\underline{K}$ and $\underline{M}$ have dimensions 25 x 25. In matrix form,

$$\left[\begin{bmatrix} \underline{K}_{11} & \underline{K}_{12} \\ \underline{K}_{21} & \underline{K}_{22} \end{bmatrix} - \lambda \begin{bmatrix} \underline{M}_{11} & \underline{M}_{12} \\ \underline{M}_{12} & \underline{M}_{22} \end{bmatrix}\right] \begin{Bmatrix} \underline{d}_c \\ \underline{d}_m \end{Bmatrix} = 0 \tag{32}$$

For the case of lumped mass, which is being considered here, $\underline{M}_{12}$ and $\underline{M}_{21}$ are zero. Thus, the eigenvalue problem is reduced to,

$$\left[\begin{bmatrix} \underline{K}_{11} & \underline{K}_{12} \\ \underline{K}_{21} & \underline{K}_{22} \end{bmatrix} - \lambda \begin{bmatrix} \underline{M}_{11} & 0 \\ 0 & \underline{M}_{22} \end{bmatrix}\right] \begin{Bmatrix} \underline{d}_c \\ \underline{d}_m \end{Bmatrix} = 0 \tag{33a}$$

Using simple algebra and solving for middle node degree-of-freedom, d_m, we have,

$$\underline{d}_m = - (\underline{K}_{22} - \lambda \underline{M}_{22})^{-1} \underline{K}_{12}^T \underline{d}_c \tag{33b}$$

and the corner node degrees-of-freedom, $\underline{d}_c$, are

$$(\underline{K}_{11} - \lambda \underline{M}_{11})\underline{d}_c + \underline{K}_{12}\underline{d}_m = 0 \tag{33c}$$

Substituting the expression for $\underline{d}_m$ into the above, we have,

$$(\underline{K}_{11} - \lambda \underline{M}_{11})\underline{d}_c + \underline{K}_{12}(-(\underline{K}_{22} - \lambda \underline{M}_{22})^{-1} \underline{K}_{12}^T \underline{d}_c) = 0 \tag{33d}$$

As is evident in the above expression, the equation is coupled containing both known, stiffness and mass, terms, and unknown, λ, quantities. Particularly the term $(\underline{K}_{22} - \lambda \underline{M}_{22})^{-1}$ presents computational difficulties as discussed by Kidder [60]. Ordinarily, some iterative process would be required to solve

the above. Most of the literature dealing with condensation in general, [61-63], has been applied to the *global* mass and stiffness matrices. That is, the focus has been in reducing extra structural degrees-of-freedom through the use of condensation techniques. Thus, iterative methods are acceptable on the global mass and stiffness matrices. But in the present case, the condensation is required on the element level. Thus, the above methods would have to be applied to *each* element which would be computationally expensive.

With the above discussion in mind, a suitable alternative to condensation is desired. One such alternative is by neglecting the middle node entirely, thereby eliminating the need for any form of condensation. Specifically, the lumped mass matrix $\underset{\sim}{M}$, as defined in Eq. 12 of Sec. 3.2, is constructed using shape functions, $\underset{\sim}{\bar{N}}$ which are based upon four boundary nodes only. By using the four-node shape functions, the mass will be "lumped" at the corner nodes only. It is believed that this approach is justifiable for the following reason. The middle node's additional displacement is very small relative to an "average" displacement interpolated from the four corner nodes. Thus by using a sufficiently fine mesh, the contribution of the middle node becomes of less importance. Therefore, the current assumption is that neglecting the middle node may not lead to significant errors in frequencies. In the remainder of this section, a series of numerical problems are investigated to determine the validity of the approach outlined above. Since this is the first implementation of the dynamic analysis capability for the element, both isotropic and anisotropic applications are required to test the new subroutines for dynamic analysis.

4.3.1 Isotropic Material Applications

4.3.1.1 Isotropic Cantilevered Plate

This first example of an isotropic cantilevered plate is chosen to provide a method of determining how significant neglecting the middle node is over range of frequencies. This particular problem, found in reference [65], provides both numerical and test results for the first twelve frequencies of vibration. In the analysis performed here, mesh sizes that range from 4x4 to 10x10, for the entire plate, are used to study the effect of mesh refinement on the convergence of the first six frequencies.

As Table 8 shows, reasonable results are obtained for the first two frequencies for all mesh sizes considered, (i.e. the error is within 8% for ω_2). When considering the higher modes, as shown, additional mesh refinement is necessary in order to produce reasonable results, (i.e. error within 7% for ω_6). Thus it appears that for the first six frequencies, the element gives accurate results.

4.3.2 Composite Material Applications

In this section, a series of composite structures are examined with the specific examples chosen to study the effects of fiber orientation, number of layers, aspect ratio, and boundary conditions on the frequency response. In most cases, due to the lack of "exact" solutions, comparisons are made to other finite element results. Specifically, comparisons are made to the displacement-based elements of Oden [24], Owen [64], and Reddy [43,51]. In all of the following examples, one quarter of the plate is modeled using a 6x6 mesh.

4.3.2.1 Anisotropic Cantilever Beam

A simple cantilevered beam which has a single layer with varying fiber orientations is considered here. The reference "solution" is that provided by Oden et.al. [24]. The material properties used are those which are said to represent cubic synonymy that simulates the single crystal structure of nickel alloy found in turbine blades [24]. Thus in this case, the fiber angle is actually the preferred direction of the single crystal material and is allowed to vary from 0 to 90, Fig. 17. Specifically, the material properties are $E_{11}=E_{22}=1.9716 \times 10^6$psi, $G_{12}=5.4758 \times 10^6$psi, $\nu_{12}=0.2875$, and $\rho=0.25$. In the analysis of Oden, both linear and quadratic two-dimensional elements are used. Namely, the analysis uses a mesh of 2x40 linear elements (I) or a mesh of 1x10 quadratic elements (II).

Tables 9 and 10 show the results of our analysis as compared to that of Oden et.al. for the first two frequencies. It should be noted that the element mesh used for this analysis was constructed so that the vibration displacement is out-of-plane of the element as compared to Oden where the displacement is in-plane. Thus, a "simpler" mesh of 1x20 elements is used. As a matter of fact, a mesh of only 1x10 elements gave satisfactory results, but a slightly finer mesh is used so that plots of the corresponding mode shapes will be more accurate. Fig. 18 shows the mode shapes corresponding to the first two frequencies of vibration for a crystal direction $\Theta = 0^o$. The mode shapes compare well to those given in [24].

4.3.2.2 Four Layer Symmetric and Anti-Symmetric Square Plates

This example is that taken from Reddy [51]. Two different laminate configurations are considered: 1) a [45/-45/-45/45] symmetric laminate, 2) a

[45/-45/45/-45] anti-symmetric laminate. Both simply supported and clamped boundary conditions are used as described in [51]. Two different materials are considered: Material I: E_{11}=25 x 10^6psi, E_{22}=1 x 10^6psi, G_{12}=0.5 x 10^6psi, G_{23}=0.2 x 10^6psi, ν_{12}=0.25. Material II: E_{11}=25 x 10^6psi, E_{22}=1 x 10^6psi, G_{12}=0.5 x 10^6psi, G_{23}=0.2 x 10^6psi, ν_{12}=0.25, with ρ=1 for both material types.

Fig. 19 shows the comparison of the present element with that of Reddy's and with closed-form solutions where noted. As is shown, the present element shows good agreement in all cases. It even shows better accuracy than Reddy, when compared to the closed-form solution for the simply supported material II case.

4.3.2.3 Simply Supported Square Laminated Plates with Varying Number of Layers

The present example is chosen to demonstrate the effect of thickness and the number of layers on the fundamental frequency. A number of cases were investigated, namely; two, three, and eight-layer anti-symmetric laminates. In all cases, layers of the same fiber orientation have the same thickness while the total laminate thickness remains constant. The plates have simply supported boundary conditions, that is, in-plane displacements are fixed in the tangential direction and symmetry boundary conditions enforced since only one quarter of the plate is modeled. Again, a 6x6 mesh is used in the present analysis. The material properties are the same as those described as Material II in section 4.3.2.1. Fig. 20 shows the results for the three-layer [0/90/0] laminate, where comparison is made to both the finite element solutions of Owen [64] and classical plate theory, CPT.

As shown, for large laminate thickness, the difference between CPT and the finite element solutions is significant, and therefore, CPT is inaccurate for thick to moderately thick laminates. Again, the pronounced difference between the CPT and finite element solutions is noted. In both figures, the present element agrees well with the results of Owen. Unfortunately for comparison purposes, Owen makes no mention of the mesh size used in the analysis. But relatively speaking, these simple problems serve to demonstrate the present element's ability to produce accurate results.

4.3.3 Additional Remarks

Considering the results presented above, it appears that the current assumption for forming the element mass may be acceptable. Of course, no firm conclusions can be made at this time because of the limited, and somewhat simplistic numerical studies performed thus far, that is, only simple beam and flat plate structures are considered. The problems of the above type have predominantly translatory mass effects. The rotary inertia terms have yet to be examined. Thus, additional studies, in which curved shell geometries are modeled, need to be investigated.

5. Final Conclusions

In this part of the report, the formulation and numerical performance of the mixed element as extended to laminated composite applications is presented with both linear static and dynamic analysis capabilities demonstrated. Even though some aspects of the element require further investigation, as outlined in Sec. 4.2.4 and 4.3.3, a certain degree of confidence is developed consider-

ing the encouraging numerical results obtained in this report. The immediate goals of the current research are as follows.

The extension to shell problems is the next immediate objective. At the present, the only extensions that are foreseen in order to make the element applicable to shell problems is the generalization of the transformation matrix. That is, a full three-dimensional transformation matrix will need to be used. Such a transformation matrix already exists in in the computer code utilized (NFAP), thus making the extension straight-forward. Additional test problems of shell type applications will be made.

Some thought has been given to possible refinements for the shear correction factor κ. As is consistent with the Reissner-Mindlin type of elements, a shear correction factor, κ, is chosen to account for shear deformation. It should be noted that the value of the shear correction factor currently used is 5/6 and is typically used for isotropic cases. It may be more appropriate to select a value for κ which depends on the laminate configuration being analyzed. A methodology for this as presented by Whitney [54] and Noor [55] has also recently proposed a method of an *a posteriori* correction of the κ values. Whether or not such modifications are necessary remains to be seen.

And finally, the extension to non-linear material behavior will be the primary focus of the research. Modifications to the element formulation to account for this type of analysis will be made. Part IV of this report will outline this aspect in more detail. In general, it is believed a firm basis is established in which future research may build upon.

PART III: COMPUTER IMPLEMENTATION AND NUMERICAL METHODS FOR VISCOPLASTIC ANALYSIS

1. Introduction

As a part of the NASA Lewis' research and development efforts for viable design of composite structures at elevated temperatures, a study was initiated to investigate efficient computational methods for the inelastic analysis of structural components subjected to thermal/mechanical cyclings. Our study is focused on large-scale computation via finite element method and heurestic numerical integration schemes for handling stiff and strongly nonlinear differential equations associated with the constitutive modeling of high-temperature composites.

It is generally known that the rate-dependent inelastic behavior (i.e. both plastic and creep responses) of composites can be better represented by a unified approach in the form of viscoplasticity theory. In this theory, the constitutive relations of composites are described by evolutionary equations which contain certain types of internal variables to model the deformation features such as inelastic strains, cyclic strain hardening or softening, and thermal ratcheting phenomenon, etc. However, the associated constitutive equations are known to have "stiff" regimes which present considerable numerical difficulty in structural analysis [66]. For example, the differential equations, when integrated numerically, are very sensitive to the time steps employed. If large time steps are used in the analysis, it may result in numerical instability or inaccurate solutions [11,13,14]. If on the other hand, small time steps are imposed, the computational cost required for an analysis may become prohibitively high. In view of these considerations, a reliable

and efficient numerical algorithm is essential for conducting practical viscoplastic analysis.

In viscoplastic analysis of structural problems via finite element method, two levels of numerical calculations are involved: namely the structural and material (or local) levels. On the structural level, global equilibrium is enforced by using either a constant stiffness [11,13,14,67] or tangent stiffness approach [68-70]. On the material level, both the explicit [11,13, 14,66,67,70] and implicit [11,69-75] integration schemes have been used to evaluate the viscoplastic rate equations. In addition, automatic time stepping in conjunction with some sort of error control may also be employed [13,14,66, 77,78]. More recently, a uniformly-valid implicit scheme proposed by Walker [12,72] appears to offer great promise for obtaining stable and reliable results in finite element analysis.

In our first year research effort, we have conducted a numerical study on various integration schemes for viscoplastic materials subjected to monotonic as well as cyclic mechanical loadings. For this purpose, four different material models were implemented into a nonlinear finite element program NFAP [18]. These include: Walker's model [2,19], Robinson's model for isotropic materials [80], Robinson's model for transversely isotropic materials [4], and Bodner's model [81]. In addition, several numerical integration schemes have also been implemented into NFAP for the intended study. These include: explicit Euler forward method, explicit and implicit trapezoidal rule with or with out iterations, an automatic time-stepping based on the Runga-Kutta operators. Three numerical examples are included to demonstrate the effectiveness of the integration schemes considered.

2. Constitutive Models

Within the framework of unified viscoplastic constitutive theories, various mathematical forms have been proposed for specific applications. In this section, we shall focus our attention to five particular models which appear to be the likely candidates for the constitutive modeling of high temperature composites. These are: Walker's model, Robinson's model for isotropic and transversely isotropic materials, Bodner's model and Freed's model. Before the outline of the aforementioned models, a brief description on the general form of the state-variable based viscoplastic equations is given below.

General Form

By limiting the scope of the present study to small deformation theory, the stress rate $\dot{\underset{\sim}{\sigma}}$ in a viscoplastic material is related to its elastic strain rate through

$$\dot{\underset{\sim}{\sigma}} = \underset{\sim}{D}(\dot{\underset{\sim}{\epsilon}} - \dot{\underset{\sim}{\epsilon}}^{I}) \tag{1}$$

where $\dot{\underset{\sim}{\sigma}}$ = stress rate

$\dot{\underset{\sim}{\epsilon}}$ = total strain rate

$\dot{\underset{\sim}{\epsilon}}^{I}$ = inelastic strain rate

$\underset{\sim}{D}$ = elastic material stiffness matrix

The inelastic strain rates are assumed to be functions of effective stresses in the form

$$\dot{\underset{\sim}{\epsilon}}^{I} = \underset{\sim}{f}\left[\frac{\underset{\sim}{\sigma} - \underset{\sim}{\alpha}}{\kappa}\right] \tag{2}$$

with the evolutional laws

$$\dot{\underline{\alpha}} = \underline{h}^{\alpha}\ \dot{\underline{\epsilon}}^{I} - \underline{\gamma}_{\alpha}$$

$$\dot{\kappa} = \underline{h}_{k}\ |\dot{\underline{\epsilon}}^{I}| - \gamma_{k} \tag{3}$$

where $\underline{\sigma}$ = vector of stresses

$\underline{\alpha}$ = vector of back stresses

κ = drag stress

$(\dot{})$ = time derivative of the quantity in question

and $\underline{h}_{\alpha}$, $\underline{h}_{k}$ and $\underline{\gamma}_{\alpha}$, γ_{k} are the work-hardening and recovery functions, respectively.

Within the framework of the above structure, a wide variety of viscoplastic models have been proposed. In the following, we shall list five models for our intended studies.

a. Walker's Model [79]

The first deviatoric invariant is defined by

$$I = \left[\frac{2}{3}\left[\frac{3}{2}S_{ij} - \alpha_{ij}\right]\left[\frac{3}{2}S_{ij} - \alpha_{ij}\right]\right]^{1/2} \tag{4}$$

with

$$\dot{R} = \left[\frac{2}{3}\dot{\epsilon}^{I}_{ij}\ \dot{\epsilon}^{I}_{ij}\right]^{1/2} \tag{5}$$

$$S_{ij} = \sigma_{ij} - \frac{1}{3}\delta_{ij}\sigma_{kk} \tag{6}$$

The inelastic strain rate is given by

$$\dot{\epsilon}^{I}_{ij} = \left[\frac{I}{K}\right]^{n}\frac{(\frac{3}{2}S_{ij} - \alpha_{ij})}{I} \tag{7}$$

The evolution equation for the back stress rate is

$$\dot{\alpha}_{ij} = (n_1+n_2)\dot{\epsilon}^I_{ij} - (\alpha_{ij} - \alpha^0_{ij} - n_1\epsilon^I_{ij})\left[(n_3+n_4e^{-n_5\dot{R}})\dot{R}+n_6(\frac{2}{3}\alpha_{kl}\alpha_{kl})^{\frac{m-1}{2}}\right] \quad (8)$$

and the drag stress rate is given by

$$\dot{K} = n_7K_2e^{-n_7\dot{R}}\dot{R} \quad (9)$$

All the material constants, i.e. $n, m, n_1, n_2, n_3, n_4, n_5, n_6, n_7, \alpha_0, K$, and K_2 may be temperature-dependent. K is the initial value of the drag stress and σ_o indicates the amount by which the stress-strain curve is rigidly shifted along the stress axis.

b. Robinson's Model for Isotropic Materials [80]

First, we define

$$x = \frac{S_{ij}(S_{ij} - \alpha_{ij})}{W_1} \quad (10)$$

$$x^* = \frac{S_{ij}\alpha_{ij}}{W_2} \quad (11)$$

$$\bar{\gamma} = \gamma e^{[(-23.8T+2635)(\frac{1}{811} - \frac{1}{T})]} \quad (12)$$

$$\bar{R} = Re^{[40000(\frac{1}{811} - \frac{1}{T})]} \quad (13)$$

$$J_2 = \frac{1}{2}[S_{ij} - \alpha_{ij}][S_{ij} - \alpha_{ij}] \quad (14)$$

The inelastic strain rate is given by

$$\dot{\epsilon}^{I}_{ij} = P(x)\frac{1}{2\bar{r}}\left[\frac{J_2}{k^2} - 1\right]^n \frac{S_{ij} - a_{ij}}{(J_2)^{1/2}} \tag{15}$$

With the evolution equations being

$$\dot{a}_{ij} = \frac{2rH}{G\beta}\dot{\epsilon}^{I}_{ij} = -\frac{RG^{m-\beta a_{ij}}}{[\frac{1}{2}a_{ij}a_{ij}]^{1/2}} \tag{16}$$

where:

$$G = (G'' - G^o)P(x^*) + G^o$$

$$G'' = \begin{cases} G & \text{for } G > 2G^o \\ \frac{G^2}{4G^o} & \text{for } G < 2G^o \end{cases} \tag{17}$$

$$P(x) = \begin{cases} 0 & \text{if } x < -1 \\ \frac{(1-x)^2}{2} & \text{if } -1 \le x \le 0 \\ 1 - \frac{(1+x)^2}{2} & \text{if } 0 \le x \le 1 \\ 1 & \text{if } x > 1 \end{cases}$$

c. Robinson's Model for Transversely Isotropic Materials [4]

Assuming the existence of a potential function:

$$\Omega = \Omega(F,G) \tag{18}$$

and that for small deformation the orientation direction of transverse plane stays the same, the two yield surfaces are defined by:

$$F = \frac{1}{K^2}\left[I_1 + \frac{1}{\eta^2} I_2 + \frac{9}{4(4\omega^2+1)} I_3\right] - 1$$

$$G = \frac{1}{K^2}\left[I_1' + \frac{1}{\eta^2} I_2' + \frac{9}{4(4\omega^2+1)} I_3'\right] \tag{19}$$

Let

$$f(F) = \frac{\partial \Omega}{\partial F} \text{ and } \frac{\gamma(G)}{h(G)} = \frac{\partial \Omega}{\partial G} \tag{20}$$

The flow law is defined by

$$\dot{\epsilon}_{ij}^{I} = f(F)\Gamma_{ij} \tag{21}$$

and the evolution law by

$$\dot{\alpha}_{ij} = h(G)\dot{\epsilon}_{ij} - \gamma(G)II_{ij} \tag{22}$$

where Γ_{ij} are functions of the effective stress tensor Σ_{ij} and the fiber director d_i

$$\Gamma_{ij} = \Gamma_{ij}(\Sigma_{ij}, d_i d_j)$$

and II_{ij} are given by

$$II_{ij} = II_{ij}(\alpha_{ij}, d_i d_j) \tag{23}$$

with

$$\Sigma_{ij} = S_{ij} - \alpha_{ij}$$

d. Bodner's Model [81]

The inelastic strain rate has the form

$$d\dot{\epsilon}_{ij}^{I} = \mu S_{ij} \tag{24}$$

with

$$\mu^2 = D_2^I J_2 \tag{25}$$

where

$$D_2^I = D_0^2 e^{\frac{-Z^2(n+1)}{n(3J_2)^n}}$$

$$J_2 = \frac{1}{2} S_{ij} S_{ij}$$

$$Z = Z_1 - (Z_1 - Z_o) e^{-m' W_I}$$

$$m' = m_o + m_1 e^{-a W_I} \tag{26}$$

$$Z = f(W_I^o + dW_I) - f(W_I^o)$$

where

$$dW_I = S_{ij} d\epsilon_{ij}^I$$

e. Freed's Model [82,83]

A viscoplastic model based on thermodynamic considerations was recently proposed by Freed and the model has been characterized for polycrystalline metals such as aluminum, copper, nickel and tungsten. In this model the constitutive relations are

$$\underline{S} = 2\mu(\underline{e} - \underline{\epsilon}^I)$$

$$tr(\underline{\sigma}) = 3K[tr(\underline{\epsilon}) - 3\alpha(T - T\omega)] \tag{27}$$

$$\Delta \underline{B} = 2H \beta \Delta t$$

$$\Delta D = h \delta \Delta t$$

where $\underline{S}$ = deviatoric stress vector

$\underline{e}$ = deviatoric strain vector

$\underline{\epsilon}^I$ = inelastic strain vector

μ = shear modulus

κ = bulk modulus

$\underline{B}$ = back stress vector

D = drag stress

H = hardening coefficient

The evolution equations are

$$\dot{\underline{\epsilon}}^I = \Theta Z \cdot \frac{\underline{\Sigma}}{\| \underline{\Sigma} \|}$$

$$\dot{\beta} = \dot{\underline{\epsilon}}^I - \frac{\underline{B}}{L} \| \dot{\underline{\epsilon}}^I \| - \Theta R \frac{\underline{B}}{\| \underline{B} \|} \tag{28}$$

$$\dot{\delta} = \| \dot{\underline{\epsilon}}^I \| - \frac{D}{\ell} \| \dot{\underline{\epsilon}}^I \| - \Theta r$$

with a constraint equation for ℓ or r

$$\frac{D}{\ell} \geq 1 - \frac{r}{z} - 2 \left[\frac{LZ \| \underline{\Sigma} \| + Z \| \underline{B} \|^2 + LR \| \underline{B} \|}{D L Z} \right] \tag{29}$$

The functional form of thermal diffusivity is adopted after Miller

$$\Theta = \begin{cases} \exp(-\frac{Q}{kT}) & ; T \geq T_t \\ \exp\left[-\frac{Q}{kT_t} (\ell n \frac{T_t}{T} + 1) \right] & ; T \leq T_t \end{cases} \tag{30}$$

where Q = activation energy for self diffusion

T_t = a transition temperature

k = Boltzmann constant

and Z is a Zener-Hollomon parameter and has the expression

$$Z = A \sinh^n \left[\frac{\| \underset{\sim}{\Sigma} \|}{D} \right] \tag{31}$$

where $\underset{\sim}{\Sigma}$ = vector of effective stress

$= \underset{\sim}{S} - \underset{\sim}{B}$

At steady state, Z assumes the value

$$Z_{ss} = A \sinh^n \left[\frac{\| \underset{\sim}{S} \|}{C} \right] \tag{32}$$

and A, C and n are the Garofalo creep constants.

The limiting functions of dynamic recovery are

$$L = \eta D$$

$$\ell = D_a + (D_u - D_a) \exp \left[-3(L - \|\underset{\sim}{B}\|)\right] \tag{33}$$

Where D_a, D_u, and η are material constants such that $0 < D_a \leq D_u < C$.

Further, the thermal recovery functions are given by

$$R = A\left[1 - \frac{\|\underset{\sim}{B}\|}{L}\right] \sinh^n\left[\frac{\|\underset{\sim}{B}\|}{C-D}\right]$$

$$r = A\left[1 - \frac{D}{Z}\right] \sinh^n\left[\frac{\|\underset{\sim}{B}\|}{C-D}\right] \tag{34}$$

It is noted that all the above models, except the last one, have already been implemented into NFAP. Freed's model is currently being implemented for future studies.

3. Finite Element Equations

For finite element analysis, we follow the conventional incremental approach in conjunction with an initial strain method for the treatment of viscoplastic effects. In this approach, numerical calculations are segregated into two levels, namely, structural and local levels. On the structural level, the targeted solution time is divided into a sequence of (global) increments and the incremental structural equilibrium equations are solved for each time step in succession. On the local level at a material point, the constitutive rate equations are integrated by a subincrementing technique so that an incremental form is obtained. With this connection, the stress rate is related to the elastic strain rate by Eq. (1). For finite element analysis, it is more expedient to transform Eq. (1) into an incremental form for a typical time step $t' \epsilon [t, t + \Delta t]$ by writing

$$\Delta \underset{\sim}{\sigma} = \underset{\sim}{D}(\Delta \underset{\sim}{\epsilon} - \Delta \underset{\sim}{\epsilon}^I) \tag{35}$$

where the vector of incremental stresses

$$\Delta\underline{\sigma} = \int_t^{t+\Delta t} \dot{\underline{\sigma}}\, dt \tag{36}$$

Similar expressions can be written for $\Delta\underline{\epsilon}$ and $\Delta\underline{\epsilon}^I$. Of course, efficient integration of Eqs. (1)-(3) to obtain Eq. (35) is the main objective which will be discussed in the next section.

Once the constitutive equations are defined according to Eq. (35), the incremental equilibrium equations for a typical displacement-based finite element are

$$\underline{K}\Delta\underline{q} = \Delta\underline{R} + \Delta\underline{J} \tag{37}$$

in which $\underline{K}$ = the element stiffness matrix, $\Delta\underline{q}$ = the vector of incremental nodal displacements, ΔR = the vector of incremental applied forces, and $\Delta\underline{J}$ = the vector of incremental forces due to viscoplastic deformations, which has the expression

$$\Delta\underline{J} = \int_V \underline{B}^T\underline{D}\,(\Delta\underline{\epsilon}^I)\, dv \tag{38}$$

where $\underline{B}$ = the strain-displacement transformation matrix.

In the above equation, the viscoplastic effect is treated as an equivalent (pseudo) nodal force vector appearing on the right hand side of the equilibrium equations. Since determination of $\Delta\underline{J}$ requires the knowledge of current state, equilibrium is approximated and is then achieved through an iterative process. For discussion purposes, we consider a solution step between (t_n, and $t_n + \Delta t$). The equilibrium equations can be written as

At the beginning of the step:

$$\underline{K}\Delta\underline{q}^{o} = \Delta\underline{R}^{o} \tag{39}$$

For the i-th iteration cycle:

$$\underline{K}\Delta\underline{q}^{i} = \Delta\underline{R}^{i} + \Delta\underline{J}^{i}; \quad i = 1,2,... \tag{40}$$

$$\Delta\underline{J}^{i} = \int_{V} \underline{B}^{T}\underline{D}\ (\Delta\underline{\epsilon}^{I})^{i-1}dv \tag{41}$$

As shown in Eq. (9) an elastic solution, and hence the strain increment, is estimated at the beginning of the global time step. Based on this strain increment, the stresses, and the state variables, one can calculate the inelastic strain increment using a subincrementing procedure to be discussed later. Once the inelastic strain increment is obtained, the incremental pseudo force $\Delta\underline{J}$ in Eq. (41) can be evaluated.

At this point, it is important to note that the success of equilibrium iterations depends upon how accurate the pseudo force $\Delta\underline{J}$ or the inelastic strain increment is calculated. Due to the "stiff" phenomenon of viscoplastic rate equations, the solution accuracy of $\Delta\underline{\epsilon}^{I}$ is highly sensitive to the values of state variables evaluated at material sampling (or integration) points. Therefore, from the numerical standpoint, a subincrementing scheme is usually necessary at each integration point. If, on the other hand, the localized inelastic strains are calculated incorrectly, structural equilibrium can not be maintained in Eq. (40).

4. Numerical Integration of Constitutive Rate Equations

In this section, we present the numerical techniques for integration of the constitutive rate equations which are essential for the finite element analysis. For discussion purpose, the constitutive rate equations are replaced by the following expression

$$\dot{\underline{y}} = \underline{f}\ (\underline{y} \cdot t) \tag{42}$$

The above equation represents a system of nonlinear, first-order ordinary differential equations. For a multi-axial stress state, the vector $\underline{y}$ consists of 19 components; six Cauchy stresses $\underline{\sigma}$, six back stresses $\underline{\alpha}$, six inelastic strains $\underline{\epsilon}^I$ and one drag stress k.

Although several numerical schemes can be used to integrate Eq. (42), three considerations must be taken: a) suitability for finite element implementation, b) solution accuracy, and c) computation cost. For example, Gear's multi-step methods were shown to be very effective for integration of viscoplastic equations under a homogeneous stress state. The methods are, however, not suitable for large scale finite element computing in view of two reasons: a) excessive computer core memory is required, and b) a special start-up procedure is needed. Therefore, one-step methods appear to be more suitable for finite element applications.

Two classes of integration schemes are normally categorized under the one-step methods, that is, explicit and implicit methods. Each class has its advantages and drawbacks. The explicit methods are only conditionally stable, although less computing effort is required. On the other hand, the implicit methods are known to be numerically stable, but the corresponding computing

cost is rather high. In the following, both the explicit and implicit schemes and automatic stepping methods are briefly reviewed.

4.1 Explicit Schemes

There are several one-step explicit integration schemes available. In the following, we consider four different methods.

Forward Euler Scheme:

We consider a typical time interval $[t_n, t_{n+1}]$ with the time increment $\Delta t = t_{n+1} - t_n$. The values of $\underline{y}$ at time t_{n+1} may be evaluated by

$$\underline{y}_{n+1} = \underline{y}_n + \Delta t\, \underline{f}_n \tag{43}$$

where

$$\underline{y}_{n+1} = \underline{y}(t_{n+1})$$

$$\underline{y}_n = \underline{y}\,(t_n) \tag{44}$$

$$\underline{f}_n = \underline{f}\,(\underline{y}_n, t_n)$$

It is apparent that $\underline{y}_{n+1}$ can be calculated directly from Eq. (43) without involving any iterations. Eq. (43) represents the first order approximation to $\underline{y}$ at t_{n+1}.

Euler-Cauchy's Scheme:

The functions of $\underline{y}$ at t_{n+1} are approximated by

$$\underline{y}_{n+1} = \underline{y}_n + \frac{1}{2}(\underline{f}_n + \underline{f}_1)\, \Delta t \tag{45}$$

where

$$\underline{y}_1 = \underline{y}_n + \Delta t \cdot \underline{f}_n$$

$$\underline{f}_1 = \underline{f}(\underline{y}_1, t_{n+1}) \tag{46}$$

Obviously, Eq. (45) represents a second-order approximation to $\underline{y}_{n+1}$.

Trapezoidal Rule:

By considering a second-order approximation to $\underline{y}_{n+1}$, one may write

$$(\underline{I} - \frac{\Delta t}{2} \underline{J}_n)\, \Delta \underline{y} = \Delta t \cdot \underline{f}_n \tag{47}$$

with

$$\underline{y}_{n+1} = \underline{y}_n + \Delta \underline{y}$$

where

$$\underline{J}_n = \frac{\partial \underline{f}}{\partial \underline{y}} \bigg|_{t=t_n} \tag{48}$$

and

$\underline{I}$ = an identity matrix

Runge-Kutta Method:

It is a higher order integration rule. At time $t_n \leq t_i \leq t_{n+1}$, the "m-stage", k-th order Runge-Kutta method has the form

$$\underline{y}_{n+1} = \underline{y}_n + \Delta t \sum_{j=1}^{m} A_j\, \underline{f}_j\, (\underline{y}_i, t_i) \tag{49}$$

where A_j's are the weighting coefficients which have different values depending on the order of approximation chosen; m defines the number of evaluations of the function $\underline{f}$ and k refers to the order of truncation error in the Taylor series expansion of $\underline{y}$ at t_{n+1}. Let E_r be the truncation error. It is given by

$$E_r = \frac{\Delta t^k}{(k+1)!}\, \underset{\sim}{y}^{k+1} \tag{50}$$

4.2 Implicit Schemes

Several different implicit schemes are available [71] for the solution of Eq. (42). Here, we will consider two different schemes: trapezoidal method with Newton-Raphson iterations and Walker's integration method.

Trapezoidal Method with Newton-Raphson Iterations:

At time t_{n+1}, the function $\underset{\sim}{y}$ is evaluated from

$$(\underset{\sim}{I} - \frac{\Delta t}{2}\, \underset{\sim}{J}^i_{n+1})\, \Delta \underset{\sim}{y}^{i+1} = \underset{\sim}{y}_n - \underset{\sim}{y}_{n+1} + \frac{\Delta t}{2}\, (\underset{\sim}{f}_n + \underset{\sim}{f}^i_{n+1}) \quad i=0,1,2... \tag{51}$$

where $$\Delta \underset{\sim}{y}^{i+1} = \underset{\sim}{y}^{i+1}_{n+1} - \underset{\sim}{y}_{n+1} \tag{52}$$

and $$\underset{\sim}{y}^0_{n+1} = \underset{\sim}{y}_n \tag{53}$$

$$\underset{\sim}{J}_{n+1} = \left[\frac{\partial \underset{\sim}{f}}{\partial \underset{\sim}{y}}\right]_{t=t_{n+1}}$$

It is noted that the coefficient matrix of $\Delta \underset{\sim}{y}^{i+1}$ on the right-hand side of Eq. (51) is asymmetric. If one is to use tangent stiffness method to solve the global equilibrium equations, cautions have to be given in the handling of the unsymmetric structural stiffness matrix. In general, the implicit method is unconditionally stable and it yields better numerical accuracy over the explicit schemes.

Walker's Integration Method [12,72]:

Walker proposed a recursive integration procedure to integrate the stiff differential equations mentioned in the above. The relationship was obtained

by converting the differential equations, i.e. Eq. (42), to a system of equivalent integral equations. For example, we consider Eq. (7), which can be written as

$$\dot{\underset{\sim}{y}} + Q\,\underset{\sim}{y} = \dot{\underset{\sim}{v}} \tag{54}$$

where $\underset{\sim}{y} = \underset{\sim}{s} - \frac{2}{3}\,\underset{\sim}{\Omega}$

$\underset{\sim}{s}$ = deviatoric stress vector

$\underset{\sim}{\Omega}$ = back stress vector

$Q = \frac{3\mu}{K}\,R^{(1-\frac{1}{n})}$

$\underset{\sim}{v} = 2\mu\underset{\sim}{e} - \frac{2}{3}\,\underset{\sim}{\Omega}$

The differential Eq. (54) can be integrated from 0 to t+Δt in the form

$$\underset{\sim}{y}(t+\Delta t) = \underset{\sim}{y}(t)\; e^{-[Q(t+\Delta t)-Q(t)]} + \int_{t}^{t+\Delta t} e^{-[Q(t+\Delta t)-Q(\xi)]}\,\frac{\partial v}{\partial \xi}\,d\xi \tag{55}$$

With an asymptotic expansion, the above equation may be approximated by

$$\underset{\sim}{y}(t+\Delta t) = \underset{\sim}{y}(t)\; e^{-\Delta Q} + \frac{(1-e^{-\Delta Q})}{\Delta Q}\,\Delta\underset{\sim}{v}(t+\Delta t)$$

$$+ \frac{1}{\Delta Q}\left\{e^{-\Delta Q} - \frac{1}{\Delta Q}\,[1-e^{-\Delta Q}]\right\}[\Delta\underset{\sim}{v}(t+\Delta t)-\Delta\underset{\sim}{v}(t)] \tag{56}$$

where $\Delta Q = \Delta Q(t+\Delta t)$

In Eq. (56), the evaluation of ΔQ and $\Delta\underset{\sim}{v}$ at t+Δt on the right-hand side of the equation requires the knowledge of $\underset{\sim}{y}(t+\Delta t)$. Hence Walker's integration method

is an implicit scheme. The method, according to the results presented in [12, 72], is very stable and highly accurate.

4.3 Automatic Time Stepping

In an automatic time stepping, the time increment for achieving a "specific" solution accuracy is determined judiciously by the computer program. Several versions of automatic step control are available [13,66,77,78]. For example, a procedure based on the Runge-Kutta method was proposed in [13]. The key elements of an automatic step control are: a) an error estimate for the calculation of $\underset{\sim}{y}$ at the end of each time step, and b) a criterion for determination of the time step Δt. The error involved for a particular integration rule is given by

$$E = \frac{\| \underset{\sim}{y}^{P+1}_{t+\Delta t} - \underset{\sim}{y}^{P}_{t+\Delta t} \|}{\Delta t} \tag{57}$$

where $\underset{\sim}{y}^{P+1}_{t+\Delta t}$ = function value of $\underset{\sim}{y}$ at the time $t+\Delta t$ evaluated by a $(p+1)$-th order integration formula

$\| \ \|$ = a Euclidean norm

A time step Δt in the calculation is retained if the error e computed from $e = E/\|\underset{\sim}{y}_n\| \ (t_f - t_o)$, t_f = final analysis time and t_o = initial analysis time, is kept within a tolerance limit, i.e.

$$e \leq \epsilon_u \tag{58}$$

If the above criterion is not satisfied, the time step must be revised according to

$$\Delta t' = \tau \cdot \Delta t \tag{59}$$

where τ is a non-negative coefficient, determined from

$$\tau = \left[\frac{\epsilon_u \ \|\underline{y}_n\|}{E(t_f - t_o)}\right]^{1/P} \tag{60}$$

5. Computer Implementation

Thus far, four viscoplastic models have been implemented into NFAP for the intended numerical studies. These include Bodner, Walker, Robinson's isotropic and transversely isotropic models. Implementation of Freed's model into NFAP will be done during the second phase of this study. In addition, we have implemented the following numerical integration procedures into the program:

- Forward Euler scheme
- Explicit trapezoidal rule
- Implicit trapezoidal rule
- An automatic subincrementing control

Walker's integration method will be considered in the second year study.

In NFAP, all the viscoplastic models and the related integration procedures were programmed in a separate material module (called Model #6). Any future coding modifications or additions can be done locally without interfering with other parts of the program.

The viscoplastic material module is called by the main program during two distinct stages of calculations: global stiffness assemblage stage and stress and strain calculation stage. The material model is being driven by all the continuum elements: 2/D continuum, 3/D continuum, plate and shell elements. As shown in Fig. 21, when the material model #6 is activated, two paths of calculations are involved and the paths are controlled by a parameter "IND". That is, at the beginning of the analysis, the following subroutines are called for assigning workspace and array initialization:

Subroutine Name	Functionality
INITWA	Initialize WA - array which contains $\underset{\sim}{\sigma}$, $\underset{\sim}{\epsilon}$, $\underset{\sim}{\epsilon}^{I}$, $\underset{\sim}{\alpha}$, and other material parameters at each integration point for all the elements of a particular element group
M06INI	Routine called by INITWA to perform the same function
M06CMC	Interpolate temperature dependent material constants.

During each typical time stpe (i.e. either element stiffness calculations, equilibrium iterations, or stress calculations), the material Model #6 (M06STR) is called by the stress-strain driver (STSTN) and the following functions are performed:

1) Formation of elastic material stiffness matrix, which may be temperature-dependent.
2) Selection of a specific viscoplastic model and integration procedure.
3) Using subincrements to calculate: $\Delta\underset{\sim}{\sigma}$, $\Delta\underset{\sim}{\epsilon}^{I}$, $\Delta\underset{\sim}{\alpha}$, etc. and update these quantities.
4) Performing error checks and revising the subincrement h if necessary.

A flow chart for the above calculations is shown in Fig. 22.

6. Numerical Examples

To demonstrate the integration methods discussed in this report, three examples are included: 1) a uniaxial plane stress problem, 2) a simple beam subjected to specified displacements, and 3) a thick wall cylinder under internal pressure. Each of these problems are described in this section.

6.1 A Uniaxial Plane Stress Problem

We consider a plane stress problem, for which a uniaxial homogeneous stress state is imposed using Walker (case A) and Robinson isotropic models (case B), respectively. The main objective of running this problem is to test the convergence characteristics of various integration rules with and without subincrement stepping.

Case A - Walker's Model

A monotonic ramp load in the form of constant strain is imposed. The following numerical schemes were exercised:

a) Forward Euler Rule (Fig. 23)

Δt(sec.)	Number of Subincrements
16.2	2
16.2	4
32.4	4
32.4	8

b) Automatic Subincrementing (Fig. 24)

Δt = 16.2 and 32.4 sec.

c) Explicit Trapezoidal Rule (Fig. 25)

Δt (sec.)	Number of Subincrements
16.2	2
16.2	4
32.2	2

d) Implicit Trapezoidal Rule (Fig. 26)

Δt = 16.2, 32.4, 54 sec.

The numerical results in the form of stress-strain plots are shown in Figs. 23-26. At first in Fig. 23, obviously the forward Euler's rule is the least reliable unless the integration step is sufficiently small, i.e., Δt = 16.2 or 32.4 sec. with number of subincrements = 4 or 8. Otherwise, numerical instability and/or gross error occurs in the responses. The automatic subincrementing procedure with an error control (see Fig. 24) is definitely much more reliable regardless of the size of the global time step being used. Both the explicit (Fig. 25) and implicit trapezoidal rules appear to give quite accurate results regardless of the step size or subincrement size used. Although the computer time is somewhat more expensive as compared to the explicit schemes, the implicit method may be particularly useful for handling complex thermal-mechanical cyclings.

Case B - Robinson's Isotropic Model

In this case, the material is subjected to uniaxial cyclic strains (2 1/2 cycles as seen in Fig. 27) with three different strain rates: $\dot{R} = 4 \times 10^{-2}$, 4

x 10^{-3}, 4 x 10^{-4}/min. The maximum strain in all three cases was 0.32%. Both the forward Euler and explicit trapezoidal rules were employed. As seen in Figs. 28 and 29, the predictions correlate closely with the experimental data in [80]. It is noted however, that some numerical difficulty was experienced for the case of low strain rate, i.e. R = 4 x 10^{-4}/min. This was induced by the discontinuous function (or shape change in the smoothing spline function) in Robinson's model. Consequently, very small time steps have to be employed in order to reach a convergent solution.

6.2 A Simple Beam

A simply supported beam subjected to specified displacement at its center is considered. Using symmetry conditions, only one half of the beam is modeled by six 8-node plane stress elements in Fig. 30. Two loading histories are considered in the analysis: case A - cyclic displacement with an amplitude of 0.095 in. and loading rate of 0.1 in/min (Fig. 31), and case B - constant displacement of the same amplitude with a hold time t_h = 168 hrs. The maximum bending stress (at the center lower fiber) vs. maximum displacement of the beam is plotted in Fig. 32. This result is very similar to that in [80]. In addition, the change in maximum stress as a function of time is shown in Fig. 33. Some stress relaxation is apparent from this plot.

When the beam is subjected to a constant displacement with a long hold time (t_h=168 hrs., significant relaxation of the maximum bending stress is expected as shown in Fig. 34.

6.3 A Thick Wall Cylinder

A cylinder, with an internal radius 0.4 cm and external radius 0.635 cm, is subjected to a ramp internal pressure shown in Fig. 35. The cylinder was modeled by twelve 8-node axisymmetric elements under plane strain deformation. A global integration procedure was chosen as the following in order to achieve convergent solution:

$$0 \leq t \leq 28 \times 10^{-4} \text{ hr.} \qquad \Delta t = 7 \times 10^{-4} \text{ hr.}$$

$$28 \times 10^{-4} \leq t \leq 42.8 \times 10^{-3} \text{ hr.} \qquad \Delta t = 5 \times 10^{-3} \text{ hr.}$$

$$42.8 \times 10^{-3} \leq t \leq 44.3 \times 10^{-2} \text{ hr.} \qquad \Delta t = 5 \times 10^{-2} \text{ hr.}$$

$$44.3 \times 10^{-2} \leq t \leq 4.44 \text{ hr.} \qquad \Delta t = 0.5 \text{ hr.}$$

$$t > 4.44 \text{ hr.} \qquad \Delta t = 5 \text{ hr.}$$

For comparison of results, four subincrementing schemes were employed:

Case A - automatic subincrementing with error checks

Case B - four subincrements for all global steps

Case C - two subincrements for all global steps

Case D - no subincrements.

Calculations were made from the forward Euler formula (of first order Runge-Kutta methods). The radial displacement at the outer wall of the cylinder versus time is shown in Fig. 36 for the four cases of integration schemes. Apparently, the results obtained from the automatic subincrements with an error control (limited to 0.1% according to Eq. (58) agree closely with those given in [80]. Solution accuracy deteriorates as the number of subincrements decrease. More noticeably from the result of Case D, no numerical instability is indicated and global equilibrium was satisfied for every incremental step. However, the solution is far from accurate due to the uncontrolled errors resulting from numerical integrations of the viscoplastic rate equations.

7. Conclusion

We have completed the implementation of four viscoplastic models into NFAP for the numerical study of integration methods. Among all the integration schemes investigated, it appears that either an automatic subincrementing procedure with an error control or an implicit scheme in the form of trapezoidal rule or Walker's integral relations is more desirable.

The major contribution of the first-year study in viscoplastic analysis consists of: 1) viscoplastic constitutive models and the associated integration methods are coded as a separate module in NFAP so that any future extension or coding modification can be done easily by a user, 2) the viscoplastic models can be applied to various structural components which can be represented by 2/D continuum, 3/D continuum, or plate/shell elements, and 3) further understanding of the numerical schemes employed for the analysis.

It is anticipated that our next phase of study will include:

1) Implementation of Walker's integration method and performing numerical study on various constitutive models as compared to other implicit schemes such as the trapezoidal rule.
2) Implementation of Freed's viscoplastic model for application purpose.
3) Investigation of solution strategy for nonlinear analysis of various structural geometries.
4) Development of an improved automatic stepping procedure with error control on the basis of an implicit integration scheme.
5) Initialization of nonlinear damage analysis.

PART IV: FULLY-NONLINEAR ANALYSIS CAPABILITY FOR SHELL APPLICATIONS

1. Introduction

The development of finite element models for the fully-nonlinear analysis of plates and arbitrary-curved shells, including the effects of both material (e.g. plasticity) and geometric nonlinearities (e.g. large displacement/rotations and finite stretches), has been a very active research area over the years, and especially in recent years [30,31,84-89]. This extensive work was prompted mainly by the many conceptual, theoretical, as well as computational difficulties and challenging problems involved in nonlinear shell formulations and solutions. In addition, there is an increased industrial need to perform large-scale computations utilizing these general shell models, such progressive failure analysis to predict damage, buckling, post-buckling and limit collapse states of stiffened plates and shells, etc.

As evidenced by numerous recent works, the degenerated-shell approach has apparently continued to be the most popular in such general developments. In particular, the important contributions here, including many variants of the displacement-based formulations, as well as a number of different hybrid/mixed developments, have been critically reviewed in [30]. However, developing a fully nonlinear solution procedure for arbitrarily-curved shells is a very demanding task. Indeed, in such a general development, it is only a minimal requirement to use a *robust* linear shell element (i.e., rank-sufficiency, locking free, accurate stress predictions, insensitivity to geometric distortions, etc.) as a starting point. Additionally, several other fundamental issues must be carefully investigated. Confining attention to the quasistatic problem, the following are of utmost importance from a theoretical standpoint:

(i) *consistent linearization* of the underlying weak, or variational, form of the governing equations [88-90]; (ii) treatment of *large rotations*, in both stiffness derivation as well as the configuration update procedure [31,91,92]; (iii) use of objective *measures* of stress and strain, and their rates, suitable for the particular form of the nonlinear material model employed (e.g. plasticity, viscoplasticity, etc.) [93-98]; and (iv) use of a valid method for stress integration (update) that maintains *incremental objectivity* in the presence of large rotations and "non-infinitesimal" stretches, when dealing with rate-type constitutive equations [75-99].

The objective in the present paper is to briefly review some of our recent work dealing with the formulation of a general theoretical framework for the analysis of finitely stretched and rotated shells using our hybrid/mixed method [30]. In particular, this is utilized here as a basis for deriving one representative nonlinear model of this type; i.e., HMSH5 (four-noded quadrilateral). Numerical results illustrating the performance of the element in some test cases are also reported in order to demonstrate the effectiveness of various proposed solution schemes. More examples can be found in [30].

We finally note that the present mixed element HMSH5 is "extended" nonlinear version of its linear counterparts; e.g. see [27] for applications to isotropic shells, and Part II for extensions to laminated plates/shells. The crucial point in its mixed formulation concerns the *judicious selection* of the parameters in the polynomial strain approximation. In particular, this was facilitated by the use of a set of *bubble functions* (i.e., kinematic degrees of freedom associated with an interior fifth node) in HMSH5.

For conciseness, the scope of the present discussion is limited to quasi-static problems. In addition, special instability phenomena and post-buckling responses are not addressed. Further, in all the applications presented later, we utilize a "semi-linear" elastic isotropic model, thus enabling the comparison of our results with other independent solutions available in the literature.

2. Geometric and Kinematic Descriptions

2.1 Basic Hypotheses

The main assumptions underlying the present mixed-element developments are summarized as follows:

(i) straight and inextensible shell "normals" (or "thickness" fibers).

(ii) zero "through-thickness" normal stress (i.e., plane-stress assumption).

(iii) "small" *transverse* shear strains, but *large* membrane and bending strain components.

The first two simplifying hypotheses (i) and (ii) are typical in any degenerated shell model [e.g., 84], based on classical Mindlin/Reissner plate theories. However, note that, even though assumption (i) is utilized as a basis for deriving the element governing "stiffness" equations , fiber "thinning" effects due to large membrane strains can still be recovered in the computations; e.g., using the incremental "average-thickness" update procedure in [86].

On the other hand, certain important implications resulting from the additional assumption (iii) can be exploited to develop simplified and effective numerical algorithms [30]. From a practical standpoint, its justification is

that "large" transverse shear strains are *not* typical in common thin or moderately-thick composite shell structures.

2.2 Coordinate Reference Frames

Three different types of Cartesian reference frames are defined here for convenience in subsequent derivations:

(1) The *fixed* or global reference frame, with its orthonormal base vectors $\underset{\sim}{e}_i (i=1,2,3)$, is used to define element geometry and its translational displacement DOF (degrees of freedom).

(2) A unique *local* fiber coordinate system is constructed at *each node*, with associated base vectors $\underset{\sim}{e}^f_i (i=1,2,3)$, where $\underset{\sim}{e}^f_3$ coincides with the nodal fiber. During the incremental analysis, this orthogonal fiber triad is continuously updated and used as a *moving basis* for defining the "finite" rotational DOF at the node.

(3) A *local* lamina system at *each integration point* in an element, $\underset{\sim}{e}^\ell_i (i=1,2,3)$, with $\underset{\sim}{e}^\ell_3$ taken to be normal to the lamina surface, and the other two in-plane lamina-tangent vectors $\underset{\sim}{e}^\ell_1$ and $\underset{\sim}{e}^\ell_2$ selected as in [30] (see Fig. 37).

This latter lamina basis rotates rigidly as the element deforms, and it is found to be most convenient for invoking the plane stress assumption in the $\underset{\sim}{e}^\ell_3$-direction in all configurations as well as for ensuring the invariant property in the interpolation of the assumed strain field given later.

2.3. Geometry and Kinematics

With its midsurface taken as the reference surface, the position vector to an arbitrary point in the shell element at any time instant "t" is defined in terms of the natural coordinates $(r,s,\bar{t})$ as follows:

$$ {}^{t}\underset{\sim}{x} = \sum_{k=1}^{n_e} N_k \, {}^{t}\underset{\sim}{x}_k + \frac{\bar{t}}{2} \sum_{k=1}^{n_e} {}^{t}h_k \, N_k \, {}^{t}\underset{\sim}{e}_3^{f(k)} \qquad (2.1) $$

where ${}^{t}\underset{\sim}{x}_k$, ${}^{t}\underset{\sim}{e}_3^{f(k)}$, and ${}^{t}h_k$ are the position vector, components of a unit pseudonormal (fiber) vector, and fiber-dimension (shell-thickness) parameter, respectively, at nodal point k on the reference surface. The $N_k(r,s)$ are the two-dimensional shape functions associated with node k [27], and n_e the number of nodes per element.

There are five DOF per node used to parameterize the element configuration in the shell space: three global translations (u,v,w), and two "fiber" rotations θ_1 and θ_2 about axes $\underset{\sim}{e}_1^f$ and $\underset{\sim}{e}_2^f$. Note that, following [30], these latter nodal rotation freedoms are appropriately viewed here as generalized *finite* rotational coordinates of the Rodrigues-Euler type [91,92], thus providing a convenient, singularity-free (no drilling freedoms) parameterization for the director fields of the elements. In total, an HMSH5 element thus contains 25 DOF.

In the context of the present incremental analysis, three successive configurations, at time "0" (initial), "t" (current) and "(t+Δt)" (incremented or neighboring) are considered. Then, the total and incremental displacement fields of the element can be expressed as

$$\underset{\sim}{u} = \sum_{k=1}^{n_e} N_k \, {}^{t}\underset{\sim}{u}_k + \frac{\bar{t}}{2} \sum_{k=1}^{n_e} N_k \, ({}^{t}h_k \, {}^{t}\underset{\sim}{e}_3^{f(k)} - {}^{o}h_k \, {}^{o}\underset{\sim}{e}_3^{f(k)}) \tag{2.2}$$

$$\Delta\underset{\sim}{u} = \sum_{k=1}^{n_e} N_k \, \Delta\underset{\sim}{u}_k + \frac{\bar{t}}{2} \sum_{k=1}^{n_e} {}^{t}h_k \, N_k \, ({}^{t+\Delta t}\underset{\sim}{e}_3^{f(k)} - {}^{t}\underset{\sim}{e}_3^{f(k)}) \tag{2.3}$$

where

$$\underset{\sim}{u}_k = {}^{t}\underset{\sim}{x}_k - {}^{o}\underset{\sim}{x}_k \quad \text{and} \quad \Delta\underset{\sim}{u}_k = {}^{t+\Delta t}\underset{\sim}{x}_k - {}^{t}\underset{\sim}{x}_k$$

The relation in Eq. (2.2) is directly employed to evaluate the total element displacements and their derivatives (i.e., total *geometric* "Almansi" strains in Eq. 3.1). In this, components of the "updated" director vectors, $\underset{\sim}{e}_3^f$, in the configuration "t" are determined in terms of nodal rotations using the (geometrically-exact) update procedure of Sec. 4.4.

On the other hand, the relation in Eq. (2.3) provides the basis for deriving the "linearized" governing equations of the element. To this end, the second term must first be expanded in terms of nodal rotation increments, and here we utilize the following "linearized" kinematic approximation:

$$\Delta\underset{\sim}{u} = \sum_{k=1}^{n_e} N_k \, \Delta\underset{\sim}{u}_k + \frac{\bar{t}}{2} \sum_{k=1}^{n_e} {}^{t}h_k \, N_k \, (-\Delta\theta_1^k \, {}^{t}\underset{\sim}{e}_2^{f(k)} + \Delta\theta \, {}^{t}\underset{\sim}{e}_1^{f(k)}) \tag{2.4}$$

for the *stiffness* evaluation of both elements considered. We particularly note that this leads to the well-known expression (i.e., similar to the "true" continuum case [84]) of a *single* geometric stiffness matrix (see Sec. 4.2).

Remark 2.1 Alternative forms for nonlinear kinematic approximations of the rotational term in Eq. (2.3) have been also employed in several recent studies [e.g. 88,89]. This led to the introduction of various *additional* geometric stiffness contributions, which were found to be necessary in order to attain quadratic rate of (asymptotic) convergence in Newton-Raphson iterative schemes for solutions of large-rotation shell problems. However, as was demonstrated in [30], even with the single geometric stiffness based on (2.4) above, the same "good" convergence rate is also exhibited by the present mixed model HMSH5; the crucial point here is the "exact" updating of the orientations of nodal fiber triads (Sec. 4.4).

Remark 2.2 In addition to its computational efficiency, it was also proved in [30] that the geometrix stiffness of HMSH5 possesses a "second-order" accuracy, thus making the element capable of appropriate modeling of instability modes; e.g. *creep buckling*.

3. Variational Principle

A modified Hellinger-Reissner variational principle [e.g. 30,100] provides the starting point for the present incremental, step-by-step analysis. This takes the following form in *updated* Lagrangian (UL) description with "t" as reference; i.e., $\delta\Delta\pi_{HR} = 0$,

$$\Delta\pi_{HR} = \int_V \left[-\frac{1}{2}\Delta\underset{\sim}{e}^T\underset{\sim}{c}\Delta\underset{\sim}{e} + \underset{\sim}{\sigma}^T\Delta\hat{\underset{\sim}{e}} + \Delta\underset{\sim}{e}^T\underset{\sim}{c}\Delta\hat{\underset{\sim}{e}} - \Delta\underset{\sim}{e}^T\underset{\sim}{c}(\underset{\sim}{e}-\hat{\underset{\sim}{e}}) \right] dV - \Delta W \qquad (3.1)$$

where $\Delta\underline{e}$ and $\Delta\hat{\underline{e}} = \Delta\hat{\underline{e}}$ (linear) + $\Delta\hat{\underline{\eta}}$ (nonlinear) are, respectively, independently-assumed and geometric (from displacements) Green strain increments; $\underline{e}$ and $\hat{\underline{e}}$ the corresponding total Alamansi strains; $\underline{c}$ the material stiffness; $\Delta\underline{\sigma} = \underline{c}\Delta\underline{e}$ the Truesdell stress increment; $\underline{\sigma}$ the true (Cauchy) stress; and ΔW is the work of prescribed forces. The last term in the bracket of Eq. (3.1) is due to compatibility-mismatch [5,45].

Note that, for the purpose of implementing element HMSH5, all strain/stress vectors in the above will be defined with respect to the *lamina* basis at "t". In particular, this implies the use of a "reduced" (5x5) material matrix, in accordance with assumption (ii) of Sec. 2.1.

4. Finite Element Formulation

4.1 Strain-Field Discretization

In addition to displacement interpolation, a polynomial for $\Delta\underline{e}$ in the present mixed element is also needed. To this end, we utilize the same specific "*least-order*" polynomial strain approximations for these elements proposed previously for linear analysis [30]. Thus, in tensor-component form, the incremental *lamina* strains $\Delta\underline{e}'$ for *undistorted* geometry are, for HMSH5 element:

$$\begin{aligned}
\Delta e'_{11} &= \beta_1 + \beta_2 r + \beta_3 s + \bar{t}(\beta_4 + \beta_5 r + \beta_6 s) \\
\Delta e'_{22} &= \beta_7 + \beta_8 r + \beta_9 s + \bar{t}(\beta_{10} + \beta_{11} r + \beta_{12} s) \\
\Delta e'_{12} &= \beta_{13} + \beta_{14}\bar{t} \\
\Delta e'_{23} &= \beta_{15} + \beta_{16} r + \beta_{17} s \\
\Delta e'_{13} &= \beta_{18} + \beta_{19} s + \beta_{17} r
\end{aligned} \tag{4.1}$$

Note that the above strain distribution needs to be further modified to account for geometric distortions; namely the "important" in-plane lamina (skewness) distortion. To this end, we use a "constant" Jacobian transformation as described in [25,30]. With this, we can finally write

$$\Delta \underset{\sim}{e} = \underset{\sim}{P}\ \Delta \underset{\sim}{\beta} \tag{4.2}$$

where $\Delta \underset{\sim}{\beta}$ are generalized strain parameters, and $\underset{\sim}{P}$ are "modified" strain-interpolation functions.

4.2 Element Stiffness Equations

In view of Eqs. (2.4) and (4.2), the appropriate "linearized" form of the variational principle in (3.1) is simply obtained as in the convectional "true" continuum case. This yields, after invoking the stationarity conditions with respect to $\Delta \underset{\sim}{\beta}$, and then $\Delta \underset{\sim}{q}$,

$$\Delta \underset{\sim}{\beta} = \underset{\sim}{H}^{-1}\ [\underset{\sim}{G}\ \Delta \underset{\sim}{q} + (\underset{\sim}{Z}_1 - \underset{\sim}{Z}_2)] \tag{4.3}$$

where

$$\underset{\sim}{H} = \int_V \underset{\sim}{P}^T\ \underset{\sim}{c}\ \underset{\sim}{P}\ dV\ ;\ \underset{\sim}{G} = \int_V \underset{\sim}{P}^T\ \underset{\sim}{c}\ \underset{\sim}{B}_L\ dV \tag{4.4}$$

$$\underset{\sim}{Z}_1 = \int_V \underset{\sim}{P}^T\ \underset{\sim}{c}\ \hat{\underset{\sim}{e}}\ dV\ ;\ \underset{\sim}{Z}_2 = \int_V \underset{\sim}{P}^T\ \underset{\sim}{c}\ \underset{\sim}{e}\ dV \tag{4.5}$$

as well as the desired final stiffness relationships:

$$(\underset{\sim}{K}_L + \underset{\sim}{K}_{NL})\ \Delta\underset{\sim}{q} = \underset{\sim}{Q} - (\underset{\sim}{Q}_1 + \underset{\sim}{Q}_2) \tag{4.6a}$$

$$\underset{\sim}{K}_L = \underset{\sim}{G}^T\ \underset{\sim}{H}^{-1}\ \underset{\sim}{G} \quad ; \quad \underset{\sim}{K}_{NL} = \int_V \underset{\sim}{B}_{NL}^T\ \bar{\sigma}\ \underset{\sim}{B}_{NL}\ dV \tag{4.6b}$$

$$\underset{\sim}{Q}_1 = \int_V \underset{\sim}{B}_L^T\ \sigma\ dV \quad ; \quad \underset{\sim}{Q}_2 = \underset{\sim}{G}^T\ \underset{\sim}{H}^{-1}\ (\underset{\sim}{Z}_1 - \underset{\sim}{Z}_2) \tag{4.6c}$$

See details in [27]. The $\underset{\sim}{K}_L$ is the element "linear" (or material) stiffness, $\underset{\sim}{K}_{NL}$ its geometric stiffness (shown in [30] to exhibit second-order "accuracy"), and the right-hand side of Eq. (4.6a) includes "correction" terms due to both equilibrium imbalance $(\underset{\sim}{Q}-\underset{\sim}{Q}_1)$ as well as compatibility mismatch terms in $\underset{\sim}{Q}_2$.

4.3 Solution Procedure

Once assembled, the linearized equations above are utilized in the following *global* incremental-iterative full Newton-Raphson scheme:

$$({}^{t+\Delta t}\underset{\sim}{K}_L + {}^{t+\Delta t}\underset{\sim}{K}_{NL})^{(n)}\ \Delta\underset{\sim}{q}^{(n+1)} = {}^{t+\Delta t}\underset{\sim}{Q} - {}^{t+\Delta t}(\underset{\sim}{Q}_1 + \underset{\sim}{Q}_2)^{(n)} \tag{4.7}$$

for the solution for the incremental nodal displacements in the (n+1)th iteration within the time step "t"→"t+Δt". A displacement-type convergence criterion is adopted here (0.001 tolerance for the ratio of norms of incremental to total nodal displacement vectors).

Remark 4.1 In applications to *viscoplastic* analyses, the above *variable stiffness* solution scheme calls for the formulation of a (material) *constitutive tangent* stiffness matrix $\underset{\sim}{C}$ (Eqs. 4.6,4.7). Although such matrices are not readily available at present for "general" unified viscoplastic models [e.g. 4,82,83], several attempts have been made [68-70] in the context of other viscoplasticity theories. This aspect will be further investigated in our future work.

Remark 4.2 Instead, the more conventional *initial strain* or *constant stiffness*, viscoplastic solution approach is obtained here by simply utilizing an *elastic* $\underset{\sim}{C}$ in all Eqs. (4.3)-(4.6) above, together with an additional "load" term (i.e., $\underset{\sim}{Q}_3$-vector) in the parenthetical term on the right-hand side of Eq. (4.6a) to account for *inelastic* strain-rate effects.

4.4 Large-Rotation Configuration Update

Configuration update involves the calculations of (i) new nodal coordinates, as well as (ii) orientations of the associated fiber triads. Although (i) is trivial, (ii) is complicated by the non-vectorial character of finite space rotations. Here, we make use of the so-called *exponential mapping* algorithm for rotational transformation of vectors [30,90-92]; i.e. at the end of the $(n+1)^{th}$ iteration,

$$\begin{bmatrix} \underset{\sim}{e}_1^{f(k)} \\ \underset{\sim}{e}_2^{f(k)} \\ \underset{\sim}{e}_3^{f(k)} \end{bmatrix}^{(n+1)} = \begin{bmatrix} 1-g_1\beta^2 & g_1\alpha\beta & -g_2\beta \\ g_1\alpha\beta & 1-g_1\alpha^2 & g_2\alpha \\ g_2\beta & -g_2\alpha & 1-g_1(\alpha^2+\beta^2) \end{bmatrix} \begin{bmatrix} \underset{\sim}{e}_1^{f(k)} \\ \underset{\sim}{e}_2^{f(k)} \\ \underset{\sim}{e}_3^{f(k)} \end{bmatrix}^{(n)} \tag{4.8}$$

$$g_1 = \frac{1 \cos \|\Delta\underline{\theta}\|}{\|\Delta\underline{\theta}\|^2} \quad ; \quad g_2 = \frac{\sin \|\Delta\underline{\theta}\|}{\|\Delta\underline{\theta}\|} \qquad \|\Delta\underline{\theta}\| = (\alpha^2 + \beta^2)^{1/2} \tag{4.9}$$

where the *local* components of the rotation pseudovector $\Delta\underline{\theta}_k^{(n+1)}$ along the fiber axes $\underline{e}_i^{f(k)}$ (at configuration "n") are conveniently defined as $(\alpha,\beta,0)$.

4.5 Strain Update

The calculation of the updated *independent* (Almansi) strain field $\underline{e}$ at the quadrature points in the element is needed to evaluate the iterative compatibility mismatch "force" vector $\underline{Q}_2$. A simple "approximate" procedure [30] is utilized here. In this, the updated $\underline{e}$ is obtained by a *push-forward* transformation [90] for the (covariant) tensor components of the total (incremented) strains using the *relative* deformation gradient for configurations (n+1) and (n). For convenience, the latter is written as follows, using the polar-decomposition theorem [90],

$$\underline{F}_{n+1} = {}^{n+1}_{n}\underline{F} = \frac{\partial \underline{x}(t_{n+1})}{\partial \underline{x}(t_n)} = \underline{R}_{n+1}\, \underline{U}_{n+1} \tag{4.10}$$

where $\underline{R}$ and $\underline{U}$ are rigid-rotation and pure stretch tensors, respectively. With appropriate reference to lamina coordinate systems in different configurations, we may then show that

$$\underline{e}^{(n+1)} = \underline{U}^{-1}_{n+1}(\underline{e}^{(n)} + \Delta\underline{e}^{(n+1)})\, \underline{U}^{-1}_{n+1} \tag{4.11}$$

where now *all* components of tensors on the right-hand side are referred to lamina coordinates in (n), whereas $\underset{\sim}{e}^{(n+1)}$ are taken with reference to lamina axes in the new configuration (n+1).

Remark 4.3 In keeping with the present mixed formulation, it is crucial to determine the relative stretches (as well as all other *pure* "strain-like" quantities) from the "true" strains. To this end, we use the following *approximation* [30]:

$$\underset{\sim}{U}_{n+1} = (1 + \frac{1}{2}I_3^e)\underset{\sim}{I}+(1 - \frac{1}{2}I_2^e)\Delta\underset{\sim}{e}^{(n+1)} - \frac{1}{2}(1-I_1^e)\Delta\underset{\sim}{e}^{(n+1)}\Delta\underset{\sim}{e}^{(n+1)} \qquad (4.12)$$

where I_i^e = (i=1,2,3) are the invariants of $\Delta\underset{\sim}{e}^{(n+1)}$.

This formula obviates the need for "costly" procedures to formally obtain the square-root of a positive-definite matrix, while it still maintains the condition of *same* principle axes for $\underset{\sim}{U}_{n+1}$ and $\Delta\underset{\sim}{e}^{(n+1)}$.

Remark 4.4 However, when needed later (Sec. 5.1), $\underset{\sim}{R}_{n+1}$ must be calculated from element displacement field. For "relatively" small strain increments, it can be approximated [30] by the coordinate-transformation matrix for lamina bases in configurations (n) and (n+1).

5. Stress Update

For a class of moderately large-strain constitutive models, a general spatial *rate-form*, consistent with the variational statement in Eq. (3.1), is considered here (a superposed dot indicates a material time derivative)

$$\overset{\circ}{\sigma}_{ij} = c_{ijkl}\, d_{kl} \quad ; \quad \overset{\circ}{\underset{\sim}{\sigma}} = \dot{\underset{\sim}{\sigma}} - \underset{\sim}{\ell}\,\underset{\sim}{\sigma} - \underset{\sim}{\sigma}\,\underset{\sim}{\ell}^{T} + (d_{kk})\,\underset{\sim}{\sigma} \tag{5.1}$$

where $\overset{\circ}{\underset{\sim}{\sigma}}$ is the (objective) Truesdell rate of Cauchy stress $\underset{\sim}{\sigma}$, $\underset{\sim}{d}$ the (spatial) deformation-rate tensor, $\underset{\sim}{\ell}$ the velocity gradient, and $\underset{\sim}{c}$ may generally depend on stress and/or deformation history (e.g. plasticity).

Remark 5.1 Considering the range of "non-infinitesimal" strains anticipated in viscoplastic/damage studies for composite space-engine components (i.e., 2-5%), the precise distinction between various "objective" stress rates becomes unimportant from the standpoint of elastic modeling of material behavior. However, from the viewpoints of both numerical implementation as well as solution accuracy/convergence, the use of Truesdell rate in Eq. (5.1) is of great advantage in the present mixed formulation, i.e. leading to "efficient" integration algorithm in Eq. (5.4) and "improved" numerical convergence (e.g. Sec. 6.3).

5.1 The Basic Stress-Integration Algorithm

In addition to the requirements of *numerical stability* and *consistency*, a time-stepping scheme for stress updating with finite strains/rotations must also satisfy the important condition of the *incremental objectivity*; [31,95].

C-2

In particular, because of its desirable numerical characteristics, the generalized *mid-point* (trapezoidal) rule has been utilized extensively to formulate "objective" stress-updating procedures. In this section, the method is adapted for the present mixed shell elements. To this end, the following definitions are introduced:

$$\underset{\sim}{F}_{n+a} = \underset{\sim}{R}_{n+a}\,\underset{\sim}{U}_{n+a} \quad , \quad J_{n+a} = \det \underset{\sim}{F}_{n+a} \tag{5.2}$$

$$\Delta\underset{\sim}{\sigma}^{(n+1/2)} = \Delta t\,\overset{\circ}{\underset{\sim}{\sigma}}_{n+1/2} = \underset{\sim}{c}_{n+1/2}\,\underset{\sim}{D}_{n+1/2} \; ; \; \underset{\sim}{D}_{n+1/2} = \Delta t\,\underset{\sim}{d}_{n+1/2} \tag{5.3}$$

in which $\underset{\sim}{c}_{n+1/2}$ is the fourth-order material moduli tensor at the mid-point configuration $t_{n+1/2}$, $\Delta t = (t_{n+1} - t_n)$, and $0 \leq a \leq 1$ (with $\underset{\sim}{F}_n = \underset{\sim}{I}$, $J_n = 1$, where $\underset{\sim}{I}$ is the unit tensor).

With the Eqs. (5.2) and (5.3) the stress update algorithm takes the following general form, giving now, the updated stress components $\underset{\sim}{\sigma}^{(n+1)}$, directly referred to the *updated* t_{n+1}-lamina basis [30]:

$$\underset{\sim}{\sigma}^{(n+1)} = J_{n+1}^{-1}\,\underset{\sim}{U}_{n+1}\,(\underset{\sim}{\sigma}^{(n)} + J_{n+1/2}\,\underset{\sim}{F}^{-1}_{n+1/2}\,\Delta\underset{\sim}{\sigma}^{(n+1/2)}\,\underset{\sim}{F}^{-T}_{n+1/2})\,\underset{\sim}{U}_{n+1} \tag{5.4}$$

in which all tensor components, except $\underset{\sim}{\sigma}^{(n+1)}$, are measured in the t_n-lamina basis.

Remark 5.2 For the important common case of *infinitesimal strain/large rotation* analysis, $\underset{\sim}{F}_{n+a} \simeq \underset{\sim}{I}$ and $J_{n+a} \simeq 1$ $(0 \leq a \leq 1)$, and Eq. (5.4) simply reduces to ($\underset{\sim}{\sigma}^{n+1}$ in lamina basis at t_{n+1}):

$$\underset{\sim}{\sigma}^{(n+1)} = \underset{\sim}{\sigma}^{(n)} + \Delta\underset{\sim}{\sigma}^{(n+1)} \; ; \; \Delta\underset{\sim}{\sigma}^{(n+1)} = \underset{\sim}{c}\, \Delta\underset{\sim}{e}^{(n+1)} \tag{5.5}$$

5.2 Approximations

Now, with Eq. (4.12) available, our remaining task is to determine *discrete approximations* for $\underset{\sim}{F}_{n+1/2}$ and $\underset{\sim}{D}_{n+1/2}$ from known (n)- and (n+1)-configurations, and $\Delta\underset{\sim}{e}^{(n+1)}$. To this end, certain additional assumptions are needed concerning the deformation ("integration") path during the incremental step. Here, two common assumptions are utilized: (i) *straightline* deformation path and *constant velocity* for each material point, or (ii) *constant material rotation and fiber extension rates.*

For Assumption (i), we can easily show that

$$\underset{\sim}{F}_{n+1/2} = \frac{1}{2}(\underset{\sim}{F}_{n+1} + \underset{\sim}{I}) \; ; \; \underset{\sim}{D}_{n+1/2} = 2[(\underset{\sim}{F}_{n+1} - \underset{\sim}{I})(\underset{\sim}{F}_{n+1} + \underset{\sim}{I})^{-1}]^{s} \tag{5.6}$$

in which "s" indicates the *symmetric* part, and again we emphasize that $\underset{\sim}{F}_{n+1}$ is calculated from its component tensors $\underset{\sim}{R}_{n+1}$ (Remark 4.4) and $\underset{\sim}{U}_{n+1}$ (Eq. 4.12).

For Assumption (ii) here, after "somewhat" lengthy derivation, we find:

$$\underset{\sim}{F}_{n+1/2} = \underset{\sim}{R}^{1/2}_{n+1}\, \underset{\sim}{U}^{1/2}_{n+1} \quad ; \quad \underset{\sim}{D}_{n+1/2} = \underset{\sim}{R}_{n+1/2}[\ell n\ \underset{\sim}{U}_{n+1}]\underset{\sim}{R}^{T}_{n+1/2} \tag{5.7}$$

where

$$\ell n\ \underset{\sim}{U}_{n+1} = \underset{\sim}{M}[\ell n\ \underset{\sim}{\Lambda}]\underset{\sim}{M}^{T} \; ; \; \underset{\sim}{U}_{n+1} = \underset{\sim}{M}\ \underset{\sim}{\Lambda}\ \underset{\sim}{M}^{T} \tag{5.8}$$

The $\underset{\sim}{M}$ is an *orthogonal* matrix containing eigenvectors of $\underset{\sim}{U}_{n+1}$, and *diagonal* matrices $\underset{\sim}{\Lambda}$ and $[\ell n\ \underset{\sim}{\Lambda}]$ contain its eigenvalues (principal stretches) λ_i (i= 1,2,3), and their natural logarithms, respectively.

Remarks 5.3 Instead of Eq. (5.8), the following first-order, Pade-type, *approximation* may be utilized:

$$\ell n\ \underset{\sim}{U}_{n+1} = 2(\underset{\sim}{U}_{n+1} - \underset{\sim}{I})(\underset{\sim}{U}_{n+1} + \underset{\sim}{I})^{-1} \tag{5.9}$$

6. Sample Applications

We consider here three numerical simulations for HMSH5. All results are obtained assuming isotropic semi-linear elastic material behavior, and *except* for some large-strain applications in Sec. 6.3, all other problems were solved using the small-strain/large-rotation assumption. We refer to [30] for additional examples.

6.1 Clamped Square Plate Under Uniform Load

This problem is taken from [31]. Figure 38 depicts the results of HMSH5 utilizing the same 4x4 mesh as for the 4-noded (reduced-integration) model Q4-UI in [31]. It is interesting to note that the average number of iterations per load step (about 3) for the two elements was the same.

6.2 A Pinched Cylinder

This problem has often been used in establishing the viability of shell elements in linear analysis [27]. But to our knowledge, there is currently no "benchmark" solution available for its nonlinear response. Only one-eighth of

the shell was modeled (because of symmetry) using a 16x16 element mesh for HMSH5 (Fig. 39). Ten equal load increments were applied to arrive at the full load of 750 (about four times the load utilized in linear solution). A total of 39 iterations were needed for HMSH5.

6.3 A Pinched Hemisphere

This is another "obstacle test" in linear analysis. It is also an excellent test of the ability of an element to handle "truly" three-dimensional finite rotations. Using symmetry, one quadrant of the shell is modeled with 10x10 mesh for HMSH5. The total load F=100 is first considered here for the small/large rotation analysis (recall that F=1 is typically used for the linear case). Only two loading steps are required for HMSH5 from F=0→10 and F=10→100 with a total of 13 iterations. Results are shown in Fig. 40, together with the solution reported in [89] using the resultant-based shell element, Q4S, with a 16x16 mesh.

In addition, a *large strain* analysis using the algorithm of Eqs. (5.4) and (5.6) and the same 10x10 mesh for HMSH5 was also performed for the above shell subjected to a very high load level F=900. We utilized two and 8 equal load steps for F=0→100 and F=100→900, respectively. Significant deformations occurred in this case; e.g. at the final load level (F=900), u_A=4.922 and v_B=12.709, with a total rotation of nearly 123 degrees at B. A summary of the results is given in Table 11, where we also report the results obtained from an independent infinitesimal-strain solution version for comparison. Note that the total (accumulated) strains at F=900 are now of the order of 3%.

As evident from Table 11, although there are no discernible differences between the two solutions above for displacements and rotations at most load levels, the "large-strain" update procedure produced *significant reductions* in the number of equilibrium iterations required for convergence at higher load (strain) levels; e.g. from 23 to 16 iterations for F=500→900. This is, of course, due to the more accurate stress calculated in this latter case, and will become even more important in cases when "stress-dependent" viscoplastic models are utilized.

7. Conclusions

We presented here the fully-nonlinear formulation of curved shells using the simple mixed model HMSH5. Several noteworthy aspects are included. A careful selection is made for the polynomial functions in the strain assumption, thus leading to robust elements (i.e., kinematically stable, free from locking, etc.). A geometrically-exact procedure is utilized for element configuration update with finite nodal rotations. Even with a "single" geometric stiffness matrix, this was shown to be capable of attaining quadratic convergence rate in practical shell applications [30]. It is also the complete geometric matrix needed for adequate modeling of "significant" instability modes; e.g. in creep buckling studies of composites under thermomechanical loadings.

For updating of the spatial stress field in the presence of non-infinitesimal strains, "objective" generalized midpoint schemes were developed by making use of the polar-decomposition of the deformation gradient. These are in keeping with the underlying mixed method.

Several numerical simulations have been presented to demonstrate the effectiveness and practical usefulness of the proposed formulation.

Our future work will focus on extensive testing of the validity of the proposed solution algorithms in the context of life prediction studies of high-temperature composite plates and shells. In particular, a variable stiffness formulation for unified viscoplastic models with damage will be developed and used in several "benchmark" solutions of static and dynamic problems.

REFERENCES

1. Chamis, C.C., and Hopkins, D.A., "Thermoviscoplastic Nonlinear Constitutive Relationships for Structural Analysis of High Temperature Metal Matrix Composites," NASA TM-87291, 1985.

2. Walker, K.P., "Research and Development Program for Nonlinear Structural Modeling with Advanced Time-Temperature Dependent Constitutive Relationships," NASA CR-165533, 1981.

3. Walker, K.P., Jordan, E.H., and Freed, A.D., "Nonlinear Mesomechanics of Composites with Periodic Microctructure: First Report," NASA, Report, 1989.

4. Robinson, D.N., Duffy, S.F., and Ellis, J.R., "A Viscoplastic Constitutive Theory for Metal Matrix Composites at High Temperature," NASA CR-179530, 1986.

5. Chaboche, J.L., "Cyclic Plasticity Modeling and Ratcheting Effects," Proceedings, 2nd Int. Conf. on Constitutive Laws for Engineering Materials (C.S. Desai, et al., eds.), Elsevier, 1987, pp. 47-58.

6. Haritos, G.K., Hager, J.W., Amos, A.K., Salkind, M.J. and Wang, A.S.D., "Mesomechanics: The Microstructure-Mechanics Connection," Int. J. Solids and Struct., Vol. 24, No. 11, 1988, pp. 1081-1096.

7. Onat, E.T., and Leckie, F.A., "Theoretical Damage Mechanics for Metal-Metal Composites," Report, NASA TR-1987.

8. Bahei-El-Din, Y.A., and Dvorak, G.J., "Plasticity Analysis of Laminated Composite Plates," J. Applied Mechanics, ASME, Vol. 49, 1982, pp. 740-746.

9. Dvorak, G.J., and Bahei-El-Din, Y.A., "Plasticity Analysis of Fibrous Composites," J. Applied Mechanics, ASME, Vol. 49, 1982, pp. 327-335.

10. Arnold, S.M., "A Transversely-Isotropic Thermoelastic Theory," NASA TM-101302, 1988.

11. Willam, K.J., "Numerical Solution of Inelastic Rate Processes," Computers & Structures, 8, May 1978, pp. 511-531.

12. Chulya, A., and Walker, K.P., "A New Valid Asymptotic Implicit Integration Algorithm for Elasto-Plastic, Creep, and Viscoplastic Theories Including Continuum Damage," to appear as a NASA TM, 1989.

13. Chang, T.Y., Chen, J.Y., and Chu, S.C., "Viscoplastic Finite Element Analysis by Automatic Subincrementing Technique," J. of Eng. Mech., ASCE, Vol. 114, No. 1, January 1988, pp. 80-96.

14. Sotolongo, W., and McDowell, D.L., "On the Integration of Elasto-Plastic Constitutive Model Structure for Non-Proportional Cyclic Loading," Computers & Structures, Vol. 24, No. 4, 1986, pp. 595-606.

15. Bathe, K.J., and Dvorkin, E.N., "On the Automatic Solution of Nonlinear Finite Element Equations," Computers & Structures, Vol. 17, 1983, pp. 871-879.

16. Park, K.C., "A Family of Solution Algorithms for Nonlinear Structural Analysis Based on Relaxation Equations," Int. J. Num. Meth. Engng., Vol. 18, 1982, pp. 1337-1347.

17. Bellini, P.X., and Chulya, A., "An Improved Automatic Incremental Algorithm for the Efficient Solution of Nonlinear Finite Element Equations," Computers & Structures, Vol. 26, No. 1/2, 1987, pp. 99-110.

18. Chang, T.Y., "NFAP - A Nonlinear Finite Element Analysis Program," Users Manual (Version 87.1), Department of Civil Engineering, University of Akron, Akron, OH, June 30, 1987.

19. Kachanov, L.M., "Introduction to Continuum Damage Mechanics," Martinus Nijhoff Publishers, 1986.

20. Simo, J.C., Ju, J.W., Taylor, R.L., and Pister, K.S., "On Strain-Based Continuum Damage Models: Formulation and Computational Aspects," Proceedings, 2nd Int. Conf. on Constitutive Laws for Engineering Materials, C.S. Desai, et. al., eds., Elsevier, 1987, pp. 233-246.

21. Bazant, Z.P., and Belytschko, T., "Strain-Softening Continuum Damage: Localization and Size Effect," Proceedings, 2nd Int. Conf. on Constitutive Laws for Engineering Materials, C.S. Desai, et.al., eds., Elsevier, 1987, pp. 11-34.

22. Chow, C.L., and Wang, J., "An Anisotropic Theory of Elasticity for Continuum Damage Mechanics," Int. J. Fracture, Vol. 33, 1987, pp. 3-16.

23. Miller, A.K., and Tanaka, T.G., "NONSS: A New Method for Integrating Unified Constitutive Equations Under Complex Histories," J. Eng. Mat. and Tech., ASME, Vol. 110, 1988, pp. 205-211.

24. Oden, J.T., Fly, F.W., and Mahadevan, L., "A Hybrid/Stress Finite Element Approach for Stress and Vibration in Linear Anisotropic Elasticity," Report TR-87-05, submitted to NASA-Marshall Space Flight Center, AL, 1987.

25. Saleeb, A.f., and Chang, T.Y., "An Efficient Quadrilateral Element for Plate Bending Analysis," Int. J. for Numerical Methods in Engng., Vol. 24, 1987, pp. 1123-1155.

26. Saleeb, A.F., and Chang, T.Y., "On the Mixed Formulation of Curved Beam Elements," J. of C omputer Method in Applied Mechanics and Engineering, Vol. 60, 1987, pp. 95-121.

27. Saleeb, A.F., Chang, T.Y., and Graf, W., "A Quadrilateral Shell Element Using a Mixed Formulation," Int. J. of Computers & Structures, Vol. 26, No. 5, 1987, pp. 787-803.

28. Saleeb, A.F., Chang, T.Y., and Yingyeungyong, S., "A Mixed Formulation of Co-Linear Triangular Plate/Shell Element - The Role of Edge Shear Constraints," to appear in Int. J. for Numerical Methods in Engng., 1988.

29. Chang, T.Y., Saleeb, A.F., and Graf, W., "On the Mixed Formulation of a 9-Node Lagrange Shell Element," submitted for publications in Computer Methods in Applied Mechanics and Engineering, 1987.

30. Saleeb, A.F., Chang, T.Y., Graf, W., and Yingyeungyong, S., "A Hybrid/Mixed Model for Nonlinear Shell Analysis and Its Applications to Large-Rotation Problems," submitted, Int. J. Num. Meth., Eng., 1988.

31. Hughes, T.J.R., and Liu, W.K., "Nonlinear Finite Element Analysis of Shells, Part I - Three Dimensional Shells," Comp. Meth. Appl. Mech. Engr. Vol. 26, 1981, pp. 331-362.

32. Spilker, R.L., "Invariant 8_node Hybrid Stress Element for Thick and Thin Multilayer Laminated Plates," Int. J. Num. Meth. Engng., Vol. 20, 573-582, 1984.

33. Bert, C.W., "A Critical Evaluation of New Plate Theories Applied to Laminated Composites," Report OU-AMNE-83-3, 1983.

34. Reddy, J.N., "A Simple Higher-Order Theory for Laminated Composite Plates," J. Appl. Mech., Vol. 51, 745-752, 1984.

35. Lo, K.H., Christensen, R.M., and Wu, E.M., "A High-Order Theory of Plate Deformation, Part 2: Laminated Plates," J. Appl. Mech., Vol. 44, 669-676, 1977.

36. Murakami, H., "Laminated Composite Plate Theory With Improved In-Plane Responses," J. Appl. Mech., Vol. 53, 661-666, 1986.

37. Spilker, R.L., "A Hybrid-Stress Finite Element Formulation for Thick Multilayer Laminates," Computers and Structures, Vol. 11, 507-514, 1980.

38. Spilker, R.L., "Hybrid-Stress Eight-Node Elements for Thin and Thick Multilayer Laminated Plates," Int. J. Num. Meth. Engng., Vol. 18, 801-828, 1982.

39. Spilker, R.L., Jakobs, D.M., Engelmann, B.E., "Efficient Hybrid Stress Isoparametric Elements for Moderately Thick and Thin Multilayer Plates," in Hybrid and Mixed Finite Element Methods, AMD-Vol. 73, ASME, 1985.

40. Chaudhuri, R.A., and Seide, P., "Triangular Finite Element for Analysis of Thick Laminated Plates," Int. J. Num. Meth. Engng., Vol. 24, 1203-1224, 1987.

41. Panda, S.C., and Natarajan, R., "Finite Element Analysis of Laminated Composite Plates," Int. J. Num. Meth. Engng., Vol. 14, 69-79, 1979.

42. Chang, T.Y., and Sawamiphakdi, K., "Large Deformation Analysis of Laminated Shells by Finite Element Method," Computers and Structures, Vol. 13, 331-340, 1981.

43. Reddy, J.N., and Phan, N.D., "Analysis of Laminated Composite Plates Using a Higher-Order Shear Deformation Theory," Int. J. Num. Meth. Engng., Vol. 21, 2201-2219, 1985.

44. Rogers, C.A., and Knight, C.E., "An Axisymmetric Linear/High-Order Finite Element for Filament - Wound Composites - I, Formulation and Algorithm," Computers and Structures, Vol. 29, 265-271, 1988.

45. Haas, D.J., and Lee, S.W., "A Nine-Node Assumed-Strain Finite Element for Composite Plates and Shells," Computers and Structures, Vol. 26, 445-452, 1987.

46. Mawenya, A.S., and Davies, J.D., "Finite Element Bending Analysis of Multilayer Plates, Int. J. Num. Meth. Engng., Vol. 8, 215-225, 1974.

47. Lakshminarayana, H.V., and Murthy, S.S., "A Shear-Flexible Triangular Finite Element Model for Laminated Composite Plates," Int. J. Num. Meth. Engng., Vol. 20, 591-623, 1984.

48. Pagano, N.J., "Exact Solutions for Composite Laminates in Cylindrical Bending," J. Comp. Maters., Vol. 3, 398-411, 1969.

49. Whitney, J.M., and Leissa, A.W., "Analysis of Heterogeneous Anisotropic Plates," J. Appl. Mech., Vol. 36, 261-266, 1969.

50. Reddy, J.N., Analysis of Layered Composite Plates Accounting for Large Deflections and Transverse Shear Strains, prepared for Recent Advances in Nonlinear Computational Mechanics, edited by E.Hinton, C. Taylor, and D.R.J. Owen, Pine Ridge Pressss, Swansea, U.K., 1981.

51. Reddy, J.N., "A Penalty Plate Bending Element for the Analysis of Laminated Anisotropic Composites Plates," Int. J. Num. Meth. Engng., Vol. 15, 1187-1206, 1980.

52. Reddy, J.N., "Exact and Finite-Element Analysis of Laminated Shells," Dept. of Engineering Science and Mechanics, VPI, November, 1983.

53. Reddy, J.N., and Chandrashekhara, K., "Geometrically Nonlinear Analysis of Laminated Shells Including Transverse Shear Strains," Department of Engineering Science and Mechanics, VPI, November, 1983.

54. Whitney, J.M., "Shear Correction Factors for Orthotropic Laminates Under Static Load," J. Appl. Mech., Vol. 40, 302-304, 1973.

55. Noor, Ahmed K., and Peters, Jeanne M., "A Posteriori Estimates for the Shear Correction Factors in Multilayered Composite Cylinders," NASA Langley Research Center, April. 1988.

56. Pagano, N.J., "Exact Solutions for Composite Laminates in Cylindrical Bending," J. Composite Materials, Vol. 3, 398-411, 1969.

57. Pagano, N.J., "Influence of Shear Coupling in Cylindrical Bending of Anisotropic Laminates," J. Composite Materials, Vol. 4, 330-343, 1970.

58. Chaudhuri, R.A., and Seide, Paul, "An Approximate Semi-analytical Method for Prediction of Interlaminate Shear Stresses in an Arbitrarily Laminated Thick Plate," Computers and Structures, Vol. 25, 627-636, 1987.

59. Chaudhuri, R.A., "An Equilibrium Method for Prediction of Transverse Shear Stresses in a Thick Laminated Plate," Computers and Structures, Vol. 23, 139-146, 1986.

60. Kidder, Robert L., "Reduction of Structural Frequency Equations," AIAA Journal, Vol. 11, p. 892, 1973.

61. Paz, Mario, "Dynamic Condensation," AIAA Journal, Vol. 22, 724-727, 1983.

62. Paz, Mario, "Modified Dynamic Condensation Method," J. of Struct. Engng., ASCE, Vol. 115, 234-238, 1989.

63. Guyan, Robert J., "Reduction of Stiffness and Mass Matrices," AIAA Journal, Vol. 3, p. 380, 1965.

64. Owen, D.R.J., and Li, Z.H., "A Refined Analysis of Laminated Plates by Finite Element Displacement Methods - II. Vibrations and Stability," Computers and Structures, Vol. 26, 915-923, 1987.

65. Anderson, R.G., Irons, B.M., and Zienkiewicz, O.C., "Vibration and Stability of Plates Using Finite Elements," Int. J. Solids and Structures, Vol. 4, 1031-1055, 1968.

66. Kumar, V., Marjaria, M., Mukherjee, S., "Numerical Integration of Some Stiff Constitutive Models of Inelastic Deformations," J. of Engng. Mat. and Tech., Vol. 102, 92-96, 1980.

67. Comereau, I., "Numerical Stability in Quasi-static Elasto/Visco Plasticity," Int. J. for Num. Meth. in Engng, Vol. 9, 107-127, 1984.

68. Miller, A.K., Tanaka, T.G., "A New Method for Integrating Unified Constitutive Equations Under Complex Histories," J. of Engng. Mat. and Tech., Vol. 2110/205, 1988.

69. Brockman, R.A., "Explicit Forms for the Tangent Modulus Tensor in Viscoplastic Stress Analysis," Int. J. for Num. Meth. in Engng., Vol. 20, 315-319, 1984.

70. Pierce, D., Shih, C.F., Needelman, A., "A Tangent Modulus Method for Rate Dependent Solids," Comp. and Struc., Vol. 18, 875-887, 1987.

71. Chaboche, J.L., "A Review of Computational Methods for Cyclic Plasticity and Viscoplasticity," Computational Plasticity, Ed. by R.J. Owen, E. Hinton, and E. Oñate, Proc. of the International Conf. held in Barcelona, Spain, April 6-10, 1987.

72. Walker, K.P., "A Uniformly Valid Asymptotic Integration Algorithm for Unified Viscoplastic Constitutive Models," Advances in Inelastic Analysis, Eds. S. Nakazawa, K. Willam, and N. Rebelo, ASME AMD-Vol. 88, PED-Vol. 28, 1987.

73. Hughes, T.J.R., Taylor, R.L., "Unconditionally Stable Algorithm for Quasi-Static Elasto Visco-Plastic Finite Element Analysis," Comp. and Struc., Vol. 8, 169-173, 1978.

74. Damjanic, F., Owen, D.R.J., "Implicit Time Integration of Elasto Visco-Plastic Solids Subject to the Mohr-Coloumb Yield Criterion," Int. J. for Num. Meth. in Engng., Vol. 18, 1873-1881, 1982.

75. Nyssen, C., "An Efficient and Accurate Iterative Method Allowing Large Incremental Steps to Solve Elasto Plastic Problems," Comp. and Struc., Vol. 13, 68-71, 1981.

76. Chang, T.Y., Chang, J.P., "Viscoplastic Analysis of Metalic Structures by Finite Elements Methods," Civil Engng. Dept., Univ. of Akron, 1985.

77. Chen, H., Krempl, E., "An Adaptive Time Stepping Scheme for the Viscoplasticity Theory Based on Over Stresses," Comp. and Struc., Vol. 22(4), 573-578, 1986.

78. Chen, H., Kremple, E., "A Two Steps Finite Element Integration Scheme for Viscoplasticity Theory Based on Over Stresses," Comp. and Struc., Vol. 22(4), 625-628, 1986.

79. Walker, K.P., "Representation of Hastelloy-X Behavior at Elevated Temperature with a Functional Theory of Viscoplasticity," United Tech. Research Center, Connecticut, 1985.

80. Robinson, D.N., "A United Creep-Plasticity Model for Structural Metals at High Temperature," ORNL Technical Report TM-5969, Oak Ridge National Laboratory, 1978.

81. Bodner, S.R., Parton, Y., "Constitutive Equations for Elastic Viscoplastic Strain Hardening Materials," J. of Appl. Mech., 385-389, 1975.

82. Freed, A.D., "A Thermoviscoplastic Model with Application to Cupper," NASA Lewis Research Center, Cleveland, OH 1988.

83. Freed, A.D., "Refinements in a Thermo-Visco-Plastic-Model for Metals: characterization of Al, Cu, Ni, W, NASA Lewis Research Center, Cleveland, OH, 1989.

84. Bathe, K.J., Finite Element Procedures in Engineering Analysis, Prentice Hall, Englewood Cliffs, NJ, 1982.

85. Boland, P.L., and Pian, T.H.H., "Large Deflection Analysis of Thin Elastic Structures by the Assumed Stress Hybrid Finite Element Method," Comp. and Struct., Vol. 1, 1-12, 1977.

86. Hughes, T.J.R., and Carnoy, E., "Nonlinear Finite Element Shell Formulation Accounting for Large Membrane Strains," Comp. Meth. Appl. Mech. Engr., Vol. 39, 69-82, 1983.

87. Parisch, H., "Large Displacements of Shells Including Material Nonlinearities," Comp. Meth. Appl. Mech. Engr., Vol. 27, 183-214, 1981.

88. Surana, K.S., "Geometrically Nonlinear Formulation for Curved Shell Elements," Int. J. Num. Meth. Engr., Vol. 19, 581-615, 1983.

89. Simo, J.C., Fox, D.D., and Rifai, M.S., "Formulation and Computational Aspects of a Stress Resultant Geometrically Exact Shell Model," in Computational Mechanics '88: Theory and Applications, Vol. 1, S.N. Atluri and G. Yagawa (eds.), Springer-Verlag, Berlin, 26.ii.1-26.ii.9, 1988.

90. Marsden, J.E., and Hughes, T.J.R., Mathematical Foundations of Elasticity Prentice Hall, Englewood Cliffs, NJ, 1983.

91. Argyris, J.H., "An Excursion into Large Rotations," Comp. Meth. Appl. Mech. Engr., Vol. 32, 85-155, 1982.

92. Simo, J.C., and Vu-Quoc, L., "A Three-Dimensional Finite Strain Rod Model Part II: Computational Aspects," Comp. Meth. Appl. Mech. Engr., Vol. 58, 79-116, 1986.

93. Atluri, S.N., "On Constitutive Relations at Finite Strain: Hypoelasticity and Elastoplasticity with Isotropic or Kinematic Hardening," Comp. Meth. Appl. Mech. Engr., Vol. 43, 137-171, 1984.

94. Simo, J.C., "A Framework for Finite Strain Elastoplasticity Based on Maximum Plastic Dissipation and the Multiplicative Decomposition: Part I Continuum Formulation," Comp. Meth. Appl. Mech. Engr., Vol. 66, 199-219, 1988.

95. Hughes, T.J.R., and Winget, J., "Finite Rotation Effects in Numerical Integration of Rate Constitutive Equations Arising in Large-Deformation Analysis," Int. J. Num. Meth. Engr., Vol. 15, 1862-1867, 1980.

96. Nagtegaal, J.C., and De Jong, J.E., "Some Computational Aspects of Elastic-Plastic Large Strain Analysis," Int. J. Num. Meth. Engr., Vol. 17, 15-41, 1981.

97. Pinsky, P.M., Ortiz, M., and Pister, K.S., "Numerical Integration of Rate Constitutive Equations in Finite Deformation Analysis," Comp. Meth. Appl. Mech. Engr., Vol. 40, 137-158, 1983.

98. Argyris, J.H., Doltsinis, J.S., Pimenta, P.M., and Wustenberg, H., "Thermomechanical Response of Solids at High Strains-Natural Approach," Comp. Meth. Appl. Mech. Engr., Vol. 32, 3-57, 1982.

99. Rubinstein, R., and Atluri, S.N., "Objectivity of Incremental Constitutive Relations over Finite Time Steps in Computational Finite Deformation Analysis," Comp. Meth. Appl. Mech. Engr., Vol. 36, 277-290, 1983.

100. Pian, T.H.H., "Variational Principles for Incremental Finite Element Methods," Journal of the Franklin Institute, Vol. 302, 473-488, 1976.

Table 1

A Cantilever Laminated Beam with In-Plane Load

Laminate	Deflection at Tip		
	Exact	Present F.E.	TRIPLT
$[0]$	0.0853	0.0862	0.0864
$[30]$	1.320	1.363	1.0956
$[\pm 30]_s$	0.4292	0.4230	0.3543
$[0/\pm 45/90]_s$	0.2351	0.2406	0.2353
$[0/90]$	0.1663	0.1671	0.1673

Table 2

Mesh Convergence Study for Clamped
1 Layer Rectangular Plate
Normalized Center Deflection

Laminate	Present F.E.				TRIPLT
	(4 x 4)	(6 x 6)	(8 x 8)	(10 x 10)	(8 x 8)
[5]	10.4598 (-0.74%)	10.9851 (+4.25%)	10.9592 (+4.0%)	10.8879 (+3.33%)	10.5375
[15]	9.3339 (-1.18%)	9.9972 (+5.84%)	10.0391 (+6.28%)	10.0215 (+6.10%)	9.4455
[25]	5.9319 (-2.53%)	6.5407 (+7.48%)	6.5245 (+7.21%)	6.5132 (+7.03%)	6.0856
[35]	2.9553 (+1.96%)	2.9991 (+3.47%)	2.9269 (+0.98%)	2.9226 (+0.83%)	2.8985
[45]	1.6414 (+16.09%)	1.3695 (-3.14%)	1.3644 (-3.50%)	1.3820 (-2.26%)	1.4139
[75]	1.1334 (+24.09%)	0.7911 (-13.39%)	0.9000 (-1.46%)	0.9133 (0.%)	0.9134
[90]	0.9962 (+24.26%)	0.6608 (-17.57%)	0.8116 (+1.23%)	0.8073 (+0.70%)	0.8017
D.O.F.	125	245	405	605	1215

Table 3

Clamped Rectangular Plate
with Uniform Pressure

Laminate	Normalized Center Deflection, $\bar{w}$	
	TRIPLT	Present F.E.
[0]	10.537	10.888
[15]	9.4455	10.022
[30]	6.0856	6.5132
[45]	2.8985	2.9226
[60]	1.4139	1.3820
[75]	0.9134	0.9133
[90]	0.8017	0.8073

Table 4

Clamped Square Plate
with Uniform Pressure

Laminate	Normalized Center Deflection, $\bar{w}$		
	Exact	Present F.E.	MQH3T
[±5]	0.0946	0.1040	0.1083
[±25]	0.2355	0.2602	0.2572
[±35]	0.2763	0.2914	0.2844
[±45]	0.2890	0.3013	0.2929

Table 5

Simply Supported Square Plate
with Uniform Pressure

Laminate	Normalized Center Deflection, $\bar{w}$			
	Exact	Present F.E.	TRIPLT	V2R
[±5]	0.592	0.614	0.606	0.595
[±25]	0.984	1.045	0.992	0.983
[±35]	0.945	1.041	0.952	0.944
[±45]	0.9150	1.033	0.922	0.914

Table 6

Bending Moment M_{xx} for a Simply Supported
2 Layer Square Plate

Laminate	M_{xx}			
	Exact	Present F.E.	TRIPLT	V2R
[±5]	1318.	1509.	1327.	1396.2
[±15]	1142.	1137.6	1150.	1176.8
[±25]	843.6	842.5	851.3	855.6
[±35]	564.6	591.9	573.1	567.8
[±45]	368.1	422.17	375.3	371.3

Table 7

Bending Moment M_{yy} for a Simply Supported
2 Layer Square Plate

Laminate	M_{yy}			
	Exact	Present F.E.	TRIPLT	V2R
[±5]	34.2	37.56	34.47	34.99
[±15]	123.4	123.64	124.4	126.4
[±25]	226.0	221.37	228.4	221.5
[±35]	304.1	314.02	308.8	305.1
[±45]	368.1	422.17	375.3	371.3

Table 8

Mesh Convergence Study for Isotropic Cantilevered Plate

Frequency	Present F.E. (4 x 4)	(6 x 6)	(8 x 8)	(10 x 10)	Ref. [65]
1	3.34	3.39	3.41	3.42	3.50
2	13.32	13.82	14.07	14.20	14.50
3	19.46	20.43	20.80	20.98	21.70
4	40.94	43.58	44.91	45.62	48.10
5	51.22	55.32	56.98	57.82	60.50
6	71.62	78.81	83.08	85.38	92.30

Table 9

Anisotropic Cantilever Beam Solution
Fundamental Frequency, ω_1

Fiber Direction	Oden et.al [24] (I)	(II)	Present F.E.
0	14.351	14.130	14.232
30	13.307	13.020	13.086
45	12.873	12.679	12.757
60	13.307	13.020	13.086
90	14.351	14.130	14.232

Table 10

Anisotropic Cantilever Beam Solution
Second Frequency, ω_2

Fiber Direction	Oden et.al [24] (I)	(II)	Present F.E.
0	85.950	83.675	84.484
30	80.673	78.264	78.147
45	78.379	76.499	76.389
60	80.379	78.264	78.147
90	85.950	83.675	84.484

Table 11

Comparison of Results for the Solutions of the Pinched Hemisphere (10 x 10 mesh); see Fig. 40

Load	Infinitesimal-Strain Solution					Large-Strain Solution				
F	u_A	v_B	$\|\underset{\sim}{e}_A\|$ (rad)	$\|\underset{\sim}{e}_B\|$ (rad)	Iterations	u_A	v_B	$\|\underset{\sim}{e}_A\|$	$\|\underset{\sim}{e}_B\|$	Iterations
50	2.562	3.797	0.543	0.745	6	2.562	3.797	0.543	0.745	6
100	3.295	5.713	0.727	1.105	5	3.295	5.711	0.727	1.105	5
200	3.867	7.637	0.907	1.470	5	3.867	7.636	0.907	1.469	5
300	4.162	8.721	1.023	1.663	4	4.164	8.725	1.023	1.663	4
400	4.426	9.712	1.138	1.802	5	4.429	9.721	1.139	1.803	5
500	4.650	10.763	1.234	1.920	6	4.652	10.772	1.235	1.921	6
600	4.782	11.559	1.269	2.008	6	4.782	11.563	1.270	2.009	4
700	4.851	12.070	1.260	2.069	5	4.851	12.067	1.260	2.069	4
800	4.894	12.432	1.224	2.114	5	4.893	12.422	1.226	2.114	4
900	4.925	12.739	1.146	2.153	7	4.922	12.709	1.165	2.150	4

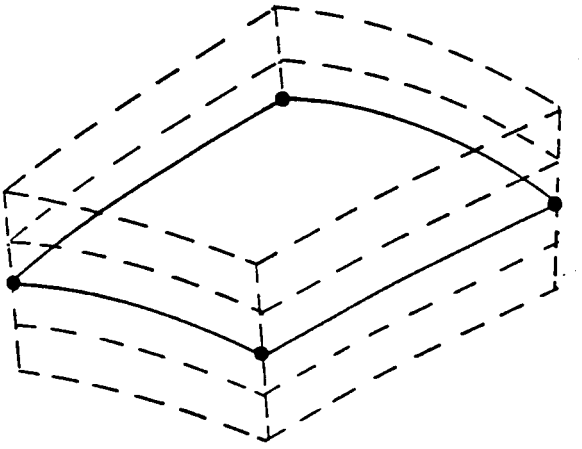

Figure 1: 4-Node element at mid-plane of multi-layered composite

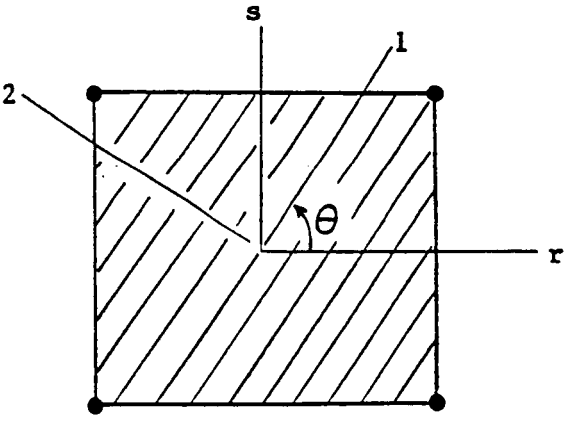

Figure 2: Local fiber orientation with respect to element coordinates

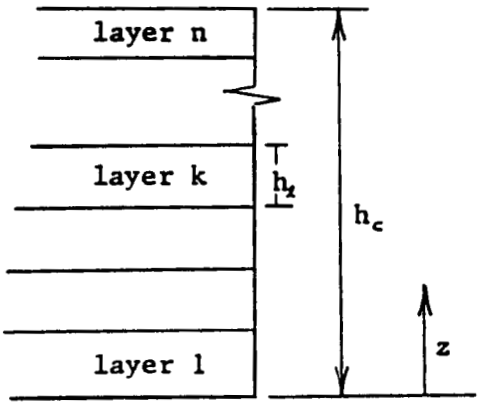

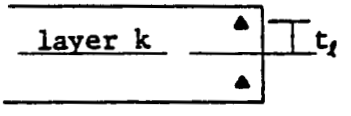

Location of layer integration points, t_l

Figure 3: Multi-layer composite

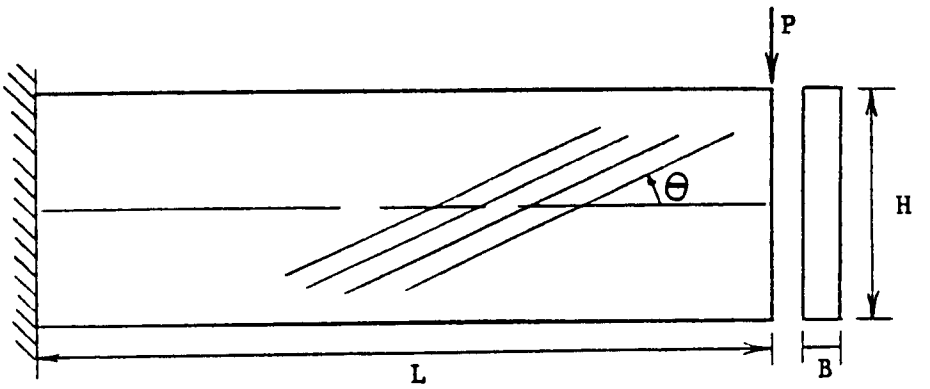

L/B=40 H/B=10 P=1.0

Figure 4: Cantilever beam subjected to in-plane point load

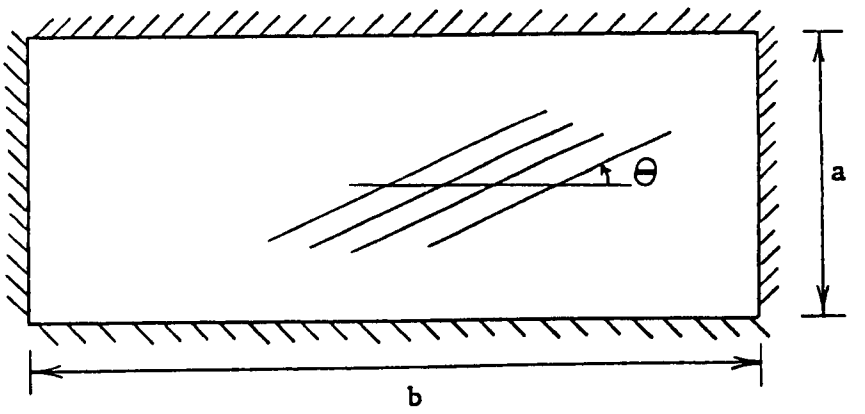

Figure 5: Clamped rectangular plate

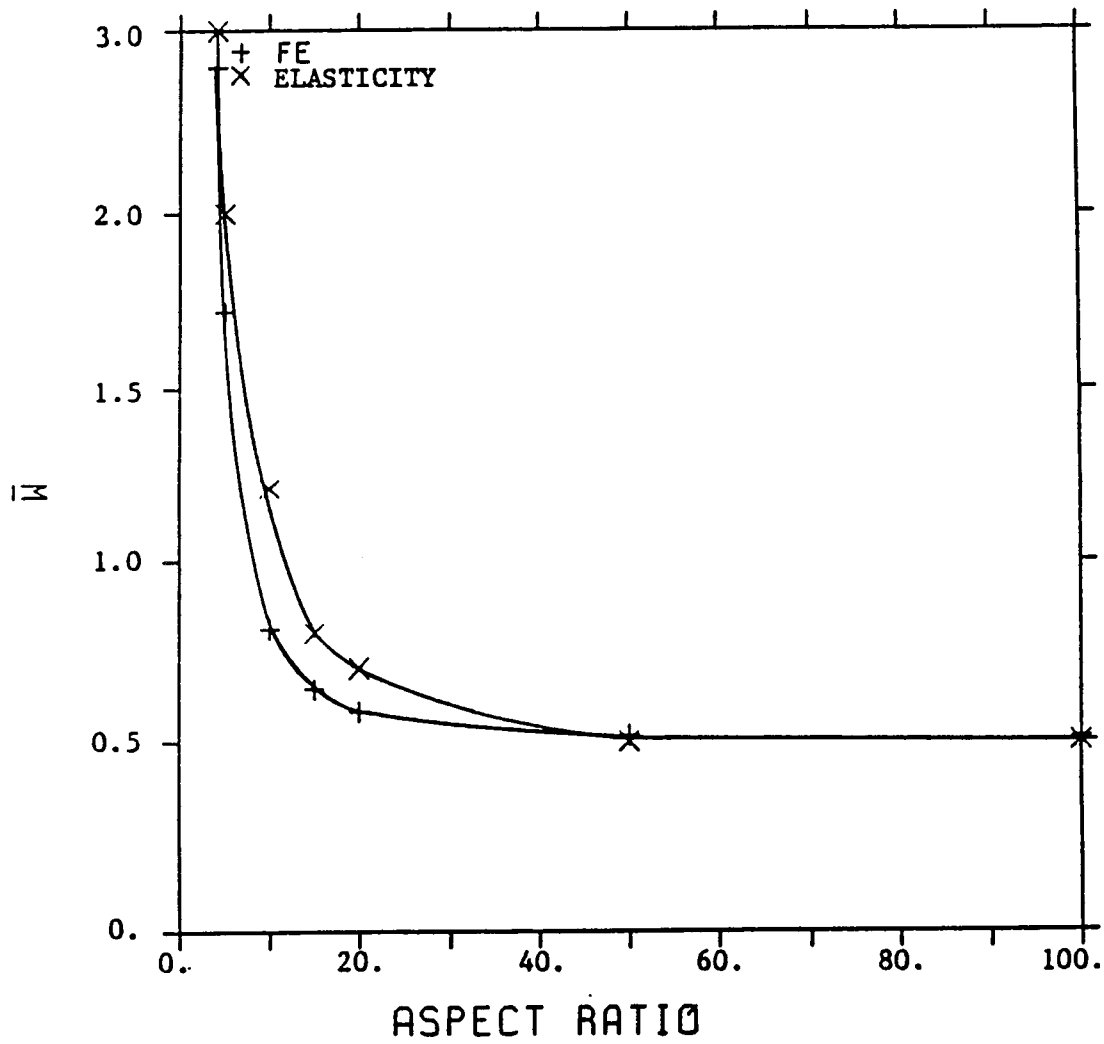

Figure 6: Deflection $\bar{w}$ for [0/90/0] laminate

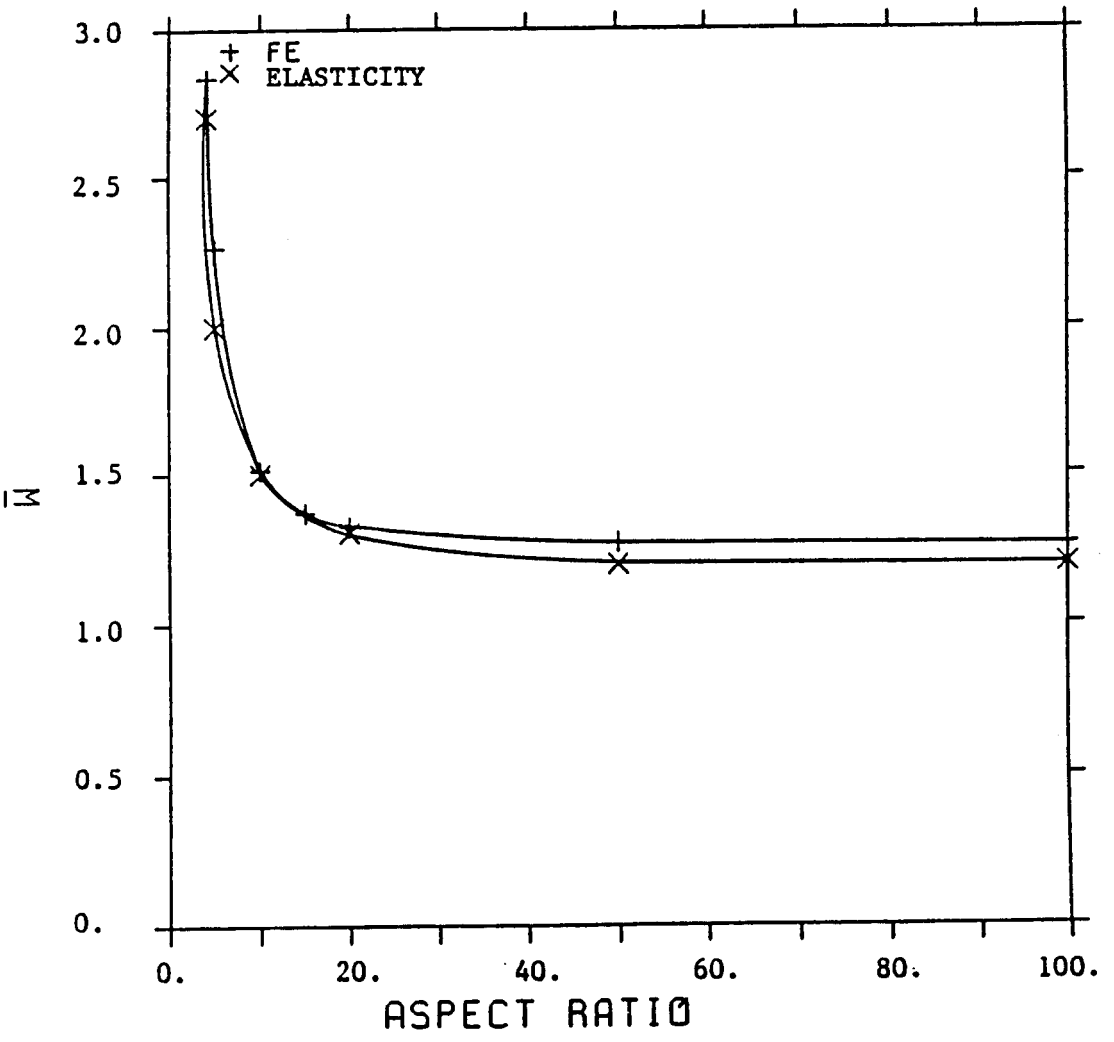

Figure 7: Deflection $\bar{w}$ for [± 15] laminate

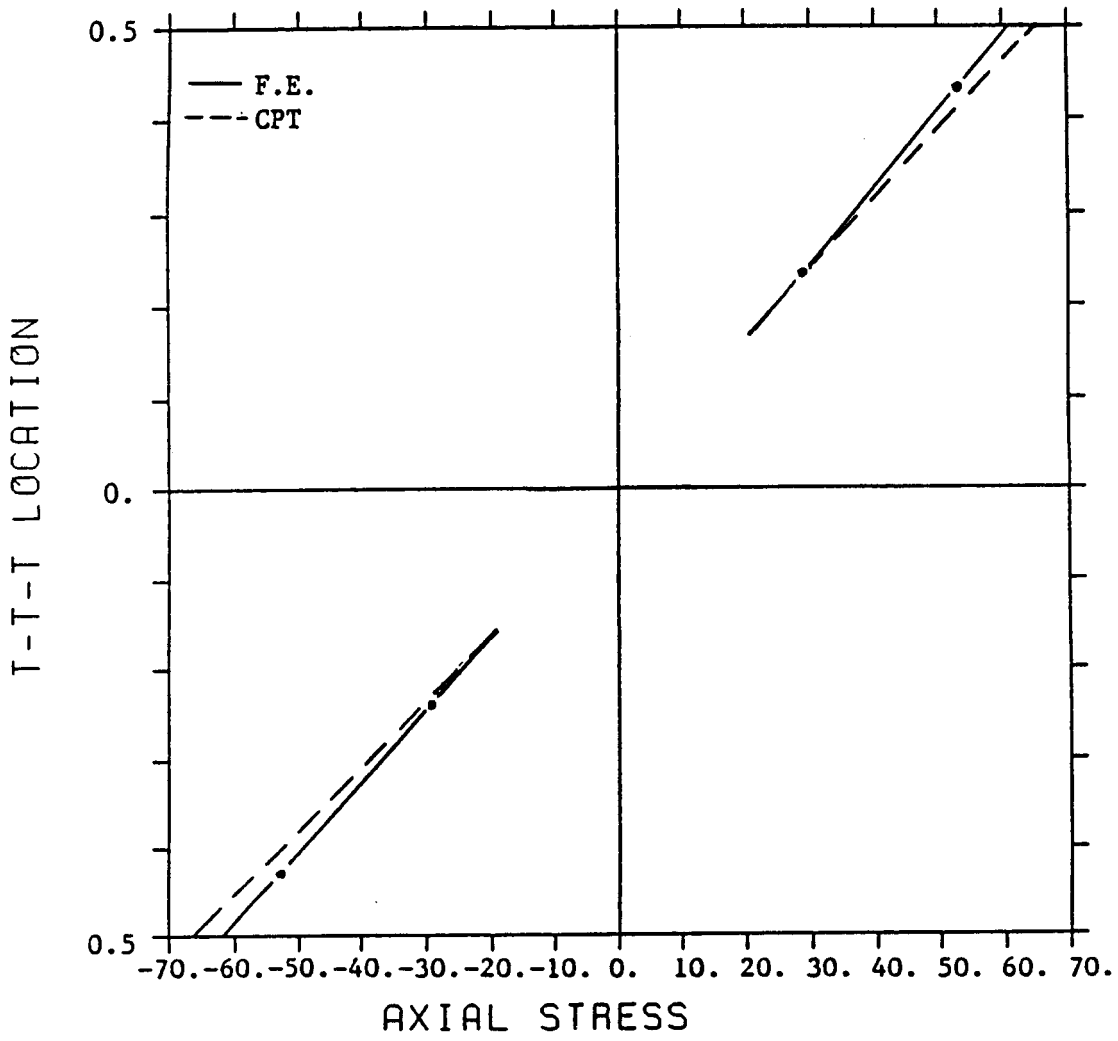

Figure 8: [0/90/0] σ_x stress distribution

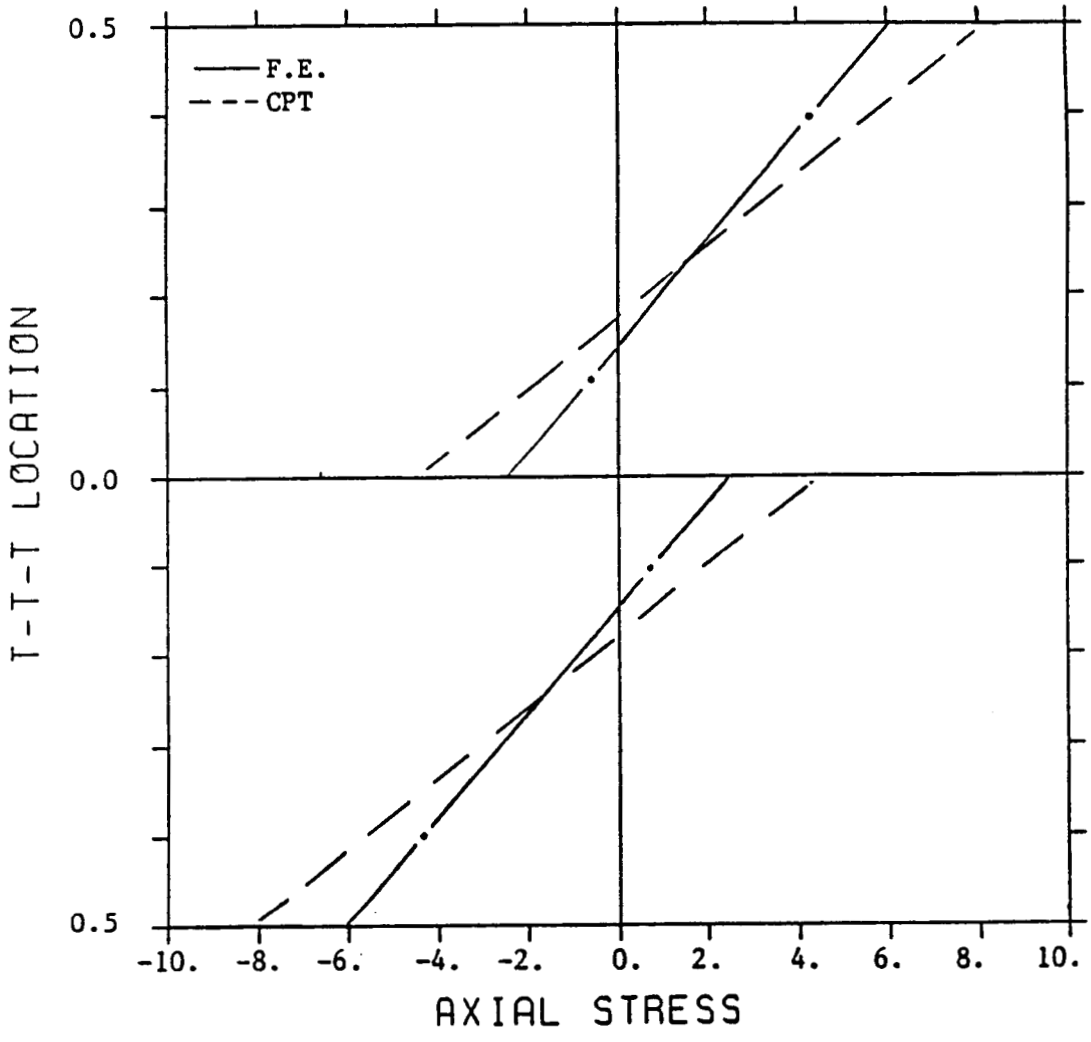

Figure 9: [± 15] σ_x stress distribution

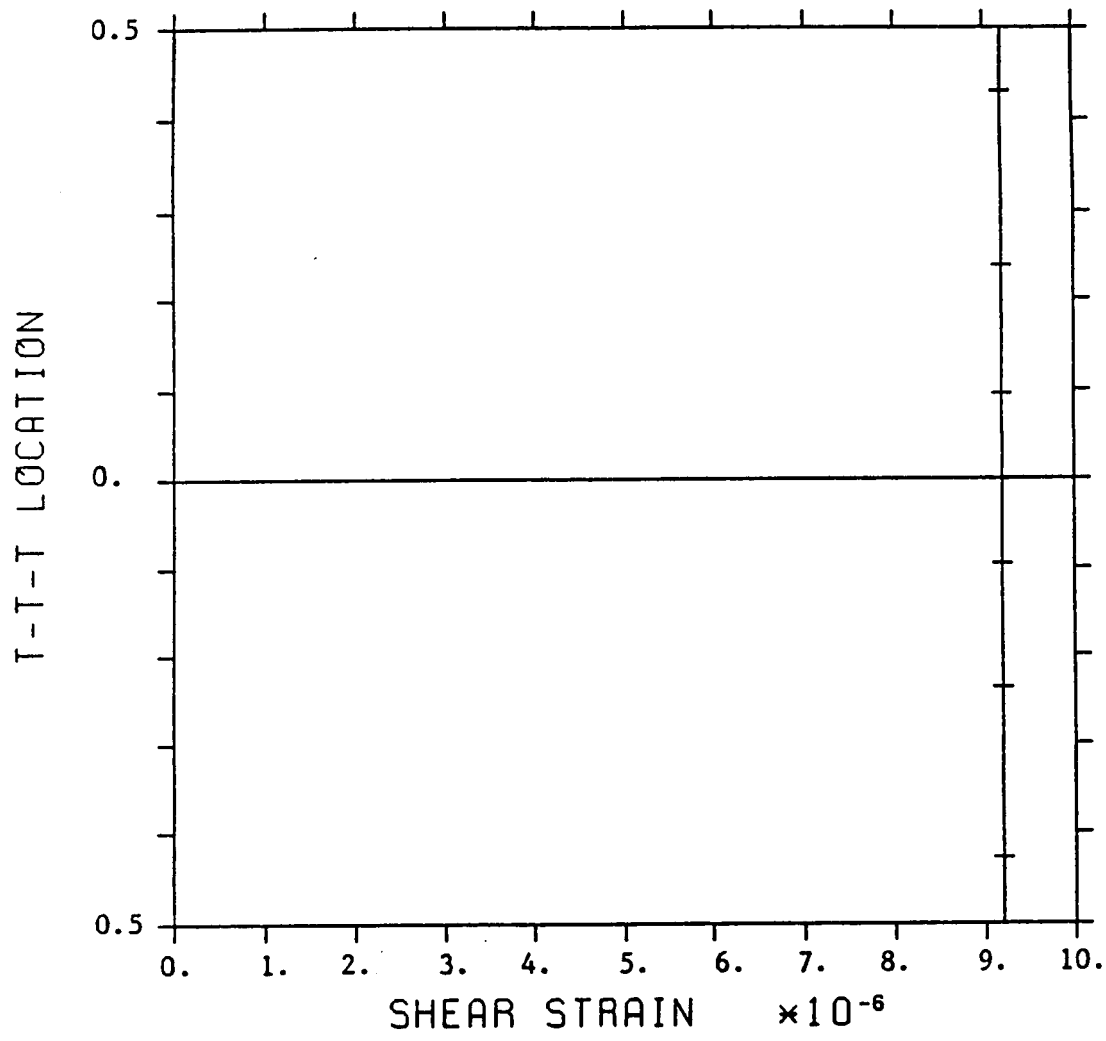

Figure 10: γ_{xz} distribution for [0/90/0] laminate directly from finite element analysis

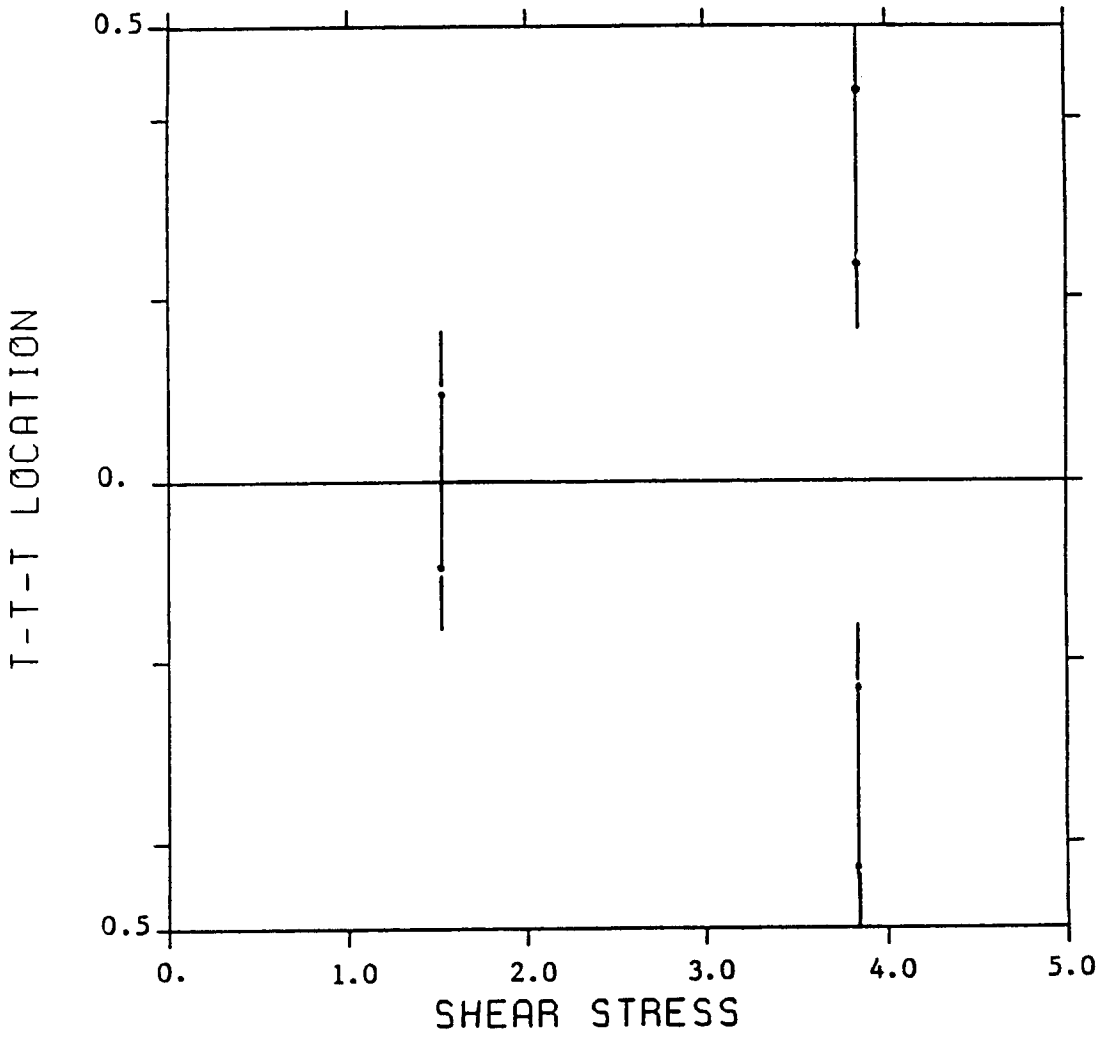

Figure 11: τ_{xz} distribution for [0/90/0] laminate directly from finite element analysis

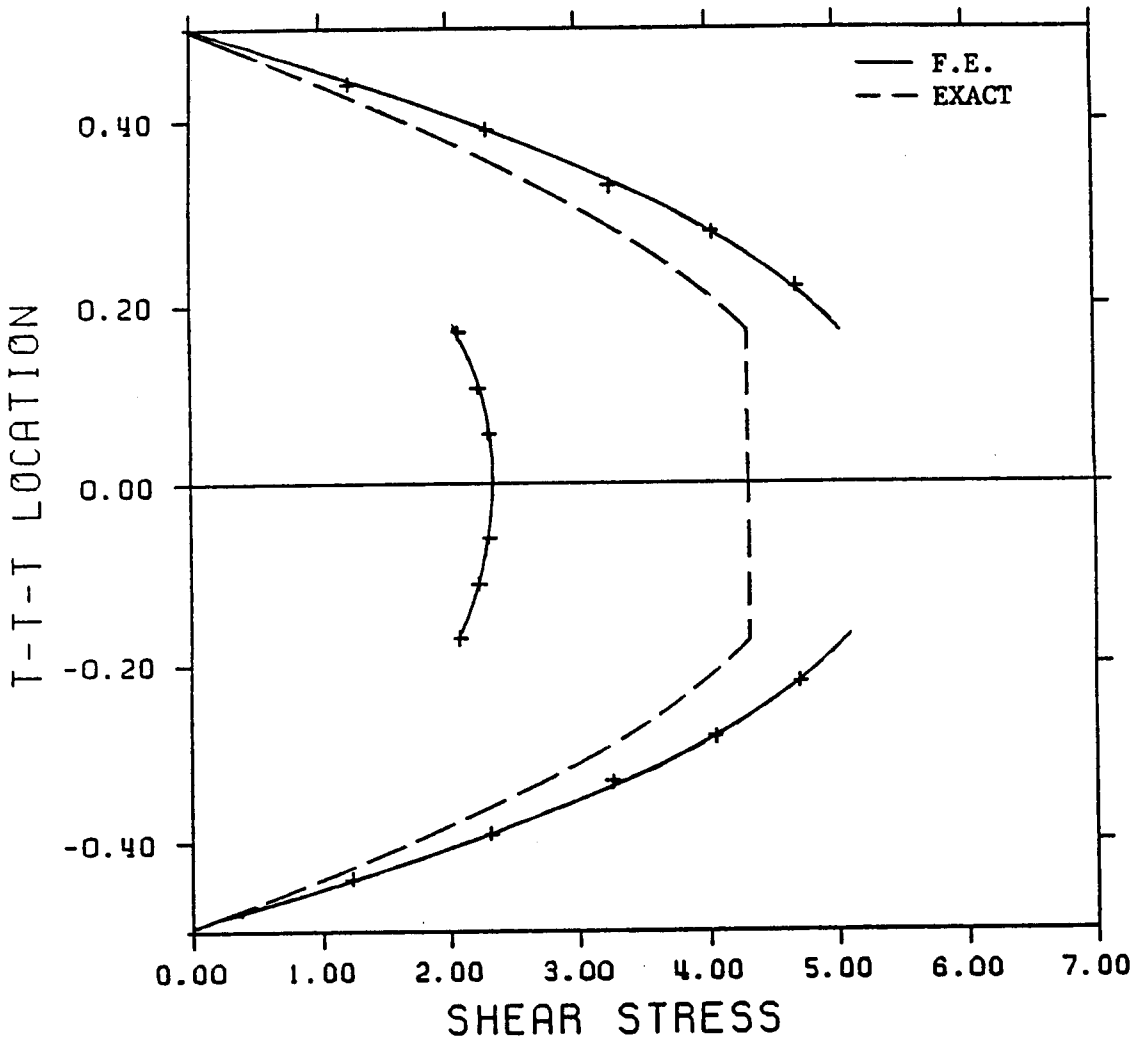

Figure 12: τ_{xz} after strain re-distribution, approach 1

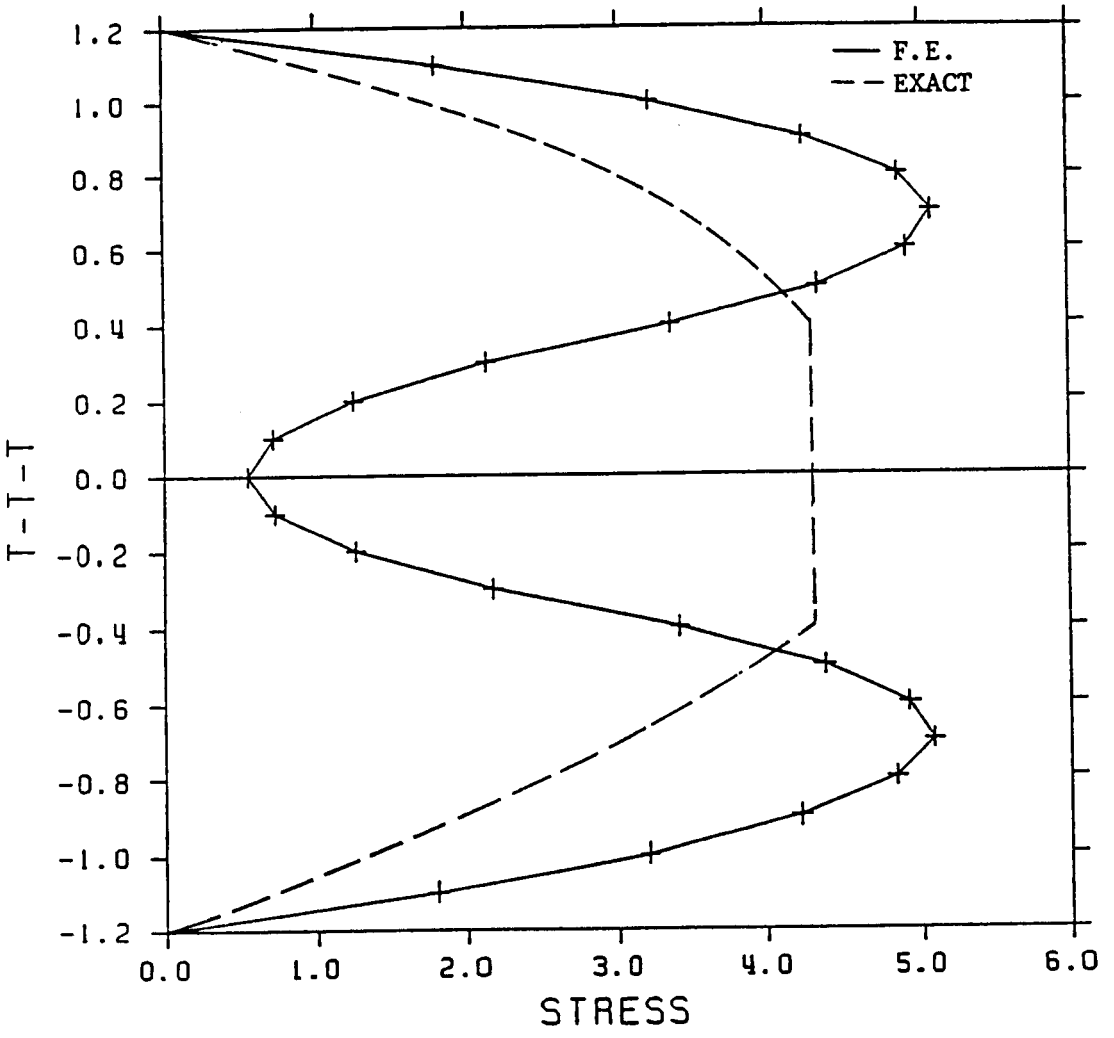

Figure 13: τ_{xz} distribution case 1, approach 2 [0/90/0] laminate

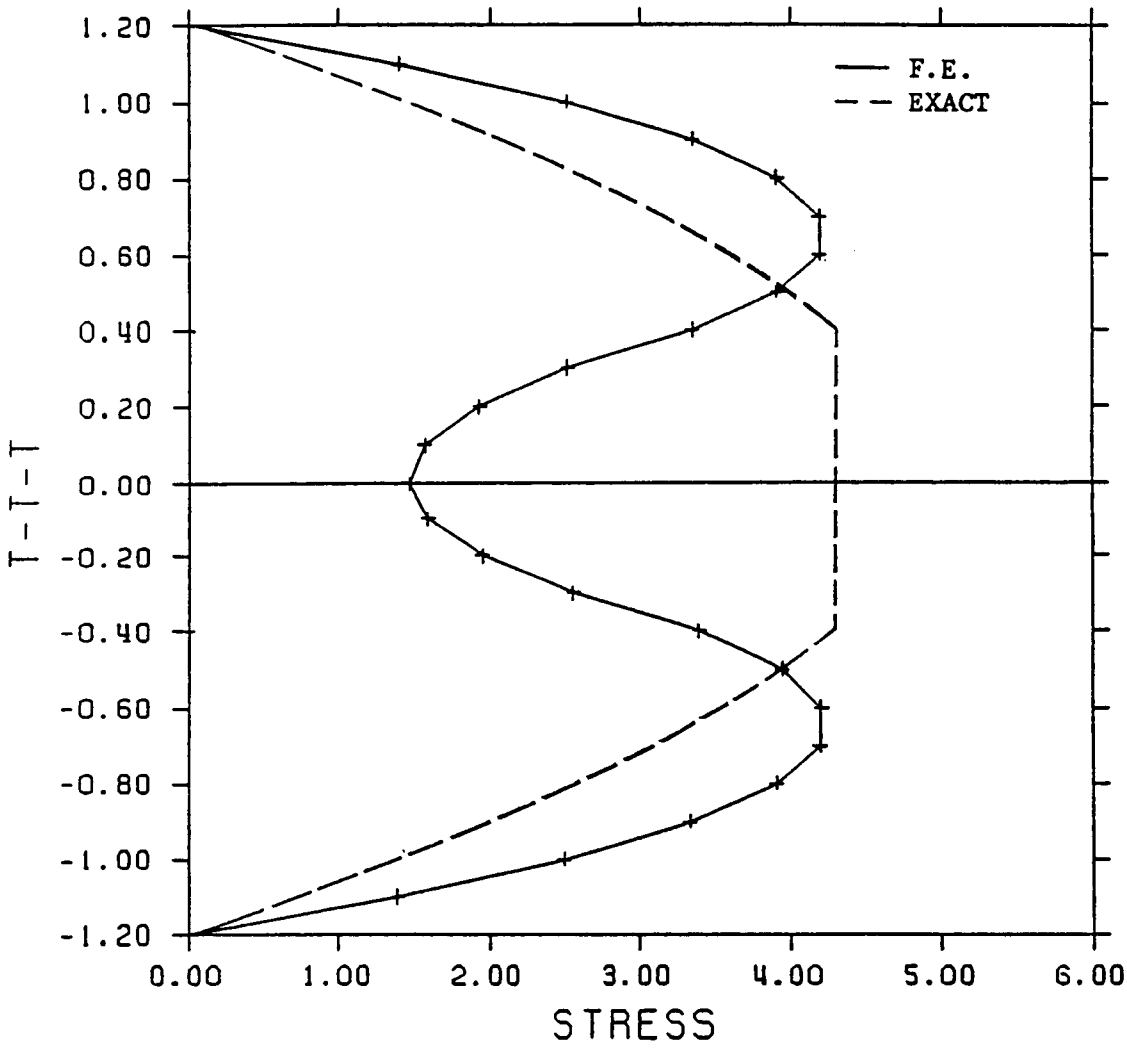

Figure 14: τ_{xz} distribution case 2, approach 2 [0/90/0] laminate

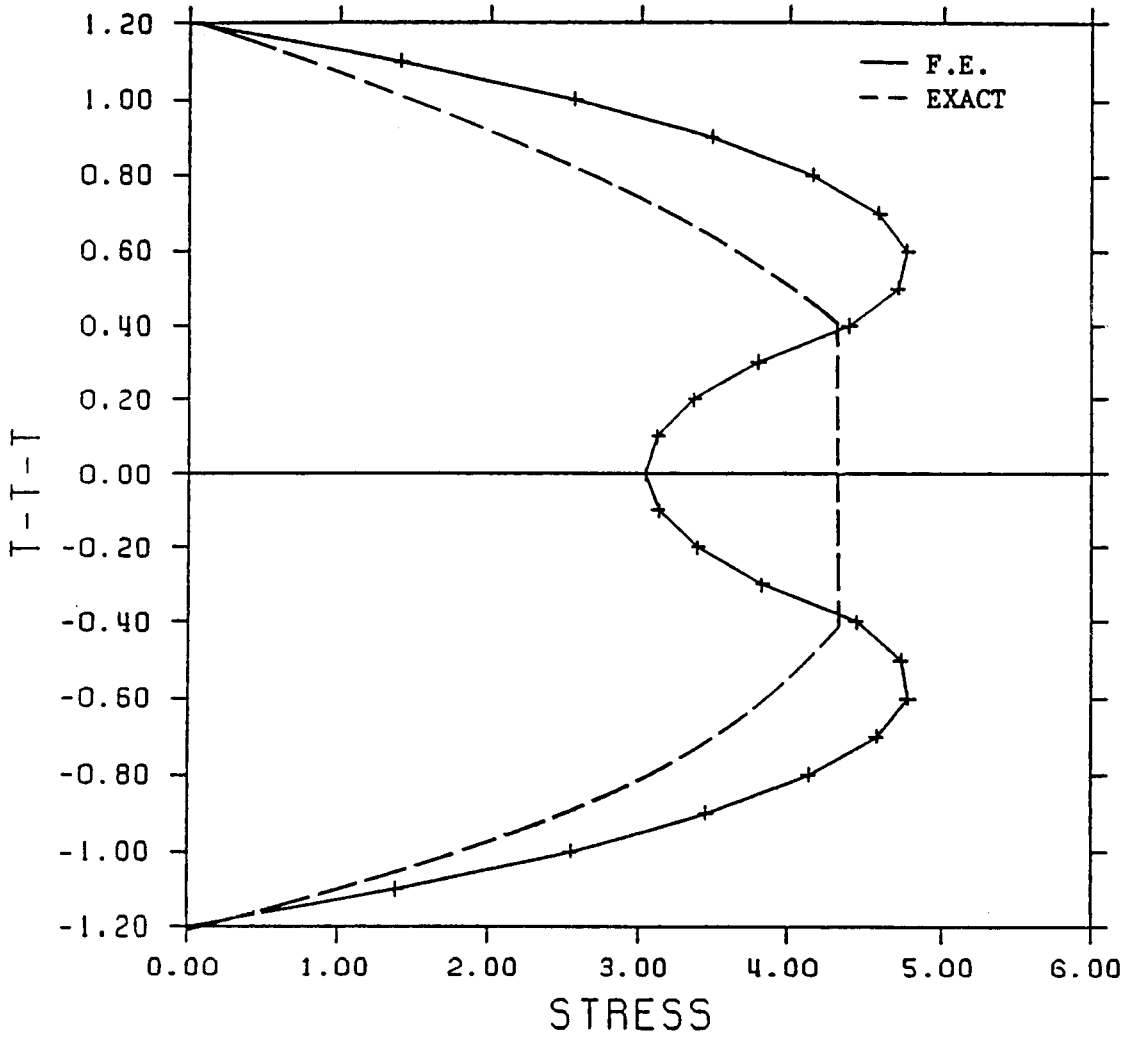

Figure 15: τ_{xz} distribution case 3, approach 2 [0/90/0] laminate

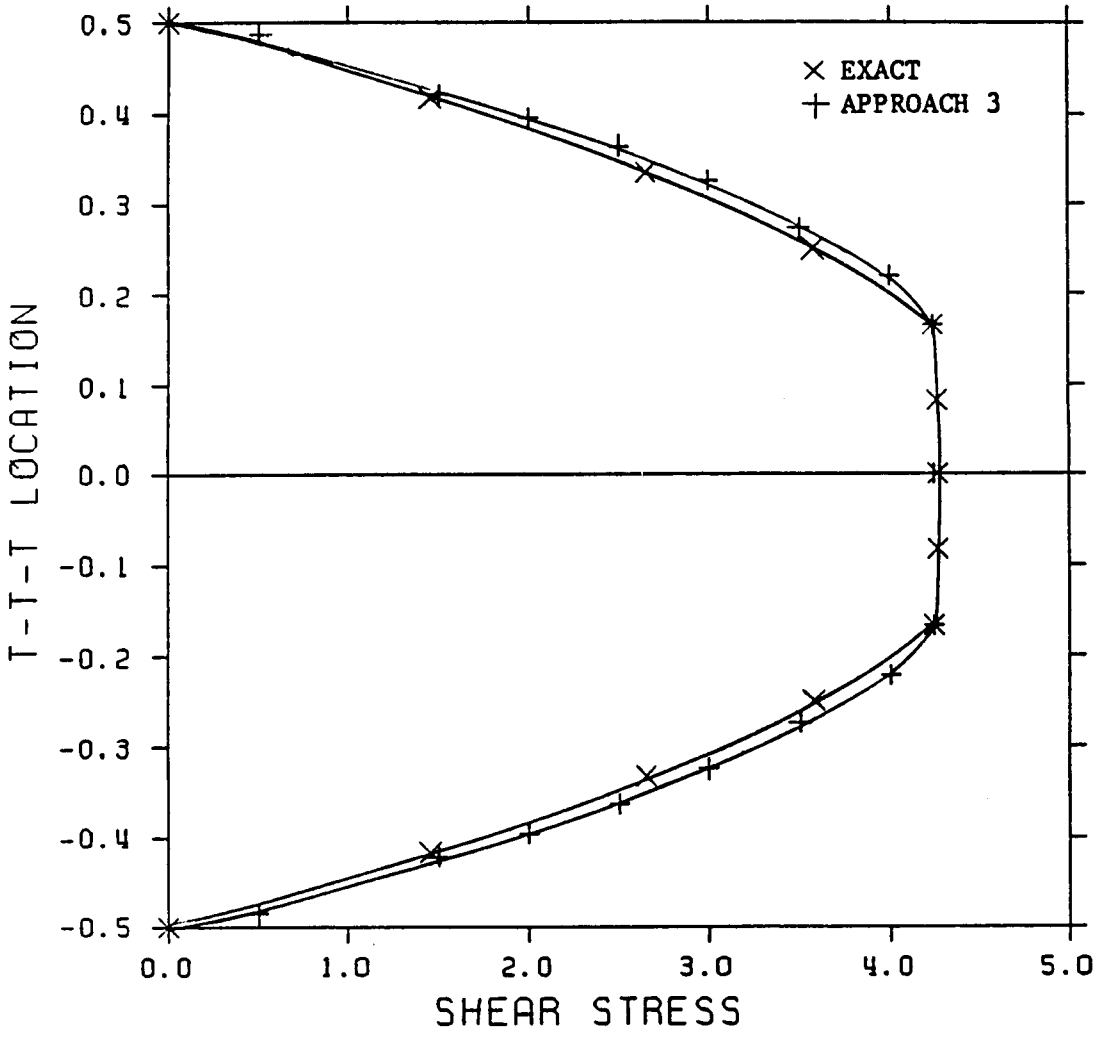

Figure 16: τ_{xz} **distribution approach 3 [0/90/0] laminate**

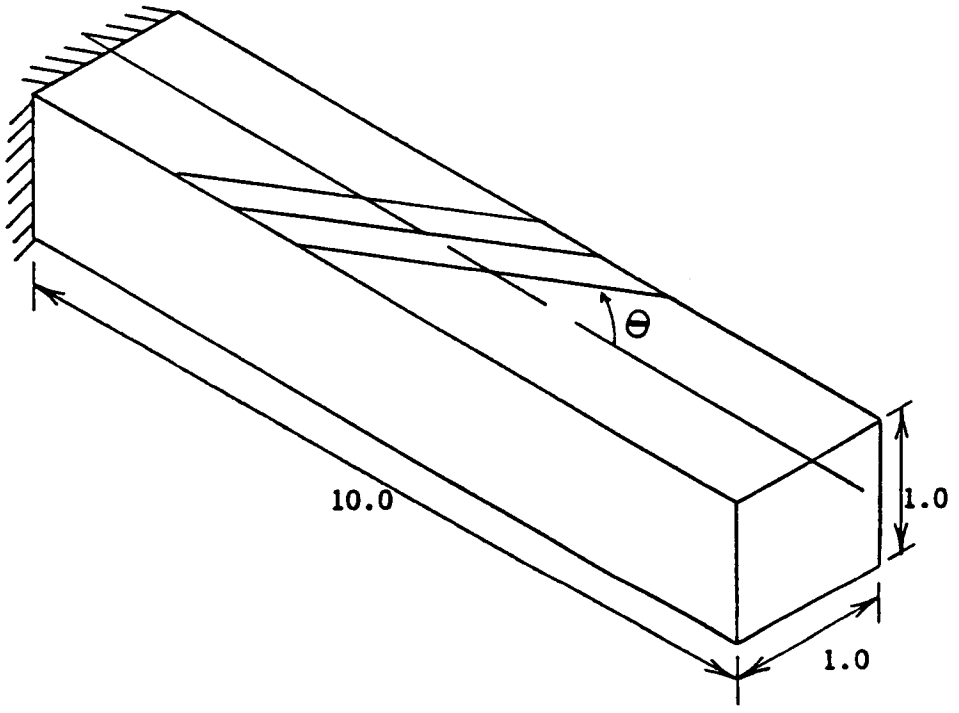

Figure 17: Anisotropic cantilever beam of Oden [24]

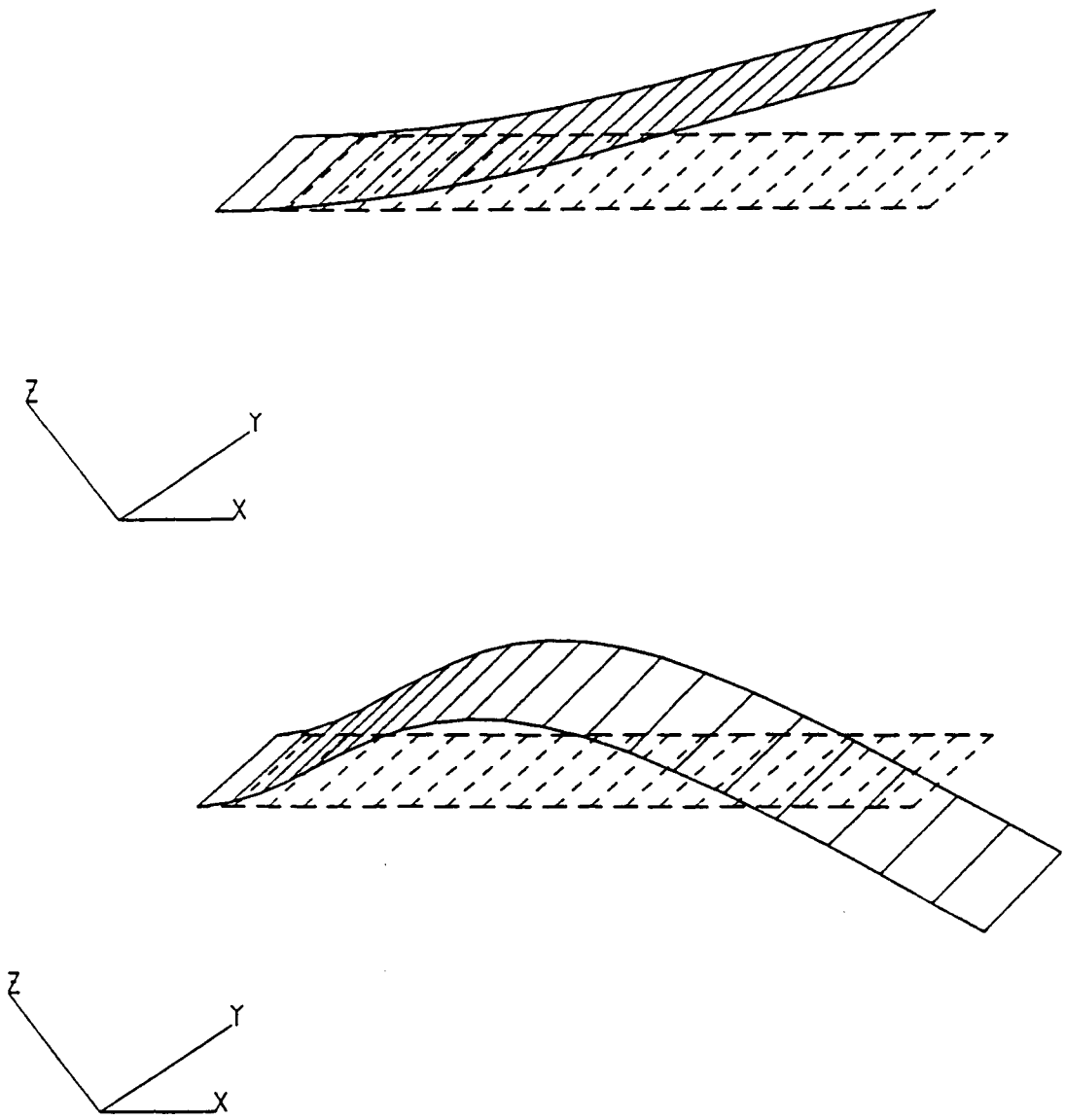

Figure 18: Mode shapes for first and second frequencies

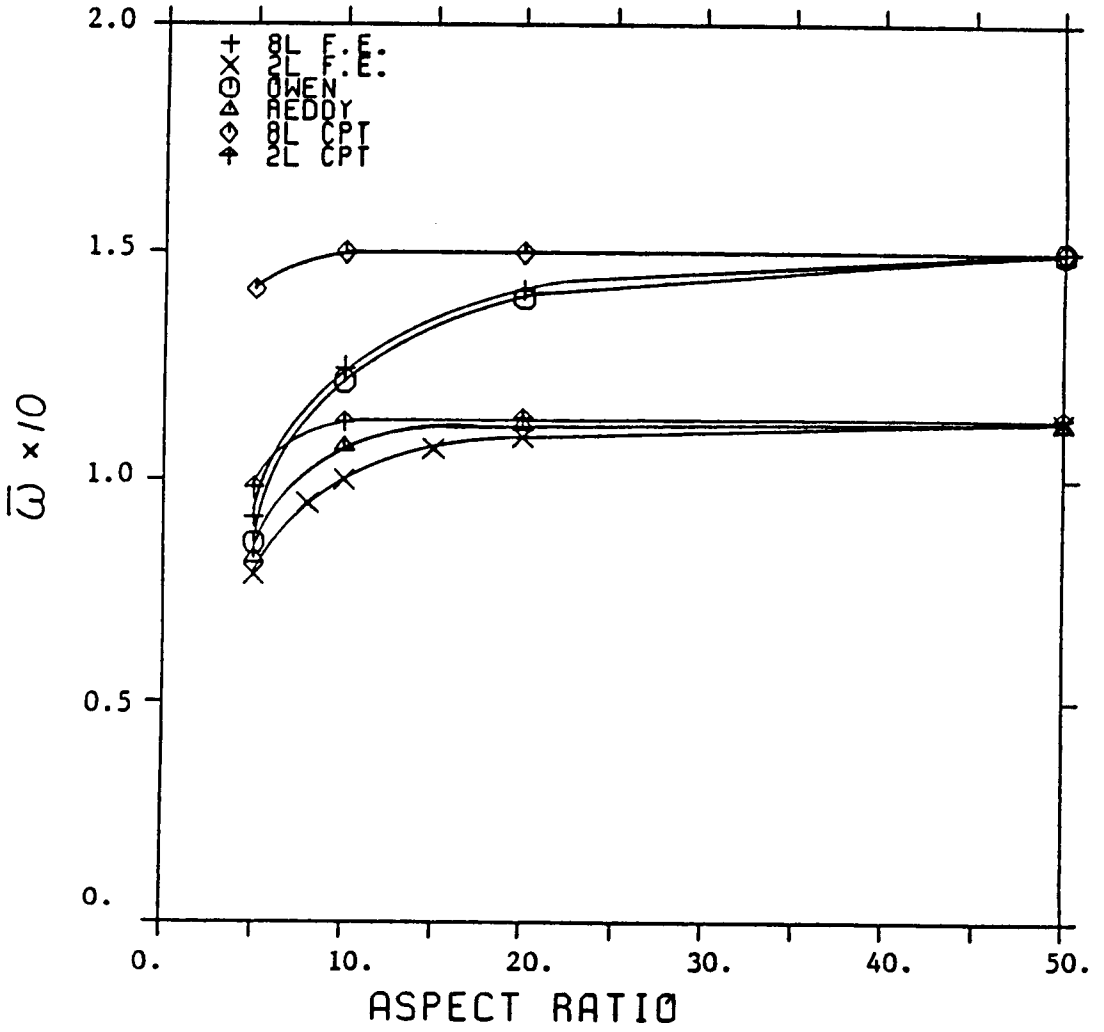

Figure 19: Effect of thickness on the fundamental frequency for two and eight-layer [0/90/...] laminates

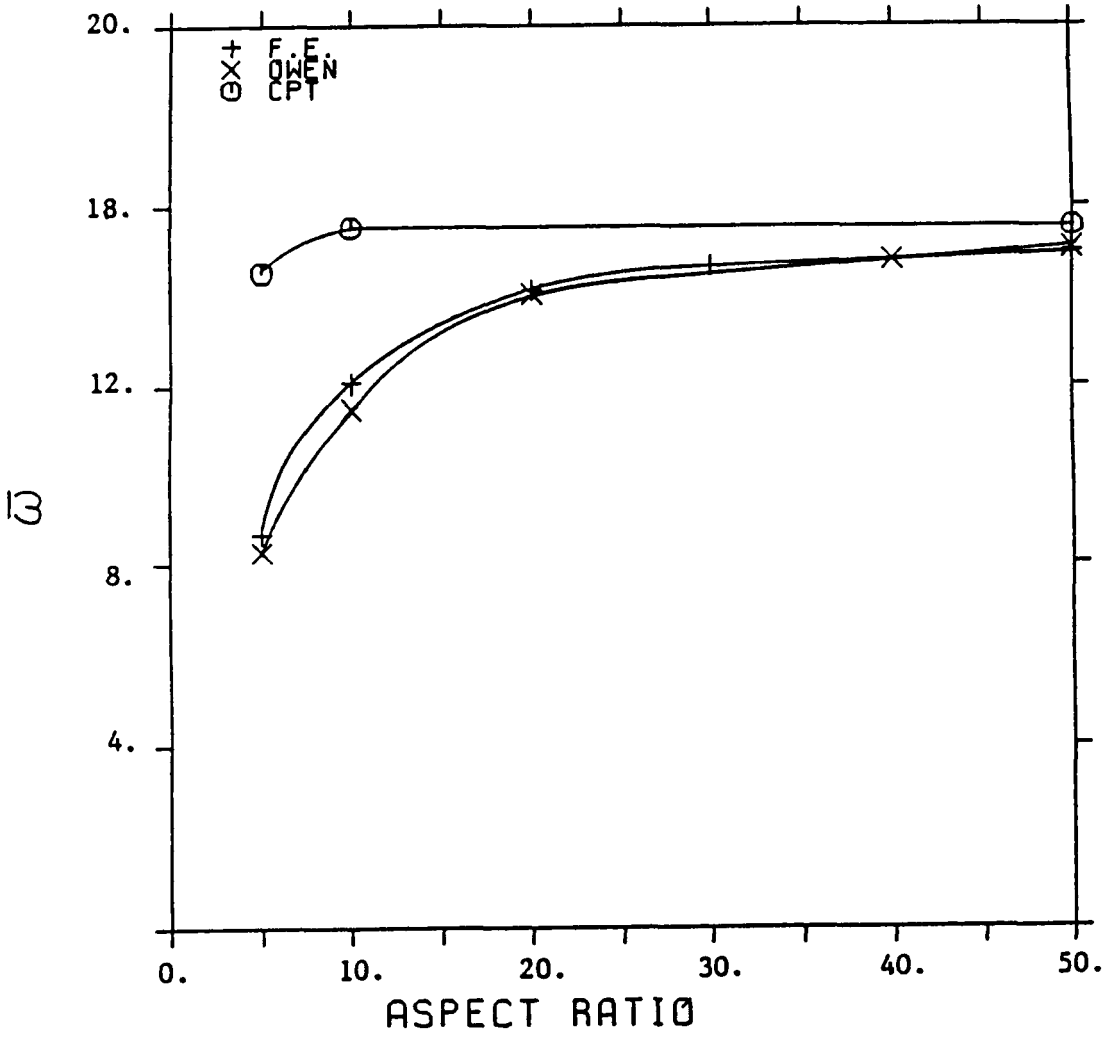

Figure 20: Fundamental frequencies vs. plate aspect ratio for [0/90/0] laminates

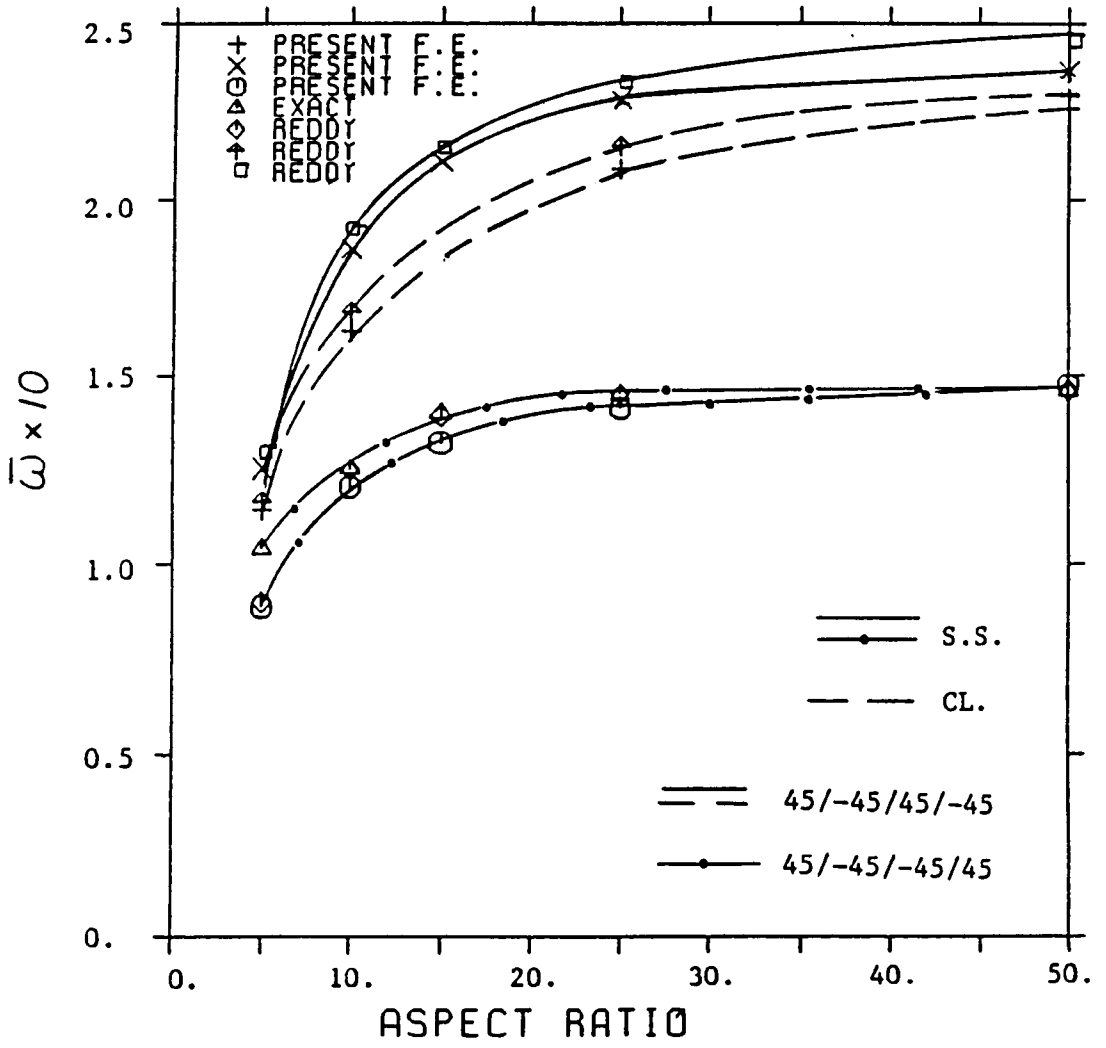

Figure 20*a*: Fundamental frequencies vs. plate aspect ratio for four-layer laminates

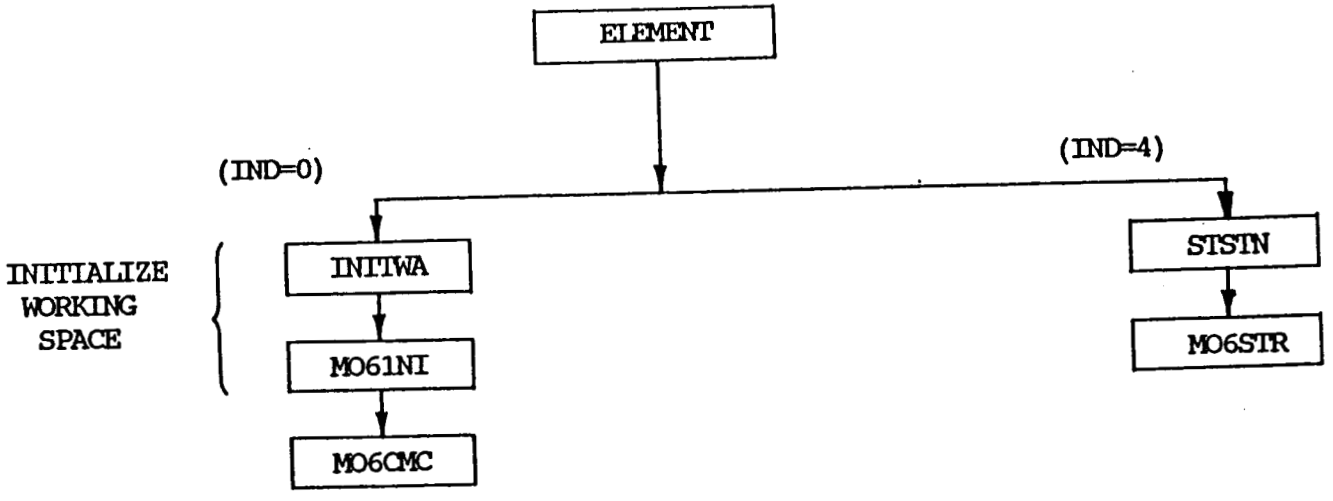

Fig. 21. Element-Material Module Relation for Viscoplastic Models

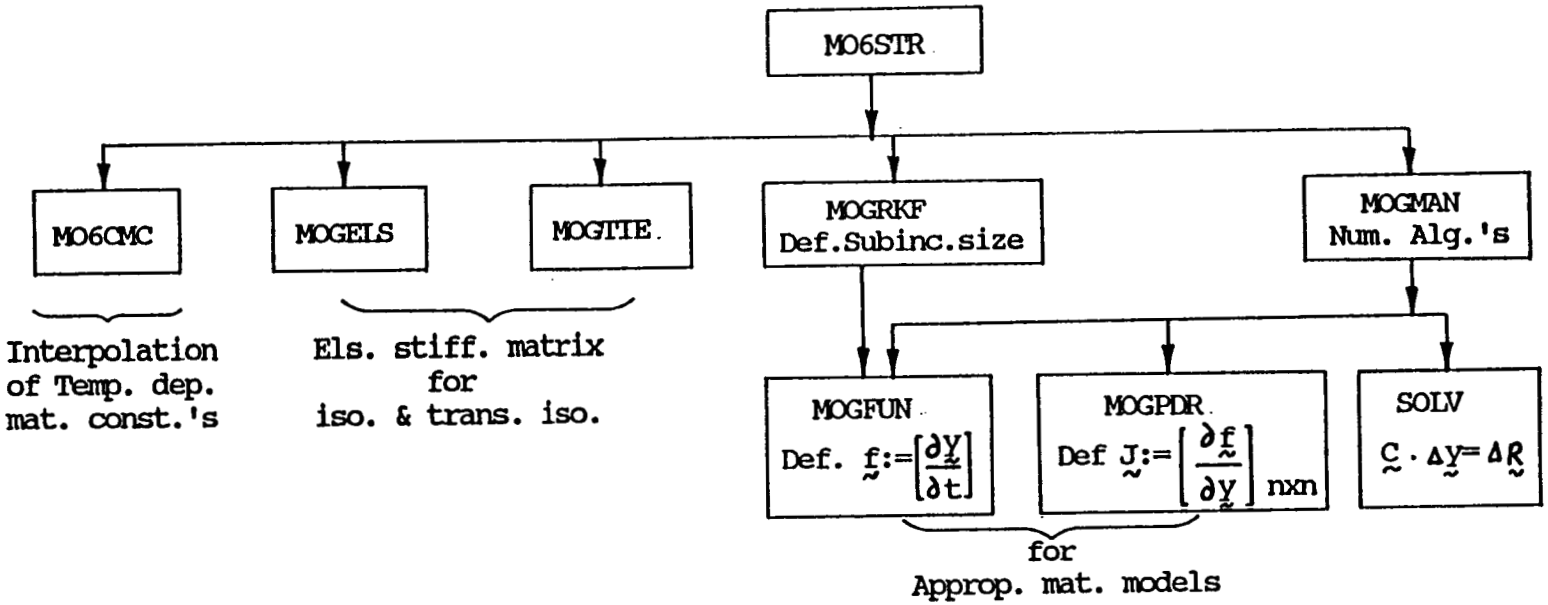

Fig. 22. Main Driver of Viscoplastic Models

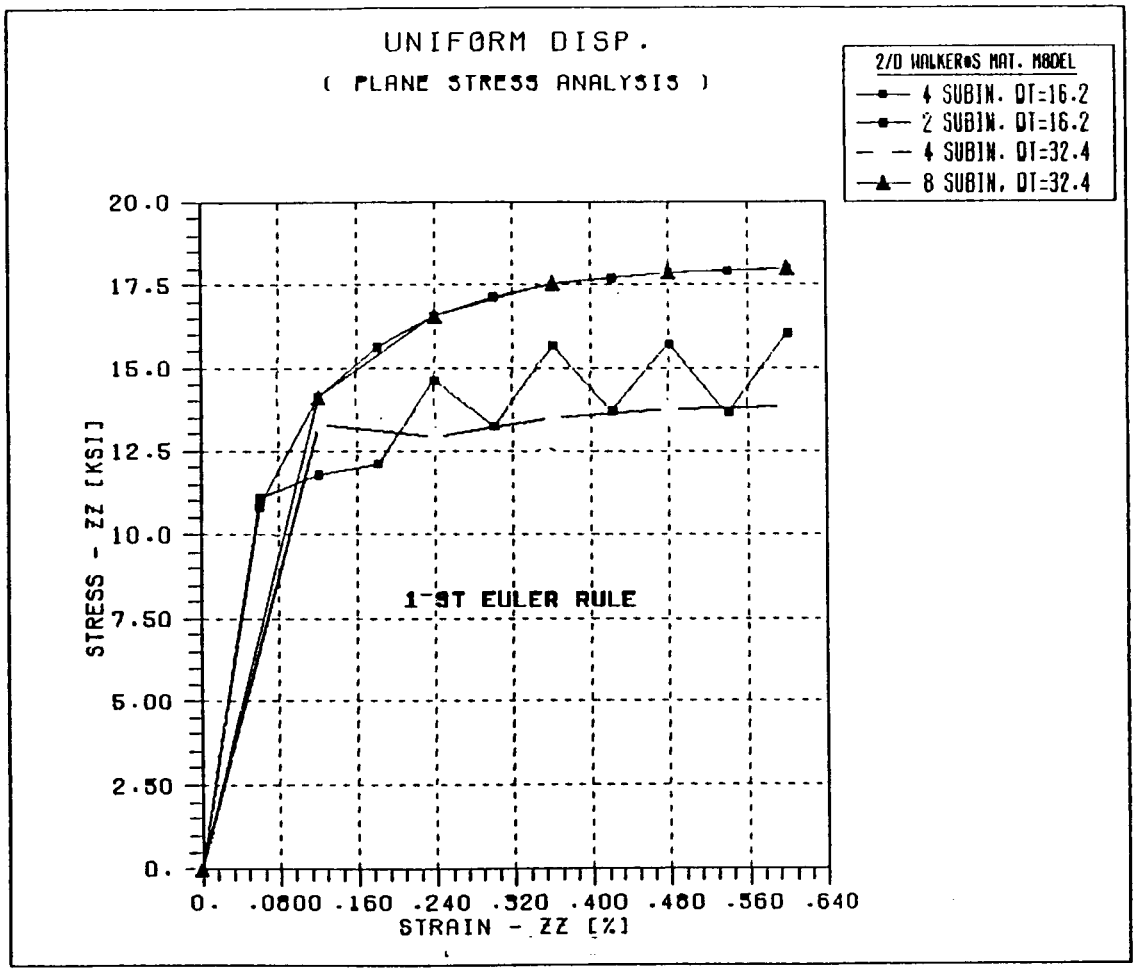

Fig. 23. Uniaxial Stress-Strain Response of Walker's Model Using Different Step Sizes

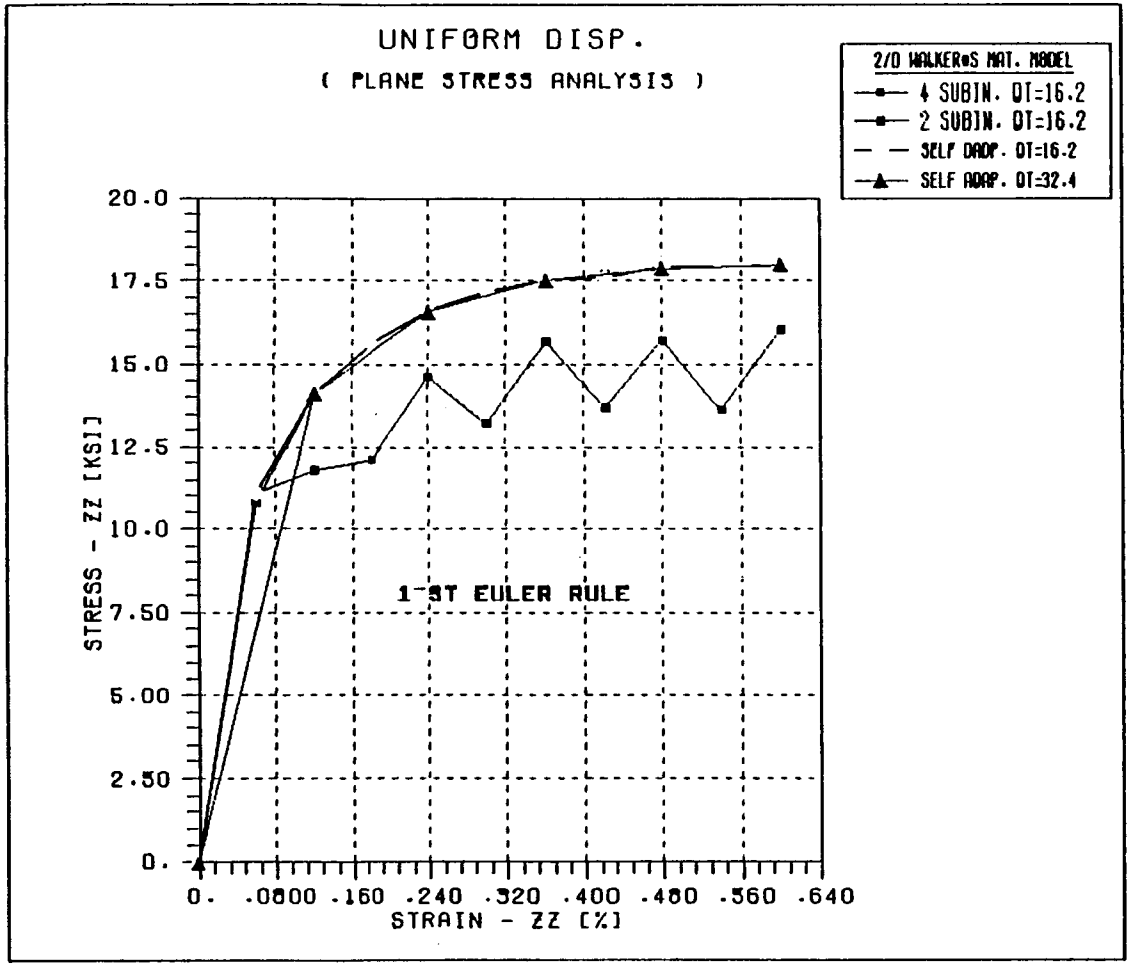

Fig. 24. Uniaxial Stress-Strain Response of Walker's Model Using Self-Adaptive (Automatic) Stepping

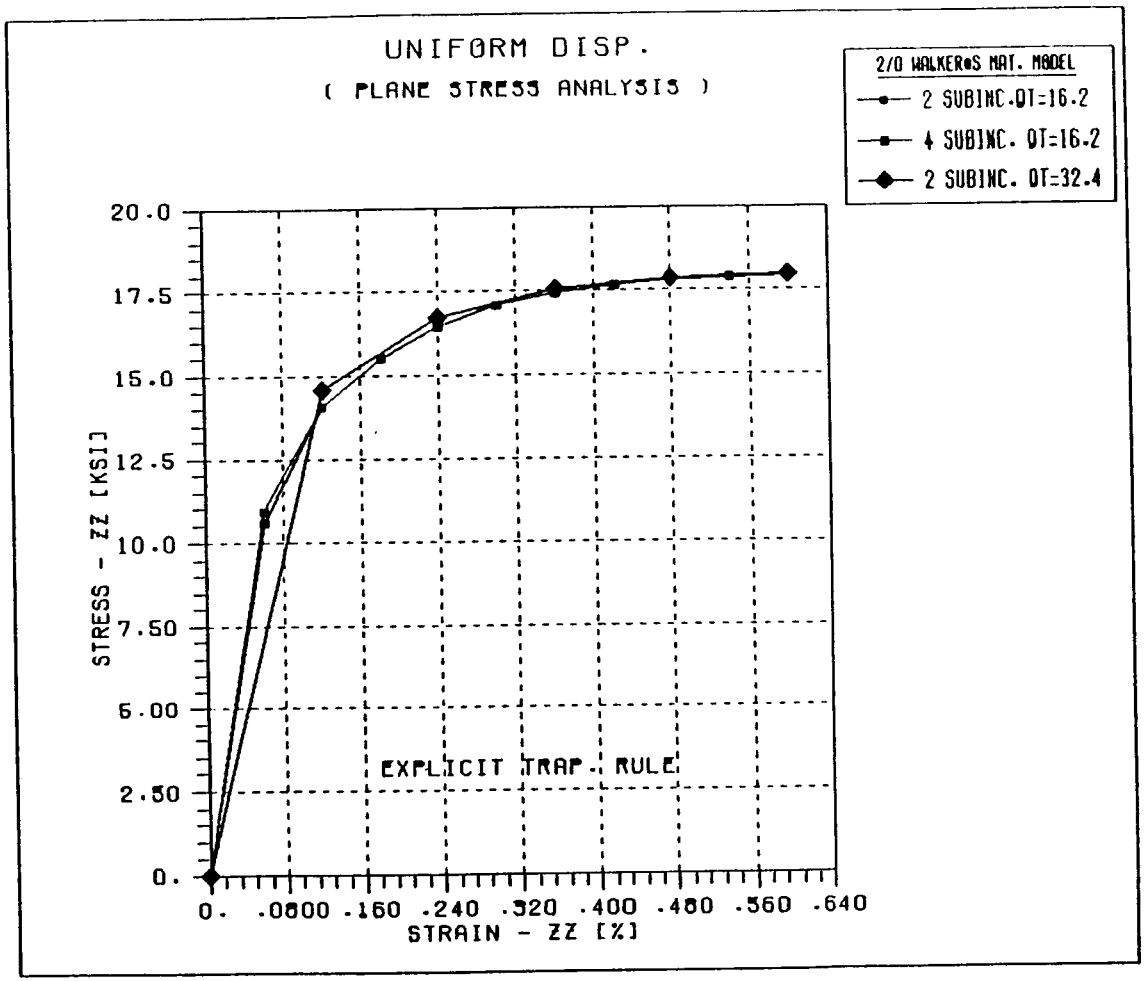

Fig. 25. Uniaxial Stress-Strain Response of Walker's Model Using Explicit Trapezoidal Rule

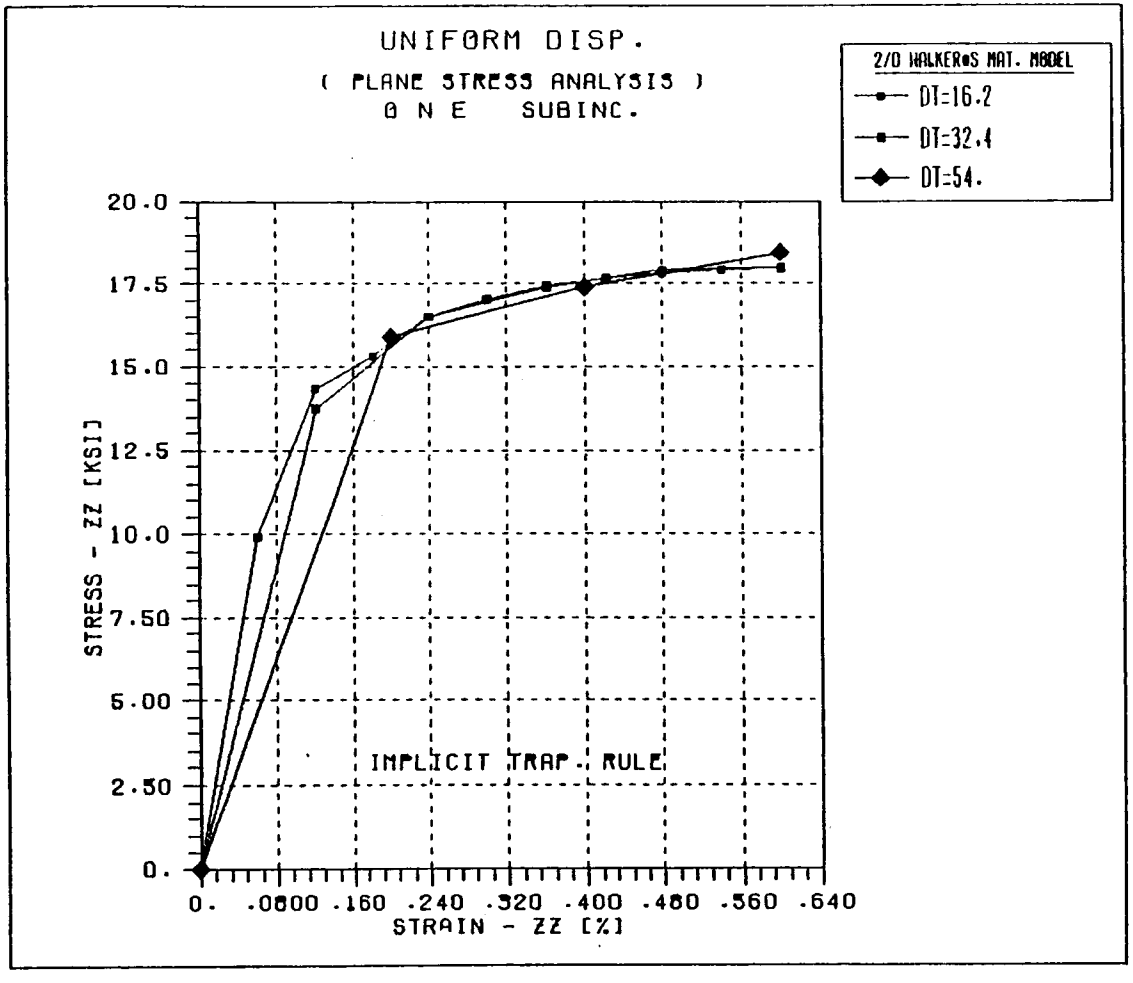

Fig. 26. Uniaxial Stress-Strain Response of Walker's Model Using Implicit Trapezoidal Rule

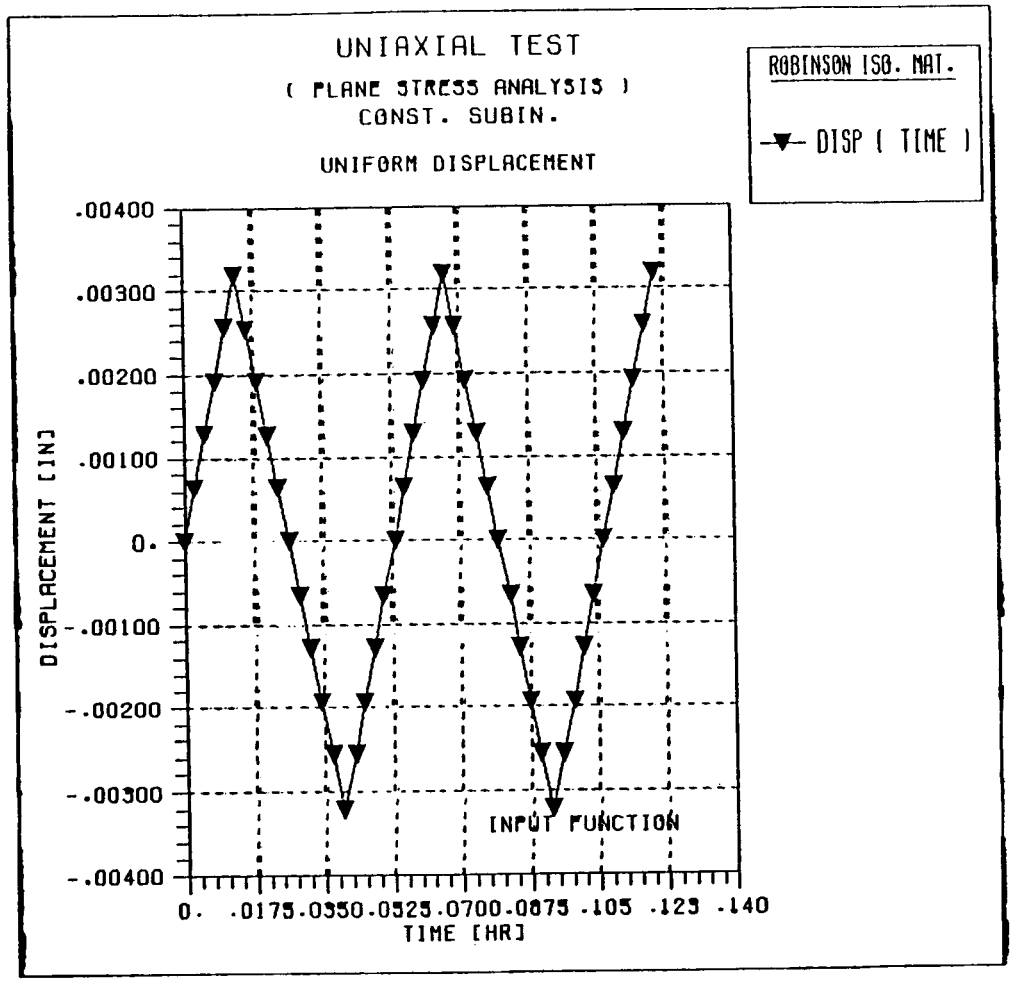

Fig. 27. Cyclic Displacement Input for a Uniaxial Test

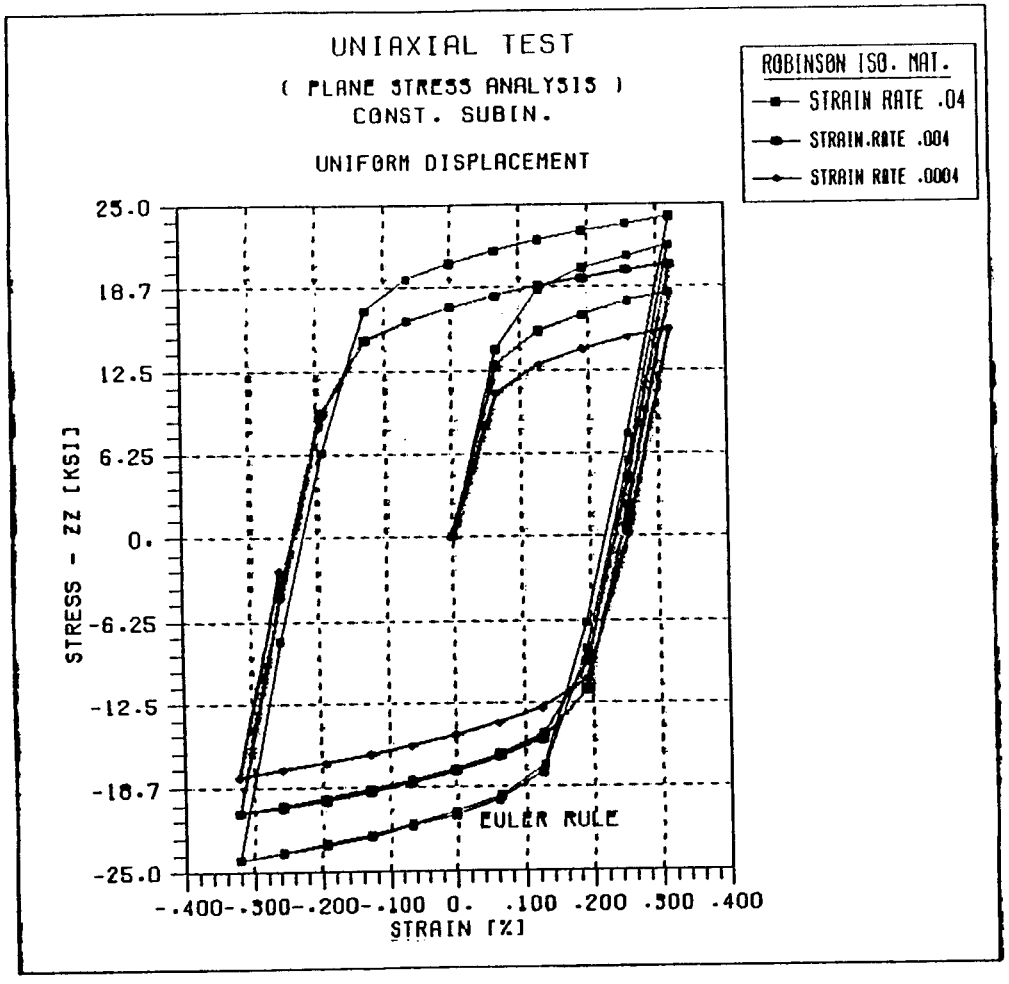

Fig. 28. Cyclic Stress-Strain Response of Robinson's Model Using a Forward Euler Method

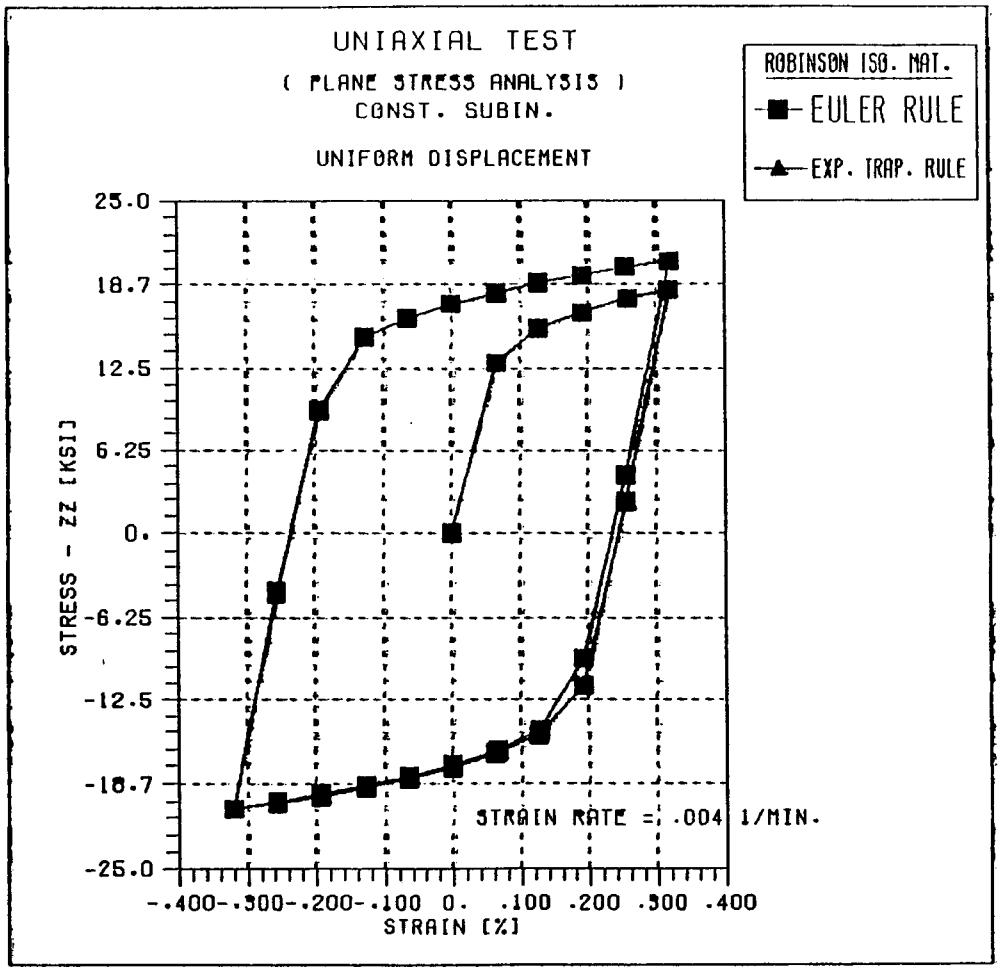

Fig. 29. Comparison of Cyclic Stress-Strain Responses of Robinson's Model Using Euler and Trapezoidal Rules

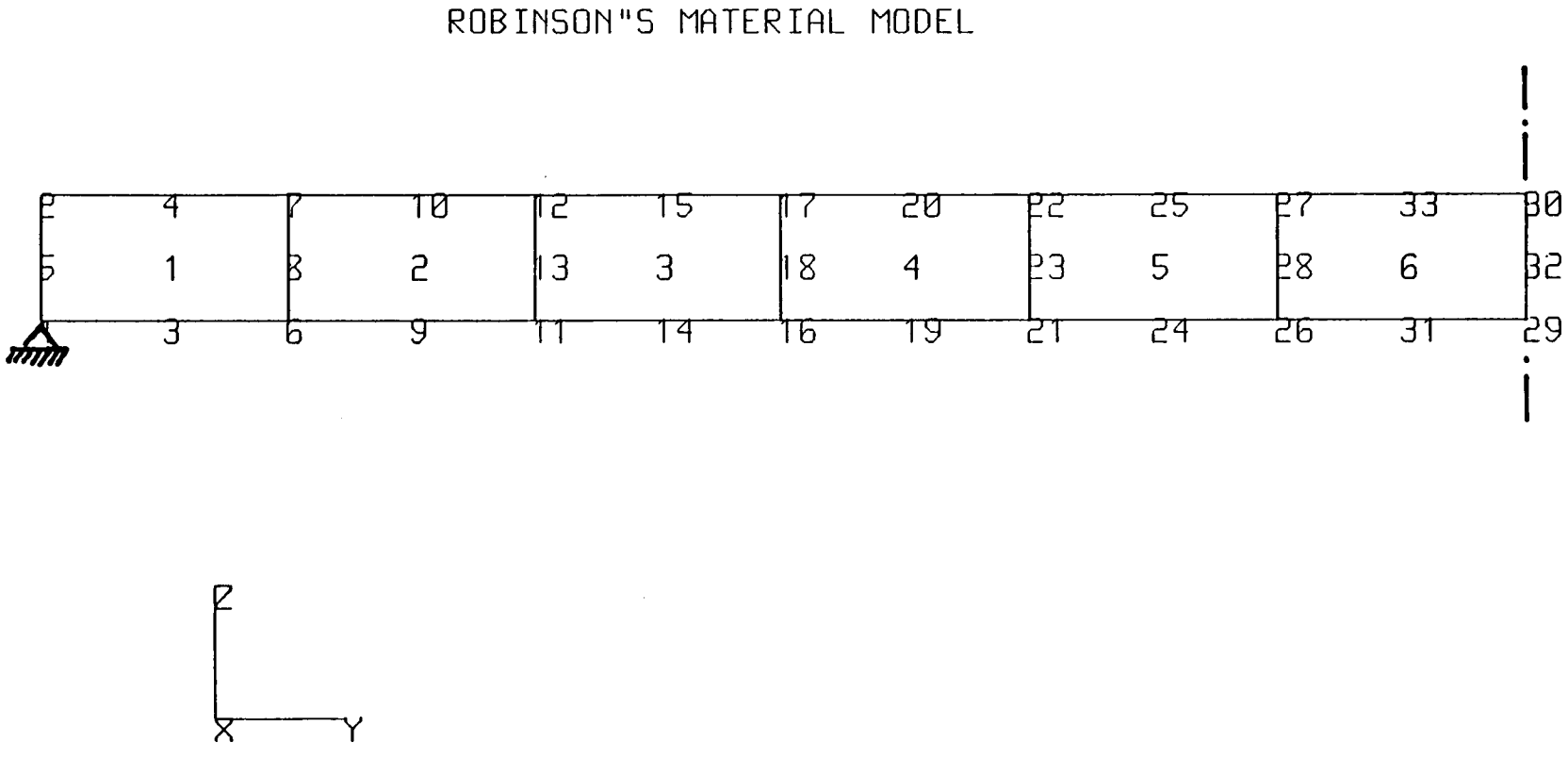

Fig. 30. Finite Element Model of a Simple Beam

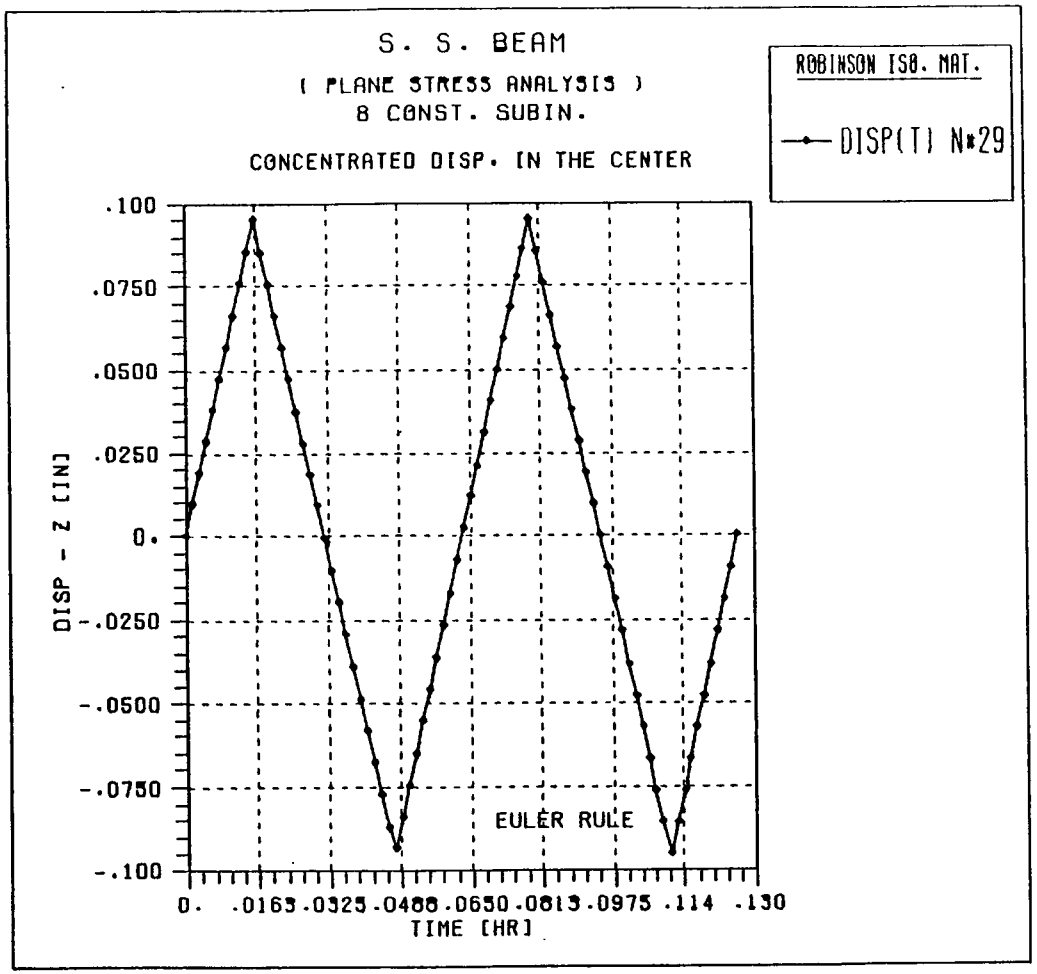

Fig. 31. Cyclic Displacement Loading for a Simple Beam

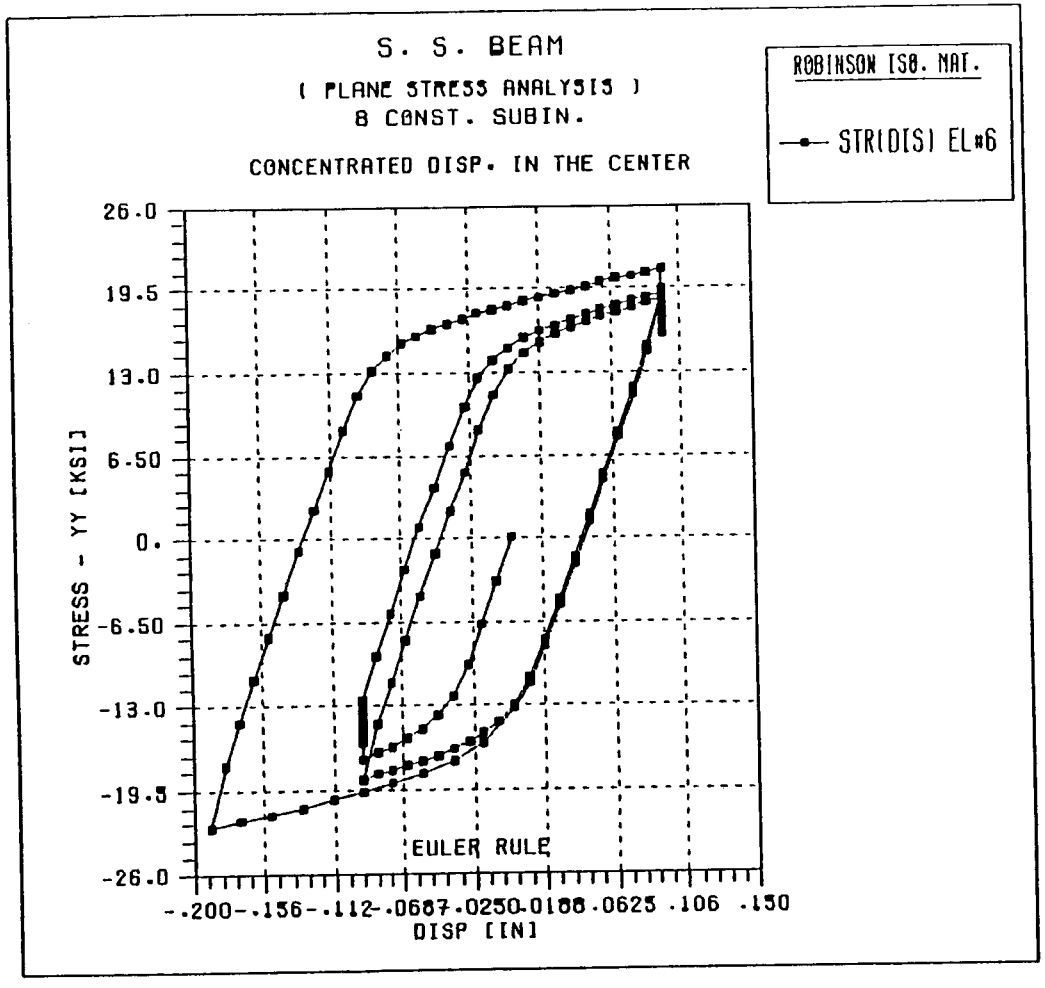

Fig. 32. Stress-Displacement Response of a Simple Beam

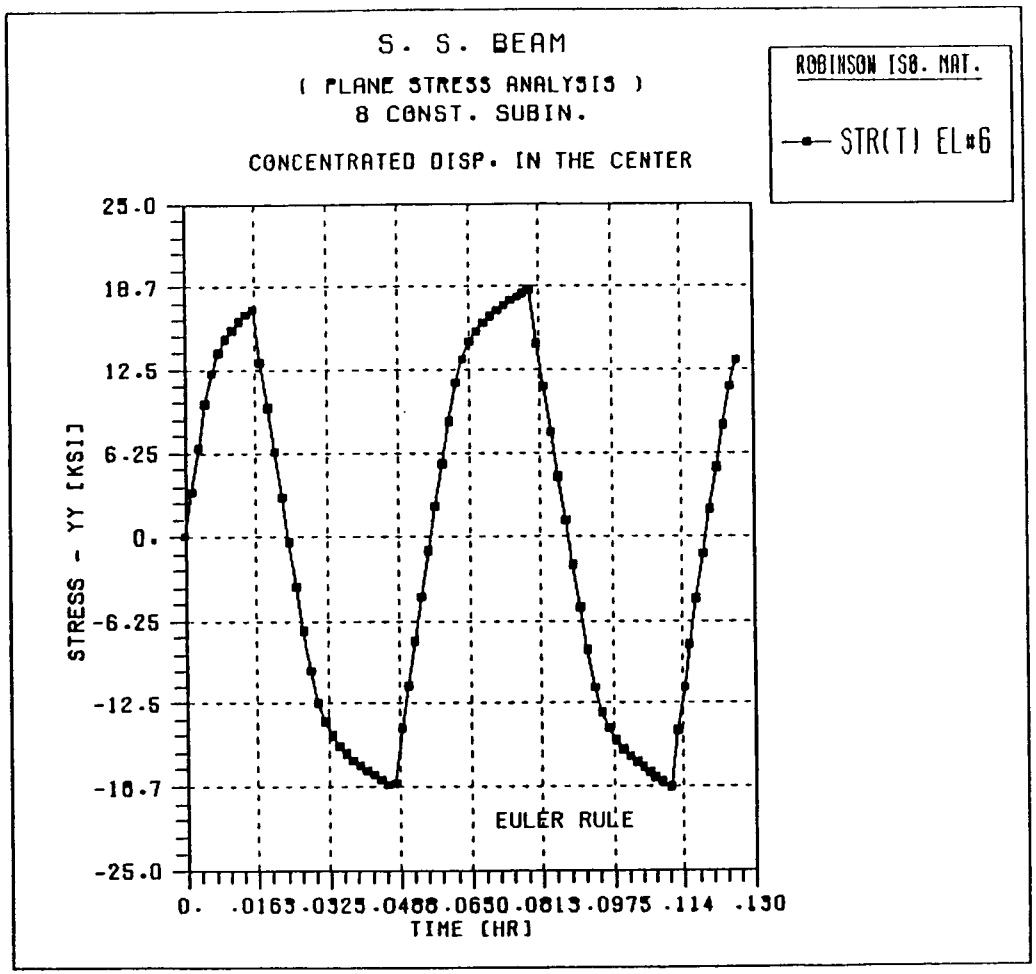

Fig. 33. Maximum Stress History in the Simply Supported Beam

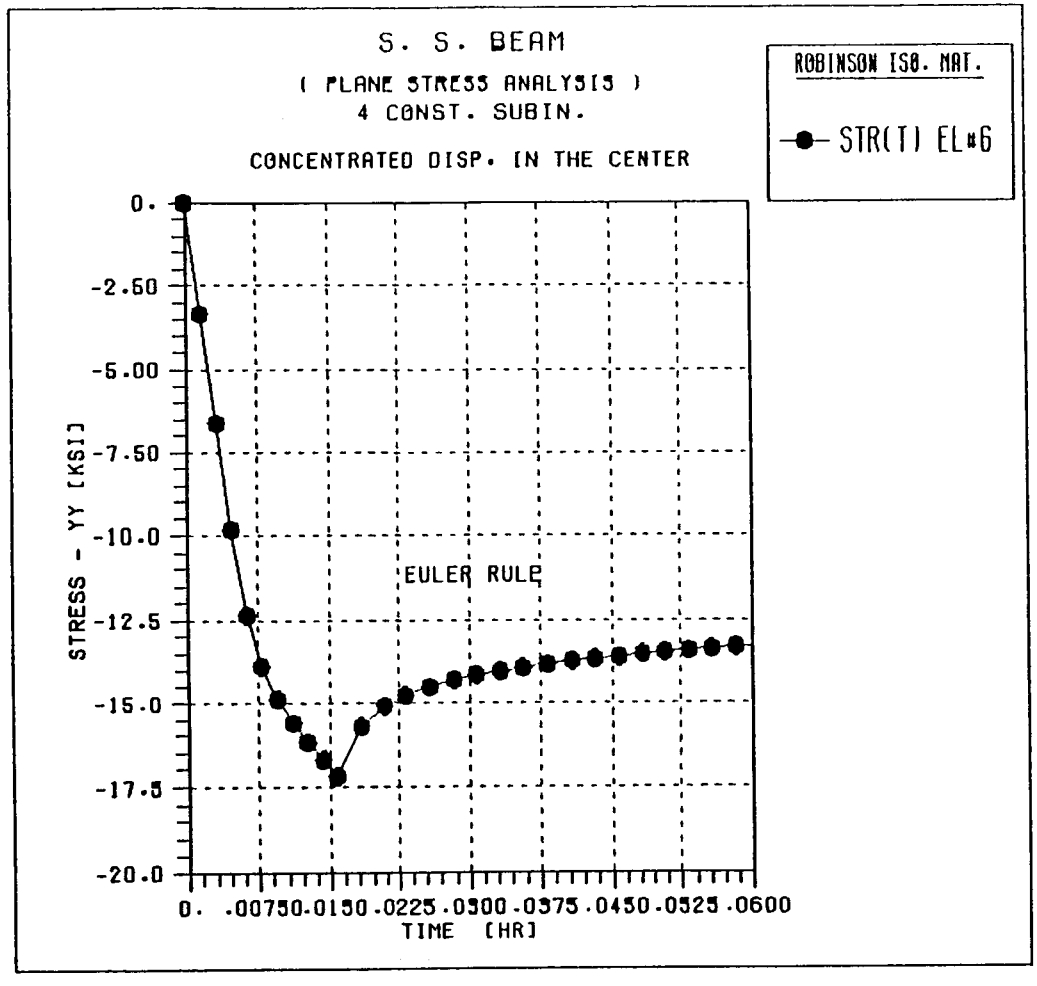

Fig. 34. Stress Relaxation in a Beam Under Constant Displacement

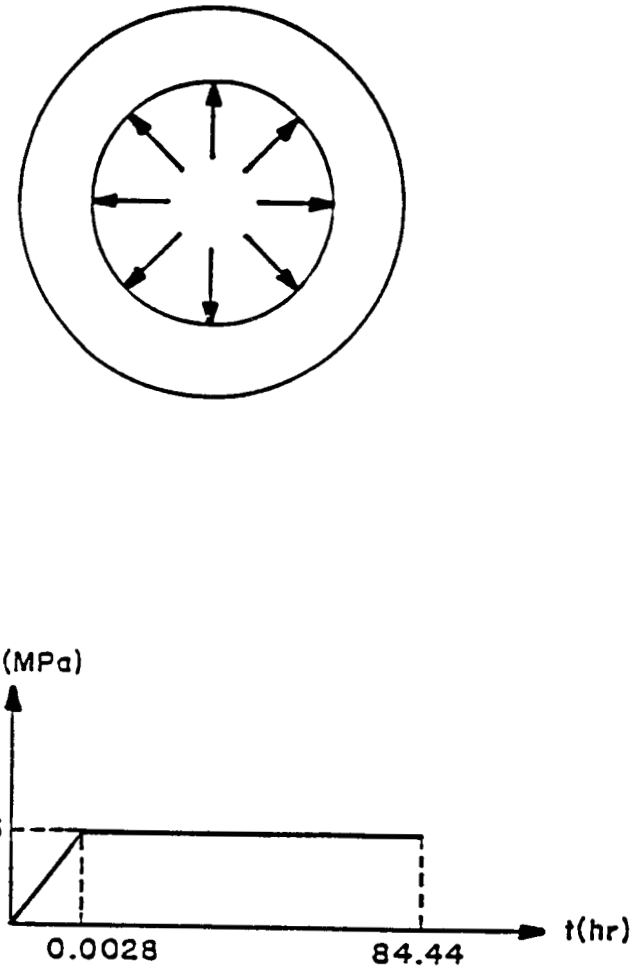

Fig. 35. A Thick Wall Cylinder

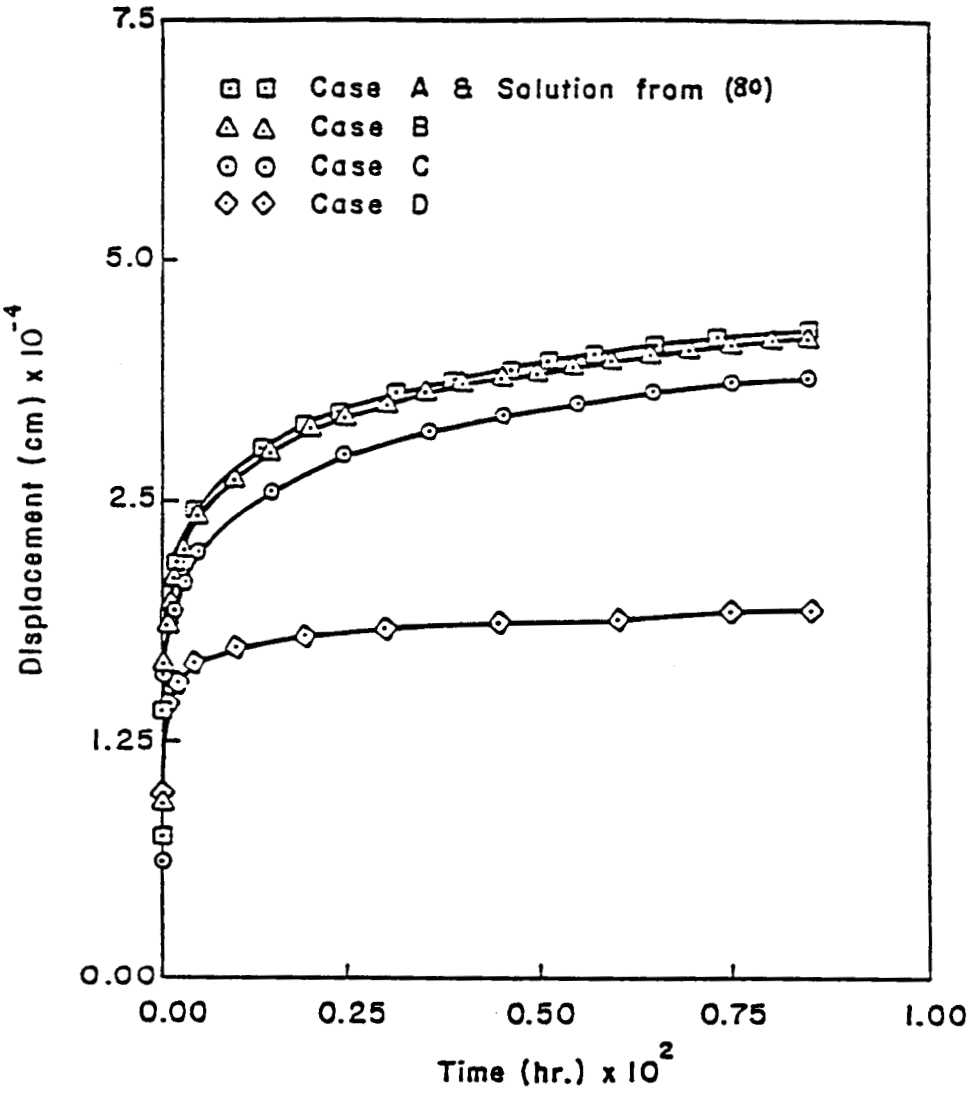

Fig. 36. Radial Displacement at the Outer Wall of the Cylinder with Different Incrementing Schemes

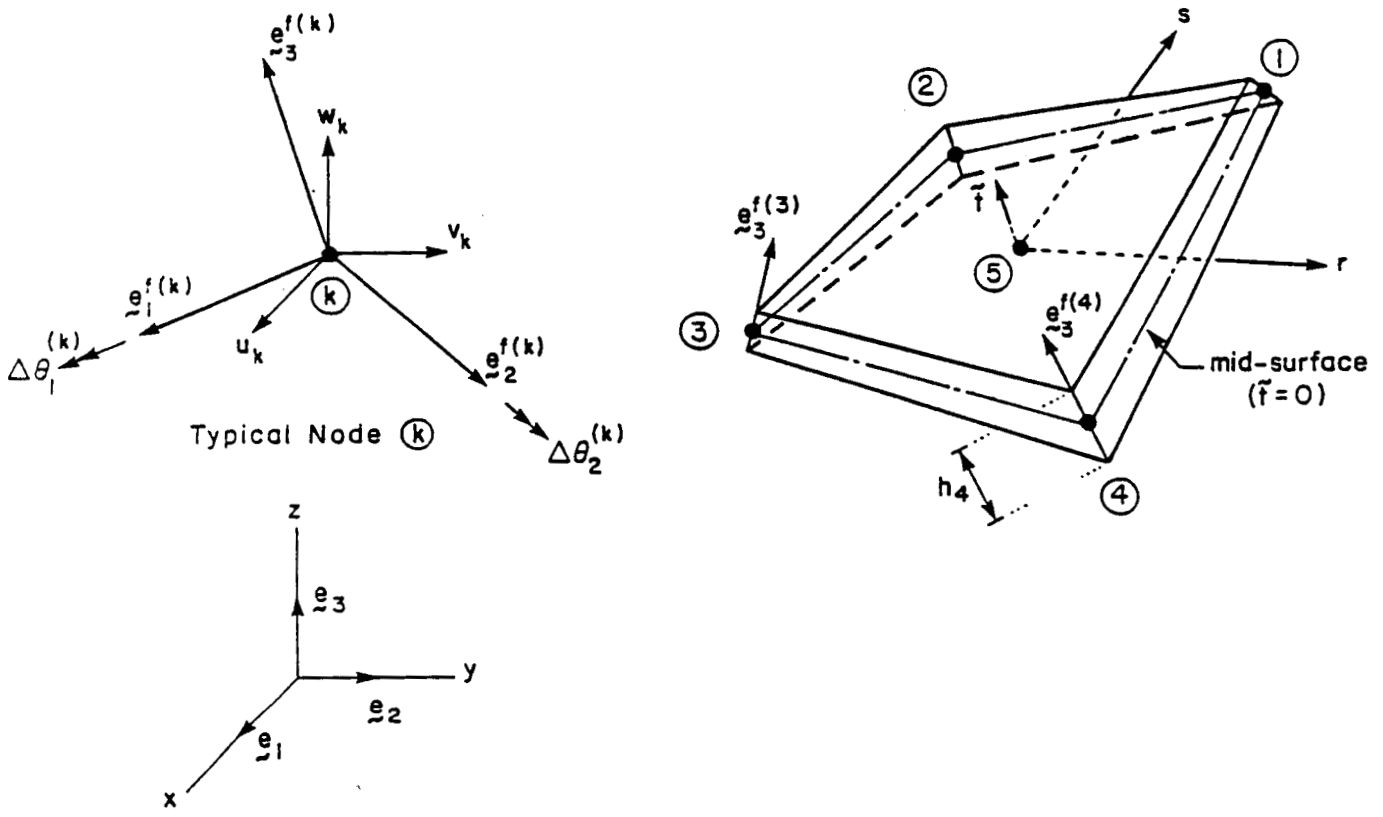

(a) Geometry, Displacement, and Fiber Basis

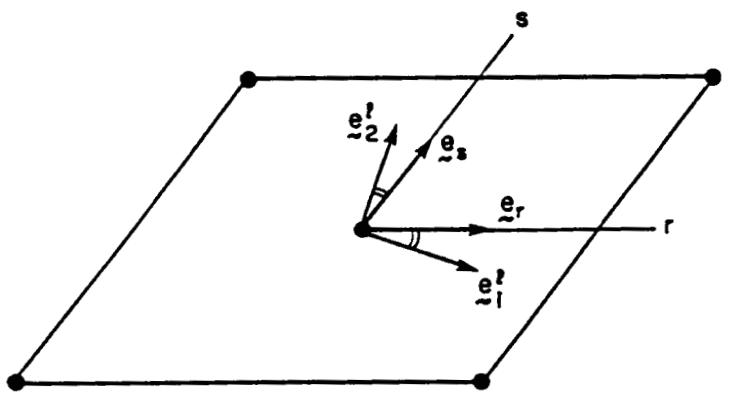

(b) Typical Lamina Coordinates and In-plane Skewness

Fig. 37. Typical Element HMSH5

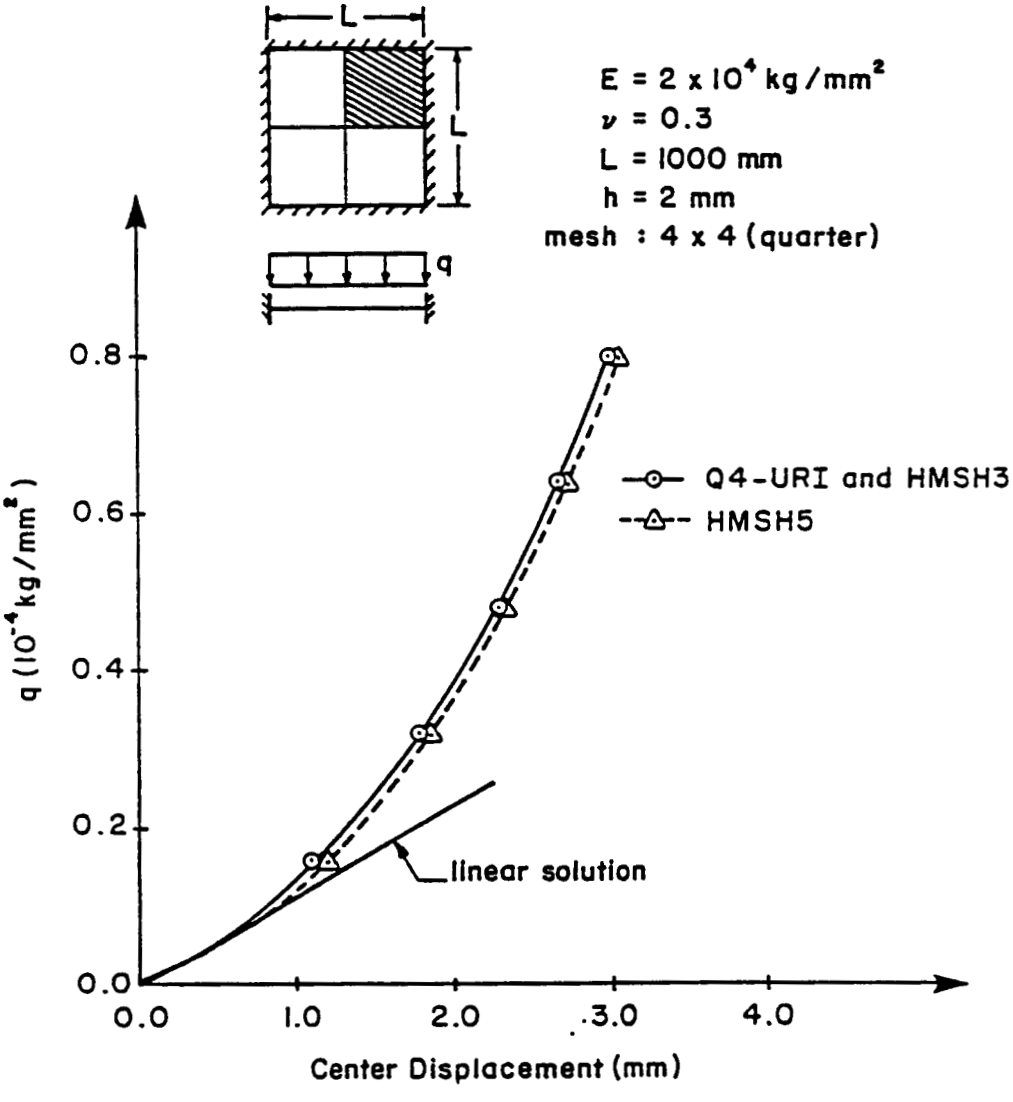

Fig. 38. A Clamped Square Plate Under Uniform Load

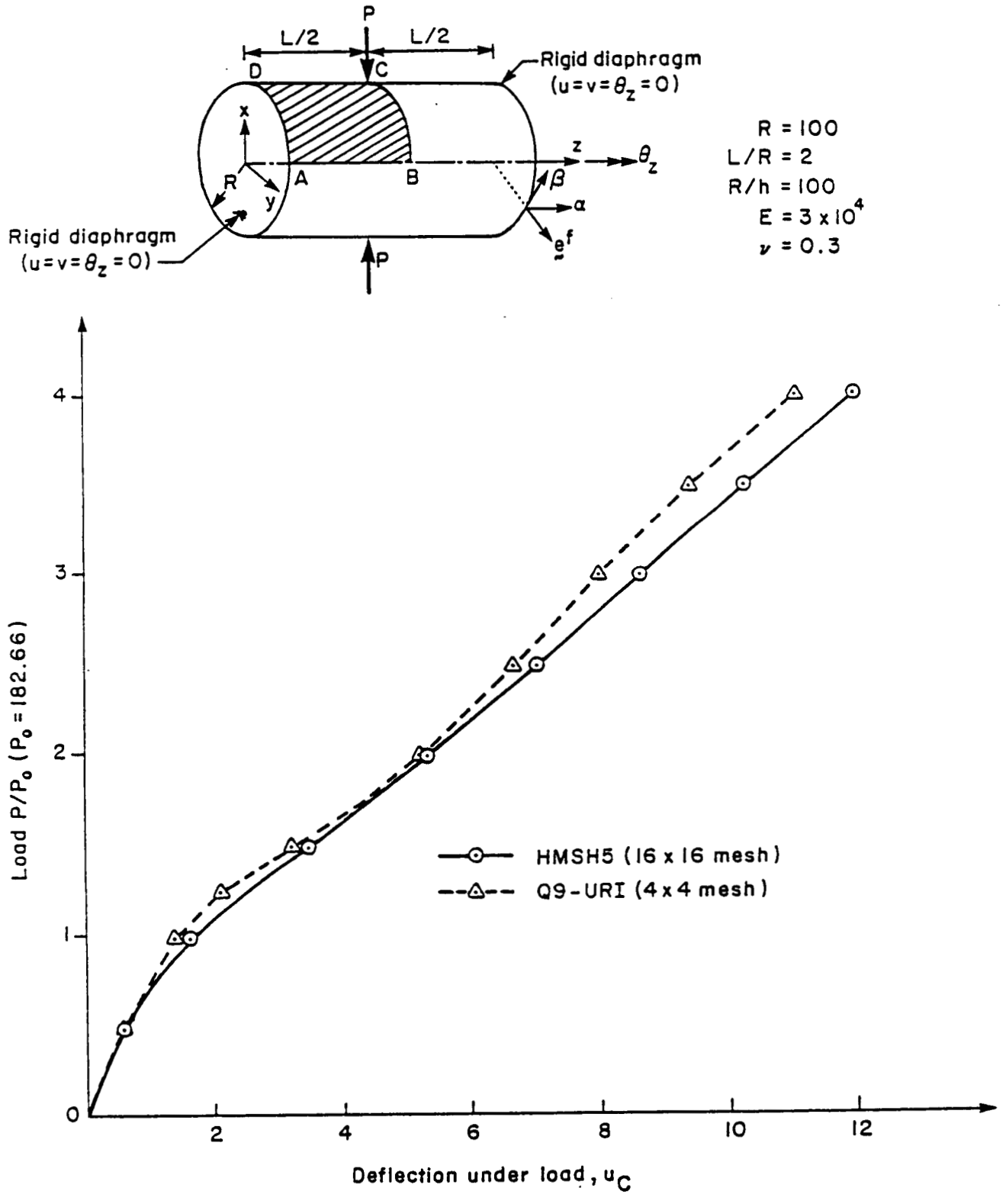

Fig. 39. A Pinched Cylinder With Rigid Diaphragms

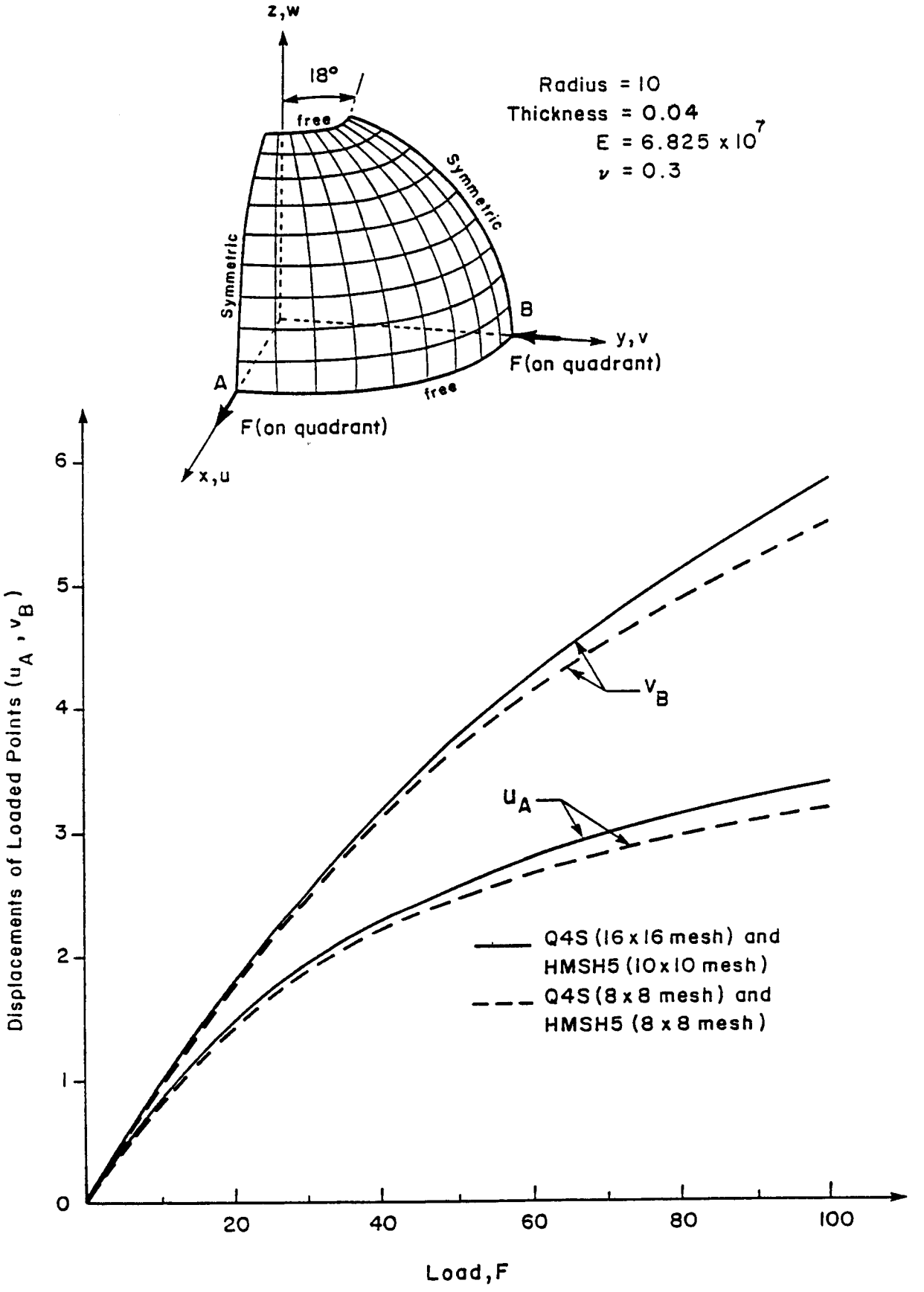

Fig. 40. A Pinched Hemispherical Shell

NASA
National Aeronautics and Space Administration

Report Documentation Page

1. Report No.	2. Government Accession No.	3. Recipient's Catalog No.
NASA CR-185120		

4. Title and Subtitle	5. Report Date
On Finite Element Implementation and Computational Techniques for Constitutive Modeling of High Temperature Composites	July 1989
	6. Performing Organization Code

7. Author(s)	8. Performing Organization Report No.
A.F. Saleeb, T.Y.P. Chang, T. Wilt, and I. Iskovitz	None
	10. Work Unit No. 505-63-31

9. Performing Organization Name and Address	11. Contract or Grant No.
University of Akron Department of Civil Engineering Akron, Ohio 44325	NAG3-901
	13. Type of Report and Period Covered Contractor Report Final

12. Sponsoring Agency Name and Address	14. Sponsoring Agency Code
National Aeronautics and Space Administration Lewis Research Center Cleveland, Ohio 44135-3191	

15. Supplementary Notes

Project Manager, Steven M. Arnold, Structures Division, NASA Lewis Research Center.

16. Abstract

This report outlines the research work performed during the past year on finite element implementation and computational techniques pertaining to high temperature composites. In the present research, two main issues are addressed: efficient geometric modeling of composite structures and expedient numerical integration techniques dealing with constitutive rate equations. In the first issue, mixed finite elements for modeling laminated plates and shells have been examined in terms of numerical accuracy, locking property and computational efficiency. Element applications include (currently available) linearly elastic analysis and future extension to material nonlinearity for damage predictions and large deformations. On the material level, various integration methods to integrate nonlinear constitutive rate equations for finite element implementation have been studied. These include explicit, implicit and automatic subincrementing schemes. In all cases, examples are included to illustrate the numerical characteristics of various methods that have been considered.

17. Key Words (Suggested by Author(s))	18. Distribution Statement
FEM; Finite element; Anisotropic materials; Composite materials; Laminates; Viscoplastic; Constitutive models; Integration techniques; Mixed elements	Unclassified – Unlimited Subject Category 39

19. Security Classif. (of this report)	20. Security Classif. (of this page)	21. No of pages	22. Price*
Unclassified	Unclassified	157	A08

*For sale by the National Technical Information Service, Springfield, Virginia 22161